Neuroanatomical relationship between cannabinoid type-1 receptors and dopamine neurons in the substantia nigra and ventral tegmental area

by

Emily Miller

BA&Sc., Quest University Canada, 2020

A Thesis Submitted in Partial Fulfillment

of the Requirements for the Degree of

MASTER OF SCIENCE

in the Division of Medical Sciences

University of Victoria

We acknowledge and respect the Lək^{w}əŋən (Songhees and X^{w}sepsəm/ Esquimalt) Peoples on whose territory the university stands, and the Lək^{w}əŋən and W̱ SÁNEĆ Peoples whose historical relationships with the land continue to this day.

Supervisory Committee

Neuroanatomical relationship between cannabinoid type-1 receptors and dopamine neurons in the substantia nigra and ventral tegmental area

by

Emily Miller

BA&Sc. Quest University Canada, 2020

Supervisory Committee

Dr. Patrick C. Nahirney, Division of Medical Sciences
Supervisor

Dr. Brian R. Christie, Division of Medical Sciences
Committee Member

Dr. Raad Nashmi, Division of Medical Sciences
Committee Member

Abstract

The substantia nigra pars compacta (SNc), substantia nigra pars reticulata (SNr) and ventral tegmental area (VTA) of the midbrain serve as the primary dopamine (DA) neuron hub of the brain. DA neurons project through distinct pathways—the mesolimbic, mesocortical, and nigrostriatal circuits—regulating critical behaviours such as motor control, motivation, and reward processing. The endocannabinoid system (ECS) is a neuromodulatory network that can influence synaptic transmission, predominantly via the cannabinoid type-1 receptor (CB1R) within the central nervous system. Although CB1Rs are widely distributed across the brain, the midbrain exhibits notably high CB1R expression. CB1Rs are proposed to modulate DA neuron activity by modulating afferent synaptic inputs. Dysregulation of CB1R distribution and function has been implicated in DA-related pathologies, including schizophrenia, Parkinson disease, and substance use disorders, making it a promising target for therapeutic intervention and mechanistic research. Despite growing interest in the DA-ECS interaction, the subcellular localization and density of CB1Rs within the SNc, SNr, and VTA remain poorly characterized. This study employed triple immunofluorescent confocal microscopy to assess the regional distribution of CB1R, tyrosine hydroxylase (TH; a DA neuron marker), and glutamate decarboxylase 67 (GAD67; an inhibitory neuron marker) across the SNc, SNr and VTA. Double pre-embedding immunoelectron microscopy was used to label CB1Rs with gold particles and TH with 3,3'-diaminobenzidine (DAB), enabling ultrastructural visualization via transmission electron microscopy. Micrographs were collected from all three regions and presynaptic terminals synapsing onto TH-positive compartments were traced and analyzed for CB1R labeling. Both immunofluorescent and immunoelectron results demonstrated that CB1Rs are most densely expressed in the SNr, followed by the SNc and VTA, and that CB1Rs preferentially localize to inhibitory presynaptic terminals. These findings suggest that CB1Rs predominantly modulate inhibitory inputs onto DA neurons. A deeper understanding of CB1R distribution and function within DA-rich midbrain regions will advance our knowledge of ECS modulation of DA neurotransmission and may inform the development of novel therapeutic strategies for DA-related disorders.

Table of Contents

List of Figures

List of Tables

List of Abbreviations

2-AG	2-Arachidonoylglycerol
AADC	Aromatic L-amino acid decarboxylase
ACh	Acetylcholine
AEA	Anandamide
Amy	Amygdala
ATP	Adenosine triphosphate
au	Arbitrary units
BLA	Basolateral amygdala
bonf	Bonferroni correction
BSA	Bovine serum albumin
BNST	Bed nucleus of the stria terminalis
cAMP	Cyclic adenosine monophosphate
Cap	Capillary
CB1R	Cannabinoid type-1 receptor
CB2R	Cannabinoid type-2 receptor
CBD	Cannabidiol
CNS	Central nervous system
CP	Cerebral peduncle
CPu	Caudate putamen
DA	Dopamine
DAB	3,3'-diaminobenzidine
DAGL	Diacylglycerol lipase
Den	Dendrite
DG	Dentate gyrus
DAPI	4’,6-diamidino-2-phenylindole
dH_2O	Deionized water
eCB	Endocannabinoid
ECS	Endocannabinoid system
EMM	Estimated marginal mean

EP	Entopeduncular nucleus
FAAH	Fatty acid amide hydrolase
GPCR	G-protein coupled receptor
GA	Glutaraldehyde
GABA	γ-aminobutyric acid
GAD67	Glutamate decarboxylase 67
GC	Granule cell
GIRK	G-protein gated inwardly rectifying potassum (K^+) channel
GL	Granule cell layer
GLMM	Generalized linear mixed model
GP	Globus pallidus
GPe	Globus pallidus externa
GPi	Globus pallidus interna
HCl	Hydrogen chloride
HCN	Hyperpolarization-activated cyclic nucleotide-gated channel
HRP	horseradish peroxidase
L-DOPA	L-3,4-dihydroxyohenylalanine
LDT	Laterodorsal tegmental nucleus
MAGL	Monoacylglycerol lipase
MFI	Mean fluorescent intensity
ML	Medial lemniscus or Molecular layer
MM	Medial mamillary nucleus
mPFC	Medial prefrontal cortex
MSN	Medium spiny neuron
nAChR	Nicotinic acetylcholine receptors
NaCl	Sodium chloride
NAPE-PLD	N-acyl phosphatidylethanolamine phospholipase D
Nu	Nucleus
NuAcc	Nucleus accumbens
PAG	Periaqueductal gray
PBP	Parabrachial pigmented nucleus

PC	Purkinje cell
PD	Parkinson disease
PFA	Paraformaldehyde
PKA	Protein kinase A
PN	Paranigral nucleus
PNS	Peripheral nervous system
PP	Peripeduncular nucleus
PPT	Pedunculopontine tegmental nucleus
PSD	Postsynaptic density
RMT	Rostromedial tegmental nucleus
SN	Substantia nigra
SNARE	Soluble N-ethylmaleimide-sensitive factor attachment protein receptor
SNc	Substantia nigra pars compacta
SNr	Substantia nigra pars reticulata
SO	Stratum oriens
SP	Stratum pyramidale
SR	Stratum radiatum
STN	Subthalamic nucleus
SUD	Substance use disorder
TBS	Trisphosphate buffered saline
TEM	Transmission electron microscopy
Ter	Terminal
TH	Tyrosine hydroxylase
THC	Δ^9-tetrahydrocannabinol
VGAT	Anti-vesicular GABA transporter
VGCC	Voltage-gated calcium channel
VGlut1	Vesicular Glutamate Transporter 1
VGlut2	Vesicular Glutamate Transporter 2
VTA	Ventral tegmental area
VTT	Ventral tegmental tail

Acknowledgements

First and foremost, I would like to thank Dr. Patrick Nahirney for teaching me that truly exceptional imaging is achieved through attention to detail—through minor adjustments in technique, patience, and adding just a bit more care in every step—and for reminding me to never surrender. I stuck with it, Pat, and I hope you agree that I've come a long way from mounting my slides backwards. I am also deeply grateful to my committee members Dr. Brian Christie and Dr. Raad Nashmi, and to my external examiner Dr. Pedro Grandes, for your invaluable support and guidance throughout my degree. Your encouragement and reassurance during my educational growing pains helped keep me sane. I also want to extent a special thank you to Kailah Sebastian—without you I'm fairly certain I would have missed every important deadline required to complete this degree. You've been an essential part of this process and I can't thank you enough.

Paige Allard and Ciara Halvorson, I'm not sure I would have made it through the first week, let alone to the end of this degree, without you both by my side. Thank you for the adventures, the post-work beers, the countless coffee walks (and little sweet treats), the times you insisted I take a break for my own good, and the hugs that held me together when I felt like giving up. Your friendship has meant the world to me.

To Sophie Thom, Jamie Morrison, Becca Pryz, Annika Ariano, and all my fellow neuroscience classmates, thank you for making these past two years truly unforgettable. This program has been one of the most welcoming and supportive communities I've ever been a part of, and it's because of all of you that I've felt so at home. I also want to extend a special thanks to Dr. Brady Reive and Mat Hammerstrom for all your help with software troubleshooting, coding and statistics. Your patience—especially in moments when I surely tested it—was something I genuinely appreciated. To Lara Solomons—thank you for your invaluable help with immunoparticle counting; your support made data collection far more manageable, and for that, I am truly grateful.

This Master's thesis would have never come to fruition if it were not for Dr. Emma Davy. Emma, I hope you know just how much you have influenced my life. Since my undergraduate years, you have supported and guided me through both academic endeavors and personal hardships, and encouraged my dream to pursue a career path that demands resilience and heart. You are an inspiration and a bad ass.

To Ryan Nordman, the love of my life, thank you for believing in me, especially when I struggled to believe in myself. Your support for my decision to begin graduate school and your strength throughout these past two years of distance mean more to me than words can express. Thank you for loving me through the stress and the chaos, for celebrating my wins, and for pushing me to keep going. Thank you for your support not only through this master's degree, but through all my past goals and through all the ones to come. I love you, and I don't know where'd I'd be without you.

To my friends outside Victoria—Brennon and Steph, Taylor, Nikki, Isabel and Steph (McCann) thank you for all your love whenever I've had the chance to see you these past two years, and every time before that. You help keep me grounded and I am grateful to you all beyond words.

To my parents, Lisa and Mike, and my sister, Christine, thank you for (literally) keeping me alive long enough not just to start this degree but to finish it. I know I've caused you worlds of stress, but know your unwavering support has not and will never go unnoticed. And thank you mum and dad for making my life easier every time you could—it mattered more than I ever said out loud. An infinite amount of thank-yous wouldn't come close to what you deserve.

Chapter 1: Introduction

1.1 Dopamine and dopaminergic pathways

In mainstream media, dopamine (DA) is often referred to as the "feel-good hormone" due to its association with the experience of pleasure. However, DA is a critical neural messenger involved not only in the mediation of pleasure, but also in motivation, motor control, and reward-based learning. DA is a catecholamine neurotransmitter synthesized from the amino acid tyrosine through a two-step enzymatic process. First, tyrosine is hydroxylated to form L-3,4-dihydroxyphenylalanine (L-DOPA) by tyrosine hydroxylase (TH), the rate-limiting enzyme of the pathway (Daubner et al., 2011). L-DOPA is then decarboxylated to DA by aromatic L-amino acid decarboxylase (AADC) (Daubner et al., 2011). The principal DA-producing nuclei of the brain—the substantia nigra (SN) and the ventral tegmental area (VTA)—are located within the midbrain and give rise to four major dopaminergic pathways, three of which are central to the present study: the nigrostriatal, mesolimbic, and mesocortical pathways (**Fig. 1**).

1.1.1 The substantia nigra and the nigrostriatal pathway

The SN was first identified and its structure illustrated by the French anatomist Félix Vicq d'Azyr in his 1786 work *Traité d'anatomie et de physiologie* (Parent & Parent, 2010; Vicq d'Azyr, 1786). However, it was not until 1910 that Japanese morphologist Torata Sano subdivided the SN into the two major regions recognized today—the substantia nigra pars compacta (SNc) and the substantia nigra pars reticulata (SNr) (Parent & Parent, 2010). Sano described the SNc as containing densely packed pigmented neurons, which we now know to be dopaminergic, and the SNr as consisting primarily of a dense fibrous meshwork with scattered non-pigmented neurons. This anatomical distinction was informed in part by Ramón y Cajal's 1899 characterization of the SN using Golgi-staining techniques (Parent & Parent, 2010; Ramón y Cajal, 1899). The question follows: when was it first recognized that these neurons are dopaminergic and critically involved in motor control?

The functional significance of the SN began to emerge in the early 1900s with Edouard Brissaud, who first postulated its role in motor control following the discovery of lesions to the region during the autopsy of a patient exhibiting symptoms consistent with Parkinson disease (PD)—a neurodegenerative disorder marked by bradykinesia, resting tremor, muscular rigidity, and postural instability (discussed further in **Section 1.4**) (Parent & Parent, 2010). In 1919,

Constantin Tretiakoff provided additional evidence in his doctoral thesis, noting that post-mortem brains of PD patients displayed a pronounced loss of pigmented nigral neurons accompanied by cellular swelling (Parent & Parent, 2010). However, it was not until the 1950s that Swedish scientists, notably Arvid Carlsson and Oleg Hornykiewicz, discovered DA, demonstrating not only that it serves as a key chemical messenger in the brain but also that DA levels are markedly diminished in the striatum of PD patients (Carlsson, 2002; Hornykiewicz, 2008; Parent & Parent, 2010). The development of fluorescence techniques during this period further evidenced their findings by allowing the researchers to trace dopaminergic projections from the SNc to the striatum. Moreover, shortly after, animal models of PD helped confirm that dopaminergic neurons originating in the SN project to the striatum via the nigrostriatal pathway, and that these neurons are critically affected in PD (Filion, 1979; Parent & Parent, 2010).

Since its anatomical and functional discovery, the SN has been extensively studied. Significant advances have been made in understanding the distinct anatomy and roles of the SNc and SNr, along with their respective inputs and outputs. Anatomically, the SN lies deep within the midbrain, positioned lateral to the ventral tegmental area (VTA; discussed further in **Section 1.1.2**) when viewed in coronal sections, and inferior and rostral to the VTA in sagittal sections (**Fig. 1**). Within the SN, the SNc is located superior to the SNr, which lies between the SNc and the underlying cerebral peduncle.

The nigrostriatal pathway is typically defined as originating from SNc dopaminergic neurons, whose axonal projections innervate the dorsal striatum (i.e., caudate-putamen, CPu), where they synapse onto medium spiny neurons (MSNs) (Prensa et al., 2009; Zhou & Lee, 2011). DA released from these projections binds to D1 and D2 receptors on MSNs, modulating their activity. Striatal MSNs contribute to either the direct or indirect basal ganglia pathways: the direct pathway involves monosynaptic projections to the globus pallidus interna (GPi)—the homolog of the rodent entopeduncular nucleus (EP)—and the SNr, whereas the indirect pathway involves polysynaptic projections through the globus pallidus externa (GPe) and subthalamic nucleus (STN) to the GPi and SNr (Zhou & Lee, 2011).

Functionally, activation of MSNs can either inhibit or enhance GPi/SNr output, thereby modulating thalamocortical activity and motor execution (Young et al., 2025). In the direct pathway, DA binds D1 receptors of striatal MSNs which once excited inhibits the GPi and SNr. Without inhibitory gamma-aminobutyric acid (GABA) signalling input from the GPi and SNr, the

thalamus activates the motor cortex and movement is facilitated. Conversely, in the indirect pathway, activation of D2 receptor-expressing MSNs inhibits the GPe, which normally suppresses the STN. Disinhibition of the STN allows it to send glutamatergic excitatory signals to the GPi and SNr, resulting in strong thalamic inhibition and suppression of motor activity. However, when DA binds to D2 receptors, it inhibits these MSNs and thus reduces inhibitory output of the GPe. This helps maintain suppression of the STN and prevents excessive activation of the GPi and SNr, thus reducing movement suppression. The pathway predominantly activated is ultimately dependent on the site of DA release and the local distribution and affinity of receptor subtypes. Regardless of these local variations, dopaminergic input from the SNc promotes motor activity by simultaneously exciting the direct pathway and inhibiting the indirect pathway (Young et al., 2025).

Within the SNc, inhibitory inputs arise from the somatosensory and motor cortices, SNr, CPu and GPe, whereas excitatory glutamatergic and cholinergic inputs originate from the pedunculopontine tegmental nucleus (PPT) and laterodorsal tegmental nucleus (LDT) (Misgeld, 2004). The SNr receives afferent inputs from the GPe (GABAergic) and the STN (glutamatergic) and sends efferent projections to the thalamus, superior colliculus, and PPT (Misgeld, 2004; Zhou & Lee, 2011). Furthermore, although local interneurons are relatively sparse, axon collaterals from SNr projection neurons provide feedback interactions within the SNr itself and with adjacent dopaminergic neurons of the SNc and VTA (Deniau et al., 1982; Partanen & Achim, 2022).

Notably, while the SNc is well established as a hub of DA neurons, the SNr contains relatively few neuronal cell bodies, the majority of which are inhibitory GABAergic neurons (Margolis et al., 2006, 2012). However, SNr GABAergic neurons are heterogeneous, differing in molecular markers, gene expression patterns, and receptor and ion channel profiles (Partanen & Achim, 2022). Notably, the SNr has been shown to contain smaller populations of other neuronal types, such as excitatory (i.e., glutamatergic) neurons, although the functional roles of these populations remain to be fully elucidated (Partanen & Achim, 2022). SNr GABAergic projection neurons exert tonic inhibitory control over their targets, regulating movement initiation and behaviour (as described). They express sodium-dependent channels that sustain inward currents, supporting spontaneous high-frequency spiking (Deniau et al., 2007; McElvain et al., 2021). Suppression of GPi and SNr activity by upstream structures results in disinhibition of target regions, while excitatory input from the STN induces burst firing (Zhou & Lee, 2011). These

afferents likely fine-tune SNr firing patterns to enable precise motor control, although the exact mechanisms linking SNr activity to specific behaviours remain unclear.

1.1.2 The ventral tegmental area and mesocortical limbic systems

The ventral tegmental area (VTA) was first distinguished anatomically by Nauta (1958), who demonstrated that limbic-associated structures preferentially project to the midbrain VTA region, but not to the adjacent SN. Given the anatomical proximity and morphological similarity of the SN and VTA, this observation was critical in differentiating these two midbrain structures. Subsequent work by Dahlström and Fuxe (1964) classified cell groups into A1–A12 and B1–B9 based on neurochemical markers (Dahlstroem & Fuxe, 1964; Ikemoto, 2007). Within this schema, dopaminergic neurons of the ventral midbrain were assigned to groups A8, A9, and A10, with the A10 group encompassing the VTA. A10 neurons were found to project predominantly to the nucleus accumbens and olfactory tubercle (components of the ventral striatum), establishing the mesolimbic DA pathway as anatomically and functionally distinct from the parallel-running nigrostriatal pathway. Further studies revealed that the VTA also sends dopaminergic projections to the hippocampus, amygdala, and prefrontal cortex (Ikemoto, 2007).

Functionally, the VTA is implicated in a wide array of processes, including positive and negative reinforcement, incentive salience attribution, decision-making, working memory, stimulus salience encoding, and aversive responses (Morales & Margolis, 2017). This functional diversity is thought to reflect the cellular heterogeneity within the VTA itself. The density of dopaminergic, GABAergic, and glutamatergic neurons varies considerably across VTA subregions, and the physiological and pharmacological properties of neurons within the same cell type also exhibit significant variability (Margolis et al., 2006, 2012). Although this thesis examines the VTA as a whole, it is worth noting that due to heterogeneity other studies frequently subdivide the VTA into four major regions based on neurochemical profiling: the paranigral nucleus (PN), parabrachial pigmented nucleus (PBP), parafasciculus retroflexus area, and ventral tegmental tail (VTT) (Ikemoto, 2007).

VTA dopaminergic neurons receive robust excitatory glutamatergic afferents from multiple structures, including the medial prefrontal cortex (mPFC), PPT, LDT, periaqueductal gray (PAG), hypothalamus, and bed nucleus of the stria terminalis (BNST) (Morales & Margolis, 2017). Inhibitory GABAergic inputs arise from the rostromedial tegmental nucleus (RMT; also referred to as the VTT), PAG, hypothalamus, local VTA interneurons, and the SNr. Although local VTA

glutamatergic and GABAergic neurons project to a variety of targets, dopaminergic neurons predominantly innervate medium spiny neurons (MSNs) of the nucleus accumbens, and to a lesser extent cells of the amygdala, mPFC, hippocampus, and other regions (Morales & Margolis, 2017).

Within the mesolimbic pathway, VTA dopaminergic neurons preferentially target MSNs of the nucleus accumbens (Morales & Margolis, 2017). DA release excites D1 receptor-expressing MSNs, facilitating the direct pathway and promoting motivated behaviours, while simultaneously inhibiting D2 receptor-expressing MSNs, thereby attenuating the indirect pathway and reducing behavioural suppression (Soares-Cunha et al., 2016). Consequently, DA enhances reward-seeking behaviours by simultaneously facilitating the activity of direct-pathway MSNs and suppressing indirect-pathway MSNs, analogous to the mechanisms operating within the dorsal striatum. Nucleus accumbens MSNs project to the ventral pallidum and thalamus, modulating cortical output, as well as to the hypothalamus and brainstem nuclei, which regulate autonomic and emotional behaviours such as feeding and stress responses (Pardo-Garcia et al., 2019; Smith et al., 2009; Soares-Cunha et al., 2016). In parallel, VTA dopaminergic neurons also innervate pyramidal neurons within the basolateral amygdala (BLA), where DA enhances the emotional salience of stimuli and facilitates reward-related and aversive learning (Tang et al., 2020). Conversely, the mesocortical pathway primarily influences cognitive and executive functions (Seamans & Yang, 2004). In this pathway, VTA DA neurons—likely arising from partially distinct subpopulations from the mesolimbic system—project directly to the hippocampus and prefrontal cortical regions. In the cortex, dopamine modulates the excitability of pyramidal neurons and local GABAergic interneurons, thereby influencing working memory, decision-making, and emotional regulation (Seamans & Yang, 2004). **Figure 1** illustrates the DA-rich mesolimbic and mesocortical pathways in the adult mouse brain.

1.1.3 DA neuron firing patterns

DA neurons of the SNc and VTA exhibit intrinsic pacemaker activity (tonic firing), characterized by the spontaneous generation of action potentials in the absence of synaptic input, as well as phasic (burst) firing in response to salient stimuli (Gantz et al., 2018). Tonic firing is maintained by "leaky" sodium currents—small, persistent inward sodium currents that gradually depolarize the membrane toward threshold—and by the activation of low-threshold voltage-gated calcium channels (primarily L-type and T-type) and hyperpolarization-activated cyclic nucleotide-gated (HCN) channels, which collectively initiate action potential generation. Repolarization is

mediated by various potassium channels, allowing the rhythmic cycling of membrane potential and resulting regular firing patterns (Gantz et al., 2018).

In contrast, phasic firing consists of high-frequency bursts of action potentials and typically requires excitatory synaptic input, primarily from the PPT and LDT. Functionally, tonic firing is thought to maintain baseline extracellular dopamine levels necessary for regulating general functions such as mood, arousal, and basic motor control, whereas phasic firing produces transient, high-concentration dopamine release critical for reward prediction and learning (Grace, 1991).

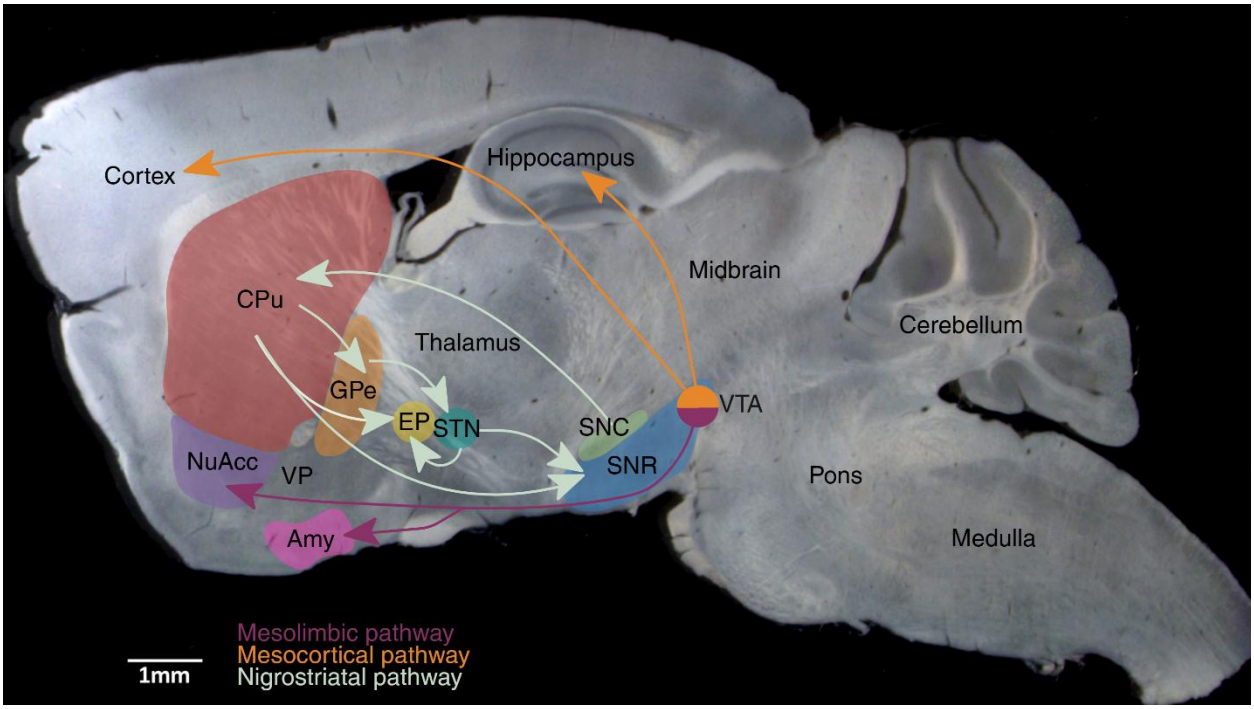

Figure 1. Mesolimbic, mesocortical, and nigrostriatal dopamine (DA) pathways of the adult mouse brain. The nigrostriatal pathway originates from the substantia nigra pars compacta (SNc), with DA projections traveling through the nigrostriatal bundle to the caudate-putamen (CPu). Medium spiny neurons (MSNs) of the CPu project either directly to the entopeduncular nucleus (EP) and substantia nigra pars reticulata (SNr) (direct pathway), or indirectly via the globus pallidus externa (GPe) and subthalamic nucleus (STN) (indirect pathway). The ventral tegmental area (VTA), central to the mesolimbic and mesocortical pathways, sends DA projections predominantly to the nucleus accumbens (NuAcc), prefrontal cortex, amygdala (Amy), and hippocampus. The nigrostriatal and mesocorticolimbic systems exert strong influence over motor control and reward-based learning, respectively.

1.2 The endocannabinoid system

The endogenous cannabinoid system, referred to as the endocannabinoid system (ECS), is a neuromodulatory network present in both the peripheral (PNS) and central nervous systems (CNS). It was initially conceptualized following the isolation of Δ^9-tetrahydrocannabinol (THC) and cannabidiol (CBD)—two primary bioactive constituents of *Cannabis sativa*—in 1964, which ultimately led to the discovery of the endogenous system they modulate in 1988 (Nazarenus &

Cox, 2019). The ECS comprises a complex interplay of enzymes, receptors, and ligands, and is intricately integrated with other signaling pathways rather than functioning in isolation (Lu & Mackie, 2016). During nervous system development, the ECS plays critical roles in neurogenesis and synaptogenesis, while in the mature CNS it regulates neuronal excitability, significantly influencing processes such as learning and memory, motor control, reward-based processing, and nociception (Skaper & Di Marzo, 2012).

The core components of the ECS include the endogenous ligands anandamide (arachidonoyl ethanolamide; AEA) and 2-arachidonoyl glycerol (2-AG) (collectively termed endocannabinoids, or eCBs); the synthetic and degradative enzymes fatty acid amide hydrolase (FAAH), monoacylglycerol lipase (MAGL), diacylglycerol lipase (DAGL), and N-acyl phosphatidylethanolamine phospholipase D (NAPE-PLD); and the cannabinoid type-1 receptor (CB1R) and cannabinoid type-2 receptor (CB2R) (Lu & Mackie, 2016). Unlike classical neurotransmitters, eCBs are synthesized "on demand" in response to neuronal activity rather than stored in synaptic vesicles. They primarily function as retrograde messengers, being produced postsynaptically and diffusing across the synaptic cleft to bind and activate presynaptic CB1Rs, typically resulting in the suppression of neurotransmitter release from the presynaptic terminal. Notably, CB2Rs are predominantly localized to the PNS, whereas CB1Rs are highly enriched in the CNS (Lu & Mackie, 2016). Accordingly, of particular relevance to this thesis is the CB1R.

1.2.1 The cannabinoid-type 1 receptor

The CB1R is a seven-transmembrane domain G protein-coupled receptor (GPCR) localized to various ultrastructural compartments, including internal organelles such as mitochondrial membranes, endosomes and lysosomes, and externally on the plasma membranes of synaptic terminals, somata, and dendrites (Bonilla-Del Río et al., 2021; Gutiérrez-Rodríguez et al., 2017; Puente et al., 2019; Soria-Gomez et al., 2021). Moreover, within the brain, CB1Rs are most abundantly expressed in the midbrain, hippocampus, cerebellum, and globus pallidus (**Fig. 2**) (Herkenham et al., 1991; Tsou et al., 1998). CB1Rs are expressed from the earliest stages of pregnancy in the fetal brain, where they play critical roles in neuronal development and circuit formation, and they persist into adulthood, functioning as key neuromodulatory receptors (Lu & Mackie, 2016). In the adult brain, CB1Rs are predominantly expressed on GABAergic interneurons and, to a lesser extent, on glutamatergic, cholinergic, glycinergic, and serotonergic neurons (Busquets-Garcia et al., 2018).

Functionally, CB1Rs can couple to multiple classes of G proteins, although they preferentially signal through Gi/o proteins (Zou & Kumar, 2018). Upon activation, CB1Rs inhibit the adenylyl cyclase pathway, reducing the conversion of ATP to cyclic AMP (cAMP). This suppression of cAMP leads to decreased activation of protein kinase A (PKA), which normally phosphorylates proteins essential for neurotransmitter release, including voltage-gated calcium channels (VGCCs) and components of the vesicle release machinery. Thus, reduced phosphorylation results in decreased neurotransmitter release. Additionally, Gi/o directly binds and inhibits presynaptic VGCCs, activates G protein-activated inwardly rectifying potassium (GIRK) channels that hyperpolarize the presynaptic terminal, and interferes with vesicle docking and fusion by disrupting SNARE complex function. All these mechanisms contribute to the inhibition of neurotransmitter release that defines CB1R activation. Interestingly, CB1Rs can also engage β-arrestin-mediated pathways, further highlighting the complexity of their signaling mechanisms (Zou & Kumar, 2018).

CB1R ligands encompass a diverse range of endogenous and exogenous compounds. Of the two principal eCBs, AEA acts as a high-affinity partial agonist at CB1Rs, producing submaximal receptor activation even at full receptor occupancy, whereas 2-AG, despite its moderate-to-weak affinity, functions as a full agonist capable of fully engaging CB1R-mediated intracellular signaling cascades (Zou & Kumar, 2018). Exogenous CB1R ligands are widely encountered both recreationally and in experimental research. THC, the primary psychoactive phytocannabinoid in *Cannabis sativa*, and CBD, the principal non-psychoactive constituent, both interact with CB1Rs, albeit with distinct pharmacodynamic profiles. THC operates as a partial agonist at CB1Rs, whereas CBD exhibits weak partial antagonist activity and can further modulate the ECS by enhancing AEA bioavailability (Soler-Cedeno & Xi, 2022). Additionally, a range of synthetic CB1R ligands have been developed, including inverse agonists such as SR141716A (rimonabant) and AM251, neutral antagonists such as AVE1625, AM6527, PIMSR, and AM4113, and potent agonists such as WIN55,212-2 (Soler-Cedeno & Xi, 2022). These compounds demonstrate varying affinities for CB1Rs and predominantly engage the orthosteric ligand-binding domain. However, increasing research attention has been directed toward the development of allosteric modulators, which offer the potential for more selective receptor modulation (Soler-

Cedeno & Xi, 2022). Many of these synthetic ligands are utilized in preclinical models or have been explored for therapeutic applications.

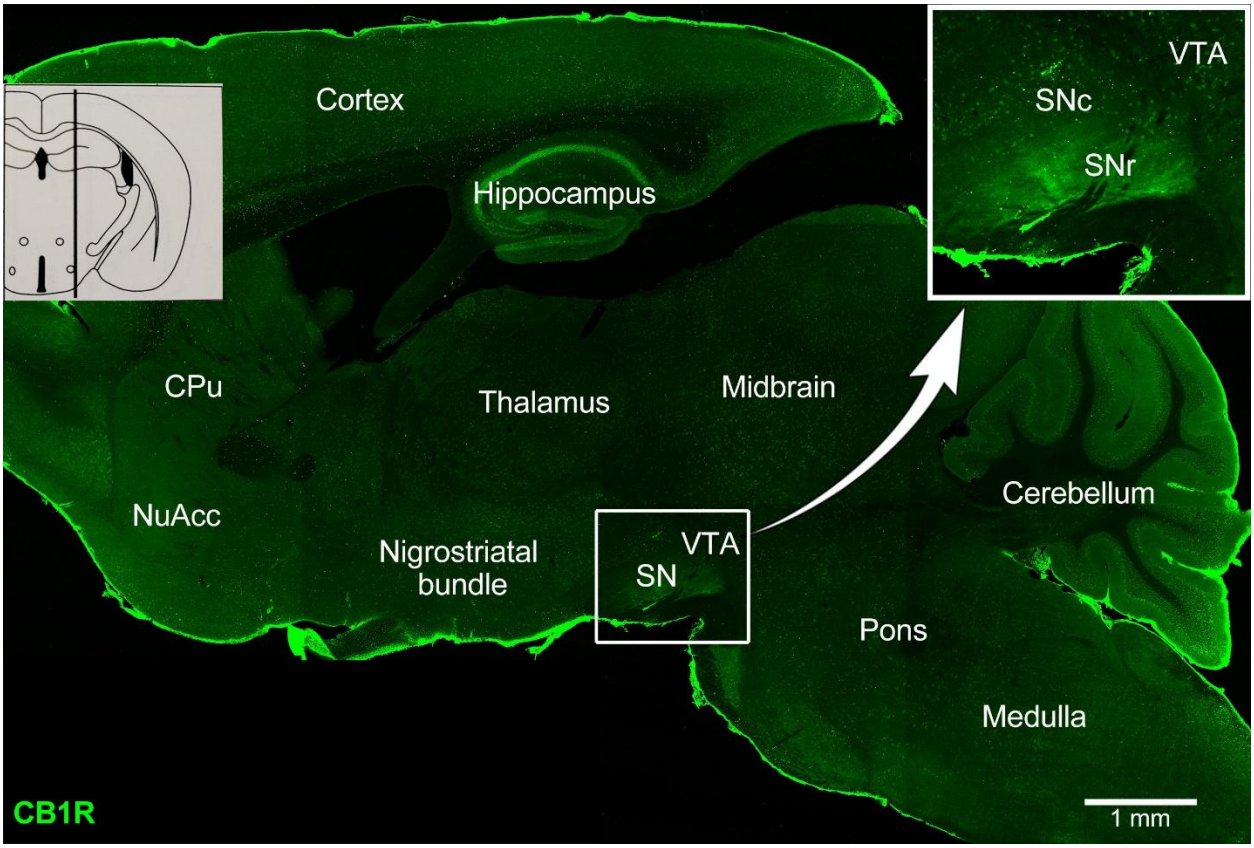

Figure 2. Epi-fluorescent montage depicting the localization of CB1Rs within a sagittal section of the adult mouse brain. Increased immunofluorescent staining is evident in the hippocampus, cerebellum, and SN region. Inset shows a higher magnification view of the boxed area, highlighting the localization of CB1R signal within the SNr compared to the SNc and VTA. At the left, a schematic illustrates the approximate position from which the sagittal section was obtained. Artifactual staining is observed along the brain perimeter, likely resulting from the use of adhesive and agarose during tissue preparation. NuAcc, nucleus accumbens; CPu, caudate-putamen.

The interaction between CB1 receptors (CB1Rs) and DA pathways has emerged as a recent focus of investigation, offering particular relevance for understanding the pathophysiology of DA-related disorders and the development of targeted therapeutics. Notably, accumulating evidence suggests that CB1Rs are not expressed directly on DA neurons themselves (Baddenhausen et al., 2024; García et al., 2016; Julian et al., 2003). Instead, CB1Rs are thought to modulate dopaminergic pathway activity indirectly, primarily by regulating GABAergic and glutamatergic neurotransmission onto midbrain DA neurons (García et al., 2016). Although significant advances have been made in delineating the anatomical distribution and functional roles of CB1Rs within DA-rich brain regions, substantial gaps in knowledge remain, warranting further investigation.

1.3 Immunoelectron microscopy of CB1Rs in the midbrain

The first electron microscope was developed by Ernst Ruska in 1931, revolutionizing the ability to visualize cellular ultrastructure (Qian, 2023). However, it was not until 1971 that Faulk and Taylor introduced the immunocolloid labeling technique, allowing specific proteins to be visualized by transmission electron microscopy (TEM) through the use of gold-conjugated antibodies (Roth, 1996). Although immunoelectron microscopy continued to advance over subsequent decades, its application to cannabinoid receptor research emerged later. One of the earliest studies to visualize CB1Rs using immunoelectron microscopy was conducted by Katona and colleagues (1999) who demonstrated prominent CB1R localization on presynaptic terminals of GABAergic interneurons in the hippocampus. Although this study provided critical insights into CB1R subcellular distribution, broader investigations into CB1R localization across various brain regions using immunoelectron microscopy techniques began to expand in the years that followed.

Although the midbrain has been recognized as a region with prominent CB1R expression, the subcellular distribution of CB1Rs within the SNc, SNr and VTA remains relatively under-characterized, particularly in relation to dopaminergic neurons. Fitzgerald et al. (Fitzgerald et al., 2012) presented a review incorporating electron micrographs that illustrated CB1R localization adjacent to TH-positive DA neurons within the VTA, SN, and striatum; however, their study did not include original experimental data or semi-quantitative analyses. More recently, Soria-Gómez and coworkers (2021) used multiple approaches, including immunogold labeling of CB1Rs in wild-type and CB1R knockout mice within the SN, and revealed that CB1R activation at distinct subcellular compartments within a single neural circuit can mediate divergent behavioural outputs. Nevertheless, their investigation predominantly focused on mitochondrial CB1Rs and did not specifically examine their location in respect to DA neurons. Despite these important contributions, detailed, quantitative analyses of CB1R subcellular distribution across the SNc, SNr, and VTA remain notably limited.

1.4 DA-related disorders and the endocannabinoid system: How foundational research could provide therapeutic insights

Dopaminergic pathways are critically implicated in a range of neurodegenerative and neuropsychiatric disorders. As a foundational project, investigating the interface between these pathways and components of the neuromodulatory ECS offers an opportunity to elucidate mechanisms underlying such conditions and to identify potential future therapeutic targets. Among

the many DA-related disorders, three are particularly associated with midbrain circuitry and will be emphasized throughout this thesis: Parkinson disease (PD), schizophrenia, and substance use disorders (SUDs).

PD is a progressive neurodegenerative disorder characterized by the degeneration of DA neurons within the SNc and the accumulation of α-synuclein protein aggregates, known as Lewy bodies, leading to hallmark motor symptoms such as bradykinesia, resting tremor, muscular rigidity, and postural instability (Morris et al., 2024; Vázquez-Vélez & Zoghbi, 2021). PD is the second most prevalent neurodegenerative disease globally and exhibits the fastest-growing rates of prevalence and disability (Su et al., 2025). In Canada, it is projected that 317,269 individuals will be living with PD by 2050 (Bach et al., 2011). The ECS, and more specifically the CB1R, has been a focal point in therapeutic investigations for PD. As CB1Rs are believed to modulate glutamatergic and GABAergic inputs onto SNc DA neurons (Fernández-Ruiz, 2009), strategic modulation of CB1R activity could influence DA output to the dorsal striatum and potentially ameliorate motor deficits (Soti et al., 2022; Urbi, Corbett, et al., 2022). Thus, a detailed understanding of the cellular and subcellular localization of CB1Rs within the SN region could inform future therapeutic strategies.

Schizophrenia is a chronic and biologically complex psychiatric disorder, presenting with a constellation of symptoms traditionally categorized as positive (e.g., hallucinations, delusions), negative (e.g., anhedonia, alogia, avolition), and cognitive (e.g., impaired executive functioning, working memory deficits) (McCutcheon et al., 2019; Weston-Green, 2022). In accordance with the DA hypothesis of schizophrenia, DA receptor antagonists have historically served as the primary pharmacological intervention for reducing positive symptoms (Weston-Green, 2022). According to Statistics Canada, approximately 1% of Canadians aged 10 years and older have been diagnosed with schizophrenia; however, this figure likely underestimates true prevalence, as it reflects only individuals who have accessed healthcare services, while a significant proportion remains undiagnosed and untreated (Canada, 2020). Emerging evidence suggests that the ECS is dysregulated in schizophrenia, contributing to aberrant DA signaling associated with the disorder (Mielnik et al., 2021). Preclinical studies, particularly those utilizing hyperdopaminergic animal models that recapitulate positive symptoms such as psychosis-like behaviours, have demonstrated that CB1R modulators can attenuate these symptoms, supporting the ECS as a promising target for therapeutic development (Mielnik et al., 2021).

SUDs are characterized by psychological and chemical dependence on psychoactive substances, such as alcohol, opioids, or stimulants, that results in disrupted brain function and impaired control over use. Drug use and SUDs represent a major public health concern globally, including in Canada where our country is currently experiencing an opioid crisis. Approximately 2.7% of Canadians are estimated to suffer from an SUD, making Canada the country with the second-highest prevalence, following the United States at 3.7% (Ritchie et al., 2022; Volkow & Blanco, 2023). The chemical dependency associated with SUDs is believed to primarily involve the mesolimbic and mesocortical DA pathways. Shortly before the identification of DA as a neurotransmitter, Olds and Milner (Olds & Milner, 1954) demonstrated that rats would repeatedly press a lever delivering electrical stimulation to regions such as the hypothalamus, septal area, and amygdala, but not to other brain areas, suggesting the existence of a brain reward system. Subsequent experiments using DA receptor antagonists further implicated DA as a critical mediator of this reward circuitry (Olds et al., 1956; Olds & Olds, 1958). In the context of drug addiction, two key markers of abnormal DA regulation have emerged: (1) reduced availability of striatal DA receptors and (2) diminished striatal DA release in response to pharmacological stimulation (Koob & Volkow, 2010; Volkow et al., 2011). Interestingly, CB1R distribution is also altered in SUDs, and antagonistic targeting of CB1Rs has shown promising results in reducing addictive behaviours, highlighting this pathway as an area of particular interest amidst the growing prevalence of addiction (Manzanares et al., 2018).

Increasing evidence suggests that the ECS exerts significant modulatory effects on dopaminergic systems, can become dysregulated in both neurodegenerative and neuropsychiatric disorders, and represents a potential therapeutic target in DA-related pathologies. Advancing our understanding of how DA neurotransmission is modulated by the ECS could provide critical insights into disease mechanisms and treatment strategies.

1.5 Questions, objectives and hypotheses

This thesis is driven by several key research questions. First, given the limited number of ultrastructural studies examining CB1R localization at the subcellular level within the midbrain, does CB1R expression indeed largely avoid colocalization with TH-positive dopaminergic neurons? Second, what are the density and localization patterns of CB1Rs within the SNr, SNc and VTA of the adult mouse brain? Specifically, how is CB1R distribution partitioned across these

three midbrain regions and, at the ultrastructural level, which presynaptic terminals are CB1Rs localized on dopaminergic neurites (i.e. inhibitory versus excitatory), and at what density?

The objectives of this study are to employ immunofluorescent and immunoelectron imaging techniques to quantify CB1R distribution within the SNr, SNc and VTA, both at regional and subcellular levels. I hypothesize that CB1Rs will exhibit the highest density within the SNr and VTA compared to the SNc, with the SNc displaying minimal CB1R expression. Furthermore, I hypothesize that CB1Rs will not colocalize with TH-positive dopaminergic compartments, but will instead be predominantly localized to inhibitory presynaptic terminals forming synaptic contacts onto DA neurons.

Chapter 2: Materials & Methods

2.1.1 Tissue processing for confocal microscopy

Wildtype C57BL/6 3–5-month-old male mice were used and all procedures carried out in these experiments were approved by the University of Victoria Animal Care Committee and in compliance with Canadian Council for Animal Care guidelines. Three mice were deeply anesthetized with isoflurane until they were unresponsive to a tail or toe pinch and they did not exhibit a corneal reflex when the eye was gently touched with a Q-tip. They were then transcardially perfused through a gravity-fed perfusion device with heparinized trisphosphate buffered solution (TBS) of pH ~7.4 until the toes and nose appeared white and the liver turned from a deep red to pale brown colour. Stock TBS (10x) was made at 2.997 M sodium chloride (NaCl), 0.160M Tris-base and 0.839 M Tris-hydrochloric acid (HCl) with a pH of ~7.4. Throughout the experiment, TBS was prepared from the stock solution and diluted to a 1x concentration. Following the heparinized flush, the perfusing fluid was changed to 4% paraformaldehyde (PFA) in TBS and ran until the hind legs and neck were stiff and the liver felt firm to the touch (~80 mL). Brains were then removed and post-fixed overnight at 4°C in the same 4% PFA solution. The next day, brains were sectioned sagittally in chilled TBS on a Leica vibratome at 50 μm and collected in labeled 24-well plates filled with TBS and 0.025% sodium azide. Sections were then stored at 4°C until further processing could commence.

Brain sections selected for fluorescent staining were chosen under a stereoscopic microscope and using a brain atlas (Paxinos & Franklin, 2001) and included the medial, middle, and lateral regions of the VTA, SNc and SNr (approximately Bregma 0.24 mm, 0.48 mm, 0.96 mm, 1.44 mm, 1.8 mm) for a total of 5 sections per mouse. One additional section was selected per mouse to run simultaneously as a negative control. This selection process aimed to obtain a fair representation of the entirety of each functionally discreet region. Sections were then treated with 10% bovine serum albumin (BSA), 0.02% saponin, and 0.01% sodium azide in TBS for 1 hour on a 30-rpm shaker at 4°C. This step was used to both block non-specific binding of antibodies and permeabilize cellular membranes to ensure antibody penetration. Saponin, a mild permeabilization agent that selectively removes cholesterol from plasma membranes to form pores in the membrane without completely disturbing it, was preferred to stronger agents like Triton-X which removes both cholesterol and phospholipids from membranes. In this way, the CB1R protein could be preserved for immunofluorescence microscopy.

Immediately after blocking and permeabilization, sections were submerged in a primary antibody solution of goat anti-CB1R antibody (1:500, Nittobo Medical Co. Ltd., cat#MSFR100610), mouse anti-glutamate decarboxylase 67 (GAD67) antibody (1:1000, ThermoFisher Scientific, cat#MA5-24909), a key enzyme in the conversion of the excitatory neurotransmitter glutamate into the inhibitory neurotransmitter GABA, and rabbit anti-TH antibody (1:1000, Pel-Freeze Biologicals, cat#P40101-150) in 1% BSA, 0.004% saponin, and 0.1% sodium azide in TBS and left overnight on a shaker at 4°C. The next morning, tissue sections underwent 3 consecutive 3-minute washes followed by two 10-minute washes in 1% BSA in TBS. Sections were then treated with a secondary antibody solution of donkey anti-goat Alexa Fluor 488 antibody (1:500, ThermoFisher Scientific Invitrogen, cat#A11055), donkey anti-rabbit Alexa Fluor 594 antibody (1:500, ThermoFisher Scientific Invitrogen cat#R37119), and donkey anti-mouse Alexa Fluor 647 antibody (1:500, ThermoFisher Scientific Invitrogen, cat#A32787) for >4 hours at room temperature (RT) on a 50-rpm shaker. The 24-well plates were covered with a tinfoil lid during this time to preserve fluorescence. After, washing was repeated with 1% BSA in TBS for 3 consecutive 10-minute periods, followed by a 10-minute treatment of 1:1000 concentration 4′,6-diamidino-2-phenylindole (DAPI; blue nuclear stain) in TBS under a tinfoil lid. Sections were then mounted on labelled microscope slides and coverslipped with PermaFluor mounting medium (ThermoFisher Scientific, cat#TA-030-FM). Slides were kept inside a pop-up slide holder at -20°C unless imaging was being completed. Slides were never imaged >72 hours after mounting to ensure the fluorescent staining was optimal for all images.

Additionally, to qualitatively assess potential co-localization of CB1Rs with other major neurotransmitter systems, supplementary experiments were conducted using 3–5-month-old male wild-type C57BL/6 mice. Tissue sections for these experiments underwent identical preparation procedures as described above but were cut either sagittally or coronally using a vibratome. Further, the primary and secondary antibodies used in these assessments included combinations of those previously mentioned, along with the following: rabbit anti-CB1R (1:500, Nittobo Medical Co. Ltd., cat# MSFR100590), donkey anti-goat Alexa Fluor 647 (1:500, ThermoFisher Scientific Invitrogen, cat# A21447), guinea pig anti-vesicular glutamate transporter 1 (VGlut1; 1:200, Synaptic Systems, cat# 135304), mouse anti-VGlut2 (1:200, Synaptic Systems, cat# 135421), and donkey anti-guinea pig Cy5 (1:400, Jackson ImmunoResearch Laboratories Inc., cat# 706175148). A full list of antibodies and their specifications is provided in **Appendix A**.

2.1.2 Confocal image acquisition and analysis

Images were acquired using an Olympus Fluoview FV1000 confocal laser scanning microscope. All images taken for data analysis were obtained using a 1024 by 1024 aspect ratio. Lasers were run sequentially on each plane to prevent fluorophore crosstalk and the Kalman filter mode was used to minimize any unwanted background signal. Lasers used included 405 nm, 488 nm, 561 nm and 635 nm, for excitation of fluorescent secondary antibodies at 358 nm (DAPI), 488 nm, 594 nm, and 647 nm, respectively. To create a map of each region of interest, low magnification images were obtained using a 20x objective lens. Two to six z-stacks of 10 planes separated by a 0.5 μm step were captured for the VTA, SNc and SNr present on each slide. Planes acquired were chosen based on strength of each signal. Z-stacks were completed in two phases using the virtual channel scan function so the quadruple stain could be acquired. The first phase operated the 405 nm and 594 nm lasers, while the second phase applied the 488 nm and 647 nm lasers. Confocal laser settings were determined according to the slide with the most intense staining and maintained for all following slides and are presented in **Table 1**. This allowed comparisons to be made across mice and regions. Representative images were obtained using a 60x oil immersion objective lens.

Table 1. Confocal Laser Scanning Microscope Channel Settings

Setting	TH-594 nm	GAD67-647 nm	CB1R-488 nm
Gain	1	2	1.25
Offset	2	3	1
High Voltage (HV)	610	610	610
Laser Percent	8.5	18	10

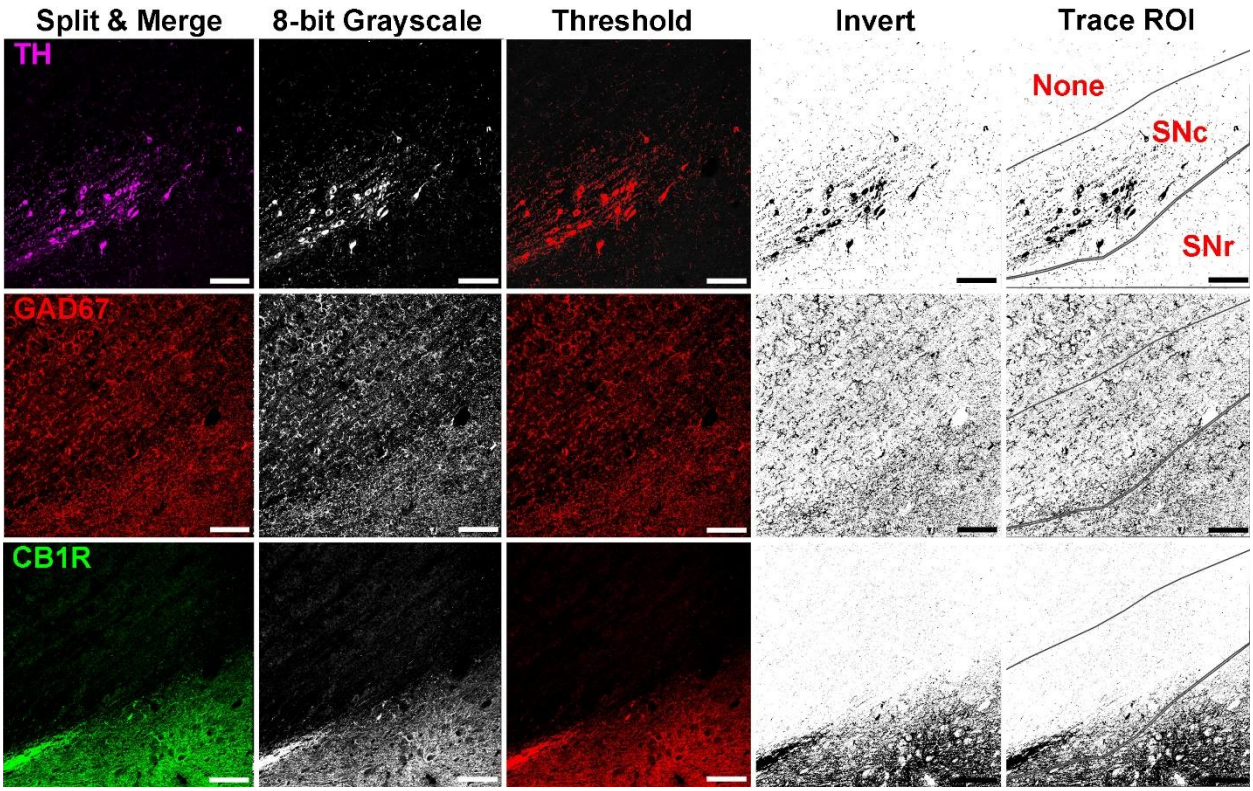

Figure 3. Mean Fluorescent Intensity Methods. Z-stacks obtained from confocal imaging were loaded into Fiji (ImageJ) software and split into single channels (i.e. TH-594 nm shown in magenta; CB1R-488 nm shown in green; GAD67-647 nm shown in red). All ten planes of each channel were then merged for a total of 5 µm depth to analyze. Individual channels were then converted to 8-bit and set to grayscale. Following, a threshold was set for the flattened image that captured the stain (shown in red), and stain mapping was reversed using the LUT invert function (shown in black). Regions of interest were traced, shown with red labels under the Trace ROI column and TH row. The GAD67 and CB1R row regions are identical and are thus not labelled. A mean gray value (arbitrary units) was measured and data was copied to Microsoft Excel (examples provided in the tables below). Values were between 0 and 255, where 0 indicated no stain present and 255 signified the region was fully stained. ROI, region of interest; MFI, mean fluorescent intensity; MGV, mean gray value. Scale bars = 100 µm.

Analysis of z-stacks was completed using Fiji (ImageJ) software (**Fig. 3**). Z-stacks were split into single channels and set to grayscale. Within each distinct channel, all slices were then merged using the z-project tool so that all ten planes obtained (5 µm total depth) could be analyzed. A threshold that captured the entirety of the stain was manually set for each channel. The display mapping was then reversed (LUT invert function) so that the mapped stain appeared black on a white background. Regions of interest where then traced referencing a brain atlas and the mean fluorescent intensity (i.e. mean gray value, MGV, arbitrary units) was measured. Values given were between 0 and 255, where 0 indicated complete white (i.e. no stain present) and a value of 255 indicated complete black (i.e. the region was entirely stained). **Tables 2-4** present data from the three slides analyzed for Mouse ID 3, provided here as a representative example.

Table 2. Mean Gray Values for TH, GAD67, and CB1R Staining in the SNc of Mouse ID 3

Slide	Z-stack	TH MGV	GAD67 MGV	CB1R MGV
1	2	61.316	27.5	49.233
1	4	59.045	42.19	89.139
1	6	14.452	58.86	63.017
2	1	36.003	21.268	33.229
2	4	48.219	50.239	23.228
2	5	13.898	46.554	139.838
2	6	42.446	50.561	34.578
3	1	33.966	39.382	9.823
3	2	58.489	35.092	10.29
3	3	33.392	25.401	14.263
3	4	12.904	29.695	2.007

Table 3. Mean Gray Values for TH, GAD67, and CB1R Staining in the SNr of Mouse ID 3

Slide	Z-stack	TH MGV	GAD67 MGV	CB1R MGV
1	1	69.48	50.606	177.663
1	2	29.921	40.578	230.262
1	3	8.11	76.825	225.258
1	4	19.992	63.043	240.361
1	5	3.647	42.122	220.586
1	6	4.95	72.909	195.213
2	1	6.808	34.029	145.017
2	2	5.717	64.881	144.151
2	3	3.637	119.927	202.257
2	4	11.033	74.255	146.141
2	5	5.206	69.291	201.541
2	6	26.068	57.584	133.885
3	1	3.225	42.16	8.514
3	2	6.994	39.414	29.195

3	3	10.625	23.986	12.498
3	4	7.188	50.438	54.227

Table 4. Mean Gray Values for TH, GAD67, and CB1R Staining in the VTA of Mouse ID 3

Slide	Z-stack	TH MGV	GAD67 MGV	CB1R MGV
3	5	26.358	15.84	1.075
4	1	48.921	15.534	1.425
4	2	40.824	11.679	0.382
5	1	28.185	13.724	2.391
5	2	29.669	17.021	2.224

2.1.3 Confocal statistical analysis

Statistical analysis was performed using Microsoft Excel, GraphPad Prism 10 and JASP software. For each mouse and region, the mean of all z-stacks per slide were found for each stain. As three slides per region were used from each mouse (n=3), this provided a total of nine data points (means) per stain per region for analysis. Normality was first confirmed for each stain, followed by a repeated measures one-way ANOVA with post-hoc t-tests to compare regions. Sphericity was not assumed and the Geisser-Greenhouse correction was applied when required.

2.2.1 Tissue processing and collection for immunoelectron microscopy

Immunoelectron microscopy methods were adapted from Puente and colleagues (2019). Three wildtype C57BL/6 male mice ages 3-5 months were deeply anesthetized and transcardially perfused using a gravity-fed perfusion device with heparinized TBS (~5 min) at RT. Following heparinized TBS, a fixative solution consisting of 0.3% glutaraldehyde (GA) and 4% PFA in TBS (~80 mL) was administered until the limbs and the liver were rigid (~10 min). The brains were then dissected and post-fixed overnight at 4˚C in labelled 20 mL glass vials filled with the same fixative solution.

The next day, brains were sectioned in the sagittal plane in chilled TBS with a Leica vibratome at 50 µm and collected into 24-well plates filled with TBS containing 0.025% sodium azide. Brains were covered with a 2% agarose solution prior to sectioning to provide extra support. For each brain, six serial sections containing the VTA, SNr and SNc were carefully selected under

a stereoscopic microscope and by referring to a brain atlas (Paxinos & Franklin, 2001), and transferred to another 24-well plate for experimentation. Sections were then treated with 0.1% sodium borohydride and 50 mM of glycine in TBS for 30 minutes at RT. Sodium borohydride is a reagent used to promote antigen retrieval by reducing the cross-linking of aldehydes that occurs with the introduction of GA and PFA. Glycine is used to quench free aldehydes that arise from GA and PFA that can continue reacting with proteins and antibodies and cause non-specific staining. After the 30 minutes, brain sections were rinsed in TBS once quickly and then 3 times for 10 minutes each. Sections were then quenched with 0.3% hydrogen peroxide in TBS for 5 minutes, and washed again in TBS quickly followed by 3 times for 10 minutes. Next, brain sections underwent blocking and permeabilization in 10% BSA, 0.02% saponin, and 0.1% sodium azide in TBS for 30 minutes on a 50-rpm shaker at RT. Immediately after, sections were transferred into a primary antibody solution of goat anti-CB1R antibody (1:100, Nittobo Medical Co. Ltd., cat#MSFR100610), 10% BSA, 0.004% saponin and 0.1% sodium azide in TBS and left on a 40-rpm shaker at 4˚C for 2 nights.

After incubation with the anti-CB1R antibody, sections were washed with 1% BSA in TBS twice for 2 minutes followed by 3 times for 10 minutes. A minimum of 4 hours of incubation in secondary antibody solution was then completed at RT on a 50-rpm shaker. The solution consisted of donkey anti-goat biotinylated secondary antibody (1:200, ThermoFisher Scientific Invitrogen, cat#A16003), 1% BSA, and 0.004% saponin in TBS. Brain sections were then rinsed again with 1% BSA in TBS 3 consecutive times of 10 minutes, and incubated in streptavidin 1.4 nm gold-conjugated secondary antibody (1:100, Nanoprobes, cat#2016-1ML) in the same secondary antibody solution for a minimum of 2 hours on a 50-rpm shaker at RT. Rinsing of sections was repeated with the same washing solution 3 times for 10 minutes each before being left in washing solution overnight on a 40-rpm shaker at 4˚C.

The next morning, 24-well plates were removed from the fridge and brain sections were submerged in 1% GA in TBS for 10 minutes to post-fix. Rinsing was then completed in 50 mM glycine in TBS 3 successive times of 10 minutes, and then in deionized water (dH_2O) for the same amount of time. Sections were then removed and placed in 4 mL glass vials with Nanoprobes HQ Silver Enhancement kit (cat#2012-45ML) solution and left for 10 minutes under the fume hood. As the silver enhancement is light sensitive, the vials were wrapped in tinfoil to ensure the stain developed in the dark. Sections were then placed back into the 24-well plates and washed

thoroughly with dH_2O prior to a 5-minute treatment of 2% sodium thiosulfate in dH_2O to cease the silver development reaction. Subsequently, washing twice for 5 minutes in dH_2O was completed before the sections were post-fixed in 2% GA in TBS for 1 hour at 4˚C. After post-fixing, all steps starting at treatment with sodium borohydride and glycine up to the completion of incubation in the secondary antibody solution, baring a few exceptions, were repeated to complete 3,3'-Diaminobenzidine (DAB) staining of TH proteins. The notable changes were as follows: 1) Quenching with hydrogen peroxide was not repeated, 2) The primary antibody solution contained rabbit anti-TH antibody (1:1000, Pel-Freeze Biologicals, cat#P40101-150) and was run for a single night only, 3) The secondary antibody solution contained donkey anti-rabbit horseradish peroxidase (HRP) secondary antibody (1:200, ThermoFisher Scientific Invitrogen, cat#A16029) and there was no second secondary antibody used. Notably, immunolabelling for CB1Rs and TH were done sequentially instead of concurrently to eliminate cross-staining that was observed during optimization experiments. Following the final antibody incubation, brain sections were rinsed with TBS 3 times for 10 minutes and then treated for 3-5 minutes with a DAB kit (Vector Labs, Burlingame, CA, USA) in the dark. Sections went through a final post-fixation of 2% GA in TBS for one hour and then left overnight in TBS at 4˚C. See **Appendix A** for details on antibodies used.

The next day, regions of interest were microdissected under a stereoscopic microscope into ~1 mm^2 sections and placed in labelled 4 mL glass vials filled with 0.15 M sodium cacodylate for electron microscopy processing. Sections were stained with 1% osmium and 1% potassium ferrocyanide for 45 minutes on a rotary mixer. Time was kept carefully as ferrocyanide decreases the silver enhancement signal, but the reagent was ultimately kept in the protocol as optimization tests showed a large decrease in contrast at the ultrastructural level without it. Once the 45 minutes elapsed, the sections were washed in dH_2O 5 times for 10 minutes to ensure all precipitate was adequately removed. They were then placed in 2% uranyl acetate (aq) for 1-1.5 hours. Timing was again carefully monitored since uranyl acetate can negatively affect silver staining (Tao-Cheng et al., 2021). Subsequently, dehydration was completed by treating tissue samples with graded ethanols of 50%, 70%, 85%, and 95% for 20 minutes each, and then rinsing twice quickly with 100% ethanol. Sections were then left to rotate overnight in 1:1 100% ethanol and Spurr resin (Spurr resin low viscosity embedding kit, Electron Microscopy Sciences, cat#14300 substituted with vinylcyclohexene dioxide, Sigma Aldrich, cat#94956-100ML). In the morning, vials were

switched to pure resin and rotated for >4 hours, and then switched with pure resin again to rotate overnight. The next day, the sections were embedded with resin in labelled BEEM size 3 embedding capsules (Electron Microscopy Sciences, cat#69910-10) placed in a 100-well plate and left to polymerize for a minimum of 1 night in a >60ºC oven. A minimum of 4 resin blocks per region per mouse were made.

Once fully polymerized, samples underwent semithin (0.5-1 μm) sectioning with an ultramicrotome (UltraCut E, Reichert-Jung) and a glass knife and were collected on glass slides and visualized under a light microscope to ensure silver enhancement and DAB staining were adequate for electron microscopy imaging. Slides were stained with 2% toluidine blue aqueous solution and visualized under the light microscope again to ensure quality of the tissue section. Only the first 1-3 semithin sections were used for quality check to ensure consistency in staining patterns once collecting TEM images. Sections were also cut at an oblique to obtain grazing sections so a gradient of stain was visible across the section. If the section was both sufficiently stained and intact with adequate surface area for imaging, ultrathin (50-70 nm) sections were then cut and collected on 200 hexagonal copper grids (Electron Microscopy Sciences, cat#H200-Cu). Grids were then visualized by transmission electron microscopy (TEM). See **Appendix B** for a detailed graphical protocol.

2.2.2 Transmission electron micrograph acquisition and analysis

Sections were visualized using a JEM-1400 transmission electron microscope (JEOL) and images captured with an Orius SC1000 digital camera (Gatan, USA). One block from each region per mouse for a total of 9 blocks were imaged for data analysis. Images were acquired at 20,000x magnification and 32-54 images with a 25% overlap between each image were captured. Image sets were then loaded into Adobe Photoshop and stitched to make a montage of the region. Images were acquired where both the DAB and silver enhancement stains were evident.

Once images were stitched together and a scale bar was added in Adobe Photoshop, montages were loaded into Fiji (ImageJ) software. The scale bar was set accordingly for each montage and gridlines added to ensure each montage was fully examined. Moving systematically through the grid, all pre-synaptic terminals synapsing onto DAB (TH) positive compartments were traced. The perimeter (μm) and area (μm^2) of each terminal was then measured and if CB1Rs were present they were counted and their density per terminal noted as CB1R count/perimeter of plasma membrane. Silver enhanced gold particles were included if they were between 10-90 nm in size to

reduce the chance of counting artifact. Positive CB1R-gold labelling was considered when at least one immunogold particle was within 30 nm of the specified membrane. To be included in quantification, terminals were required to have intact plasma membranes for tracing and a visible synaptic cleft. The tracing of terminals was saved to ensure terminals were not counted more than once. If silver particles were present on mitochondria within pre-synaptic terminals this was noted, but otherwise analysis of mitochondria was excluded from this study. Synapses were also determined as either excitatory or inhibitory based on their ultrastructural features (**Fig. 4**). A synapse was considered excitatory if it appeared asymmetrical with a strong post synaptic density (PSD) and abundant small spherical pre-synaptic vesicles, and inhibitory if it presented with a symmetric membrane density with an absence of a strong PSD signal and pleomorphic pre-synaptic vesicles. Finally, all silver-enhanced gold particles present in each montage between 10-90 nm were counted and total area of the montage was calculated to determine the density of CB1Rs per region. This was completed with the crosshair tool where counted particles were labelled to ensure particles were not counted more than once. **Table 5** displays data from the SNr of Mouse ID 2 (corresponding to **Fig. 4**), included as a representative example of montage-level data collection.

2.2.3 Transmission electron micrograph statistical analysis

Similar to analysis of confocal data, statistical analysis for TEM data was performed using Microsoft Excel, GraphPad Prism 10 and JASP software. Regional CB1R immunoparticle density (counts/μm^2) was quantified from one montage image per region per mouse, resulting in a total of nine measurements (n = 9; three regions across three mice). Due to the small sample size, normality could not be reliably assessed; therefore, a non-parametric approach was used by default. A Friedman test was conducted to evaluate differences in CB1R density across the SNc, SNr, and VTA, as the data represented repeated measures within subjects. Post hoc comparisons were performed using Bonferroni-corrected Dunn's tests.

To assess differences in CB1R terminal positivity, the percentage of CB1R-positive synapses was first calculated per mouse and brain region, separately for all synapses, excitatory synapses, and inhibitory synapses (n = 9 per condition). Given the small sample size and limited power to assess normality, non-parametric Friedman tests were initially used to evaluate regional differences. However, these tests did not yield statistically significant results in any condition. To improve sensitivity and account for repeated measures, generalized linear mixed models

(GLMMs) were subsequently employed. CB1R positivity (binary: positive or negative) was entered as the dependent variable, and models were run separately with either brain region or synapse type as the fixed effect. Mouse ID was included as a random effect. This approach allowed inclusion of all raw synapse-level data. GLMMs were conducted using JASP, and post hoc pairwise comparisons were Holm-adjusted for multiple comparisons.

CB1R density was calculated for each CB1R-positive pre-synaptic terminal as the number of immunoparticles per μm^2 of membrane. To determine the appropriate statistical approach, Shapiro–Wilk tests were used to assess normality for each brain region and mouse, separately for inhibitory and excitatory synapses. While some inhibitory data met normality assumptions, others did not, and excitatory synapse data could not be reliably tested due to small sample size. As a result, non-parametric methods were used for all analyses. To assess inter-mouse variability, Kruskal–Wallis tests were conducted within each brain region, separately for inhibitory and excitatory terminals. As no significant differences were found between mice, data were pooled across animals. Two additional Kruskal–Wallis tests were then conducted to assess regional differences in CB1R density, one for inhibitory and one for excitatory terminals, followed by Bonferroni-corrected Dunn's post hoc tests where applicable. Finally, to evaluate within-region differences between synapse types, three Mann–Whitney U tests were conducted—one per region—to compare CB1R density between excitatory and inhibitory terminals in the SNc, SNr, and VTA. False discovery rate correction was applied to control for multiple comparisons.

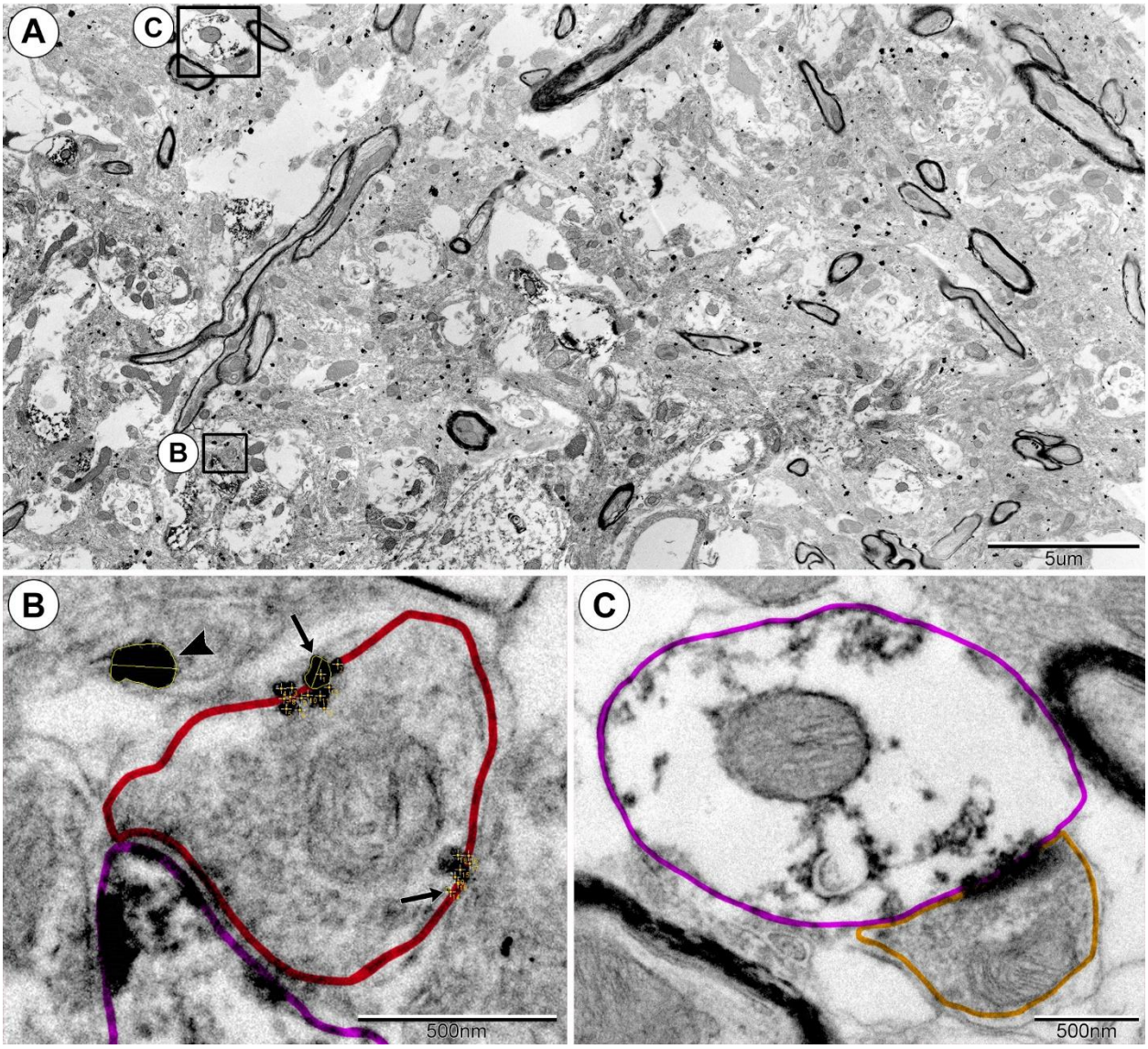

Figure 4. Immunoelectron Micrograph Tracing Methods. Montages of stitched images were loaded into Fiji software, scale bars set and gridlines added (not shown). Each montage was then systematically surveyed following gridlines and all synaptic terminals synapsing onto DAB (TH) positive compartments were traced. The top image is a low magnification example of the SNr from Mouse ID 2 (A). Panels B and C are high magnification images of the regions boxed in A. B shows an inhibitory synapse with symmetrical synaptic density. The pre-synaptic terminal is traced in red and CB1Rs counted with the Fiji crosshair tool. The large arrowhead points to an example of a silver particle (traced and diameter found in Fiji) that would not be counted if it were on the pre-synaptic membrane as it does not lie within the 10-90 nm diameter requirement for inclusion (diameter = 162 nm). Arrows point to a larger (diameter = 76 nm) and smaller (diameter = 11 nm) silver particle that represent the edge of the 10-90 nm limit of what particles would be included. Panel C shows an example of an excitatory synapse with a strong PSD signal and no CB1Rs. The pre-synaptic terminal is traced in orange. TH terminals are traced in magenta. Table 5 below represents the data collected for the montage (Gigapan): Total area, total CB1Rs for all silver particles between 10-90 nm, and for all traced synapses their type, area, perimeter, CB1R count and CB1R density calculated as CB1R count/perimeter.

Table 5. SNr Mouse ID 2 Immunoelectron Microscopy Data (Corresponding to Fig. 4)

Synapse Type (excitatory = 1, inhibitory = 0)	Terminal Membrane Perimeter (nm)	Terminal area (nm^2)	CB1R Present (1 = yes, 0 = no)	CB1R on Membrane	CB1R on Mitochondria	CB1R Density
0	1.858	0.186	0	0	0	0
0	2.997	0.107	1	5	0	1.668335002
0	2.238	0.337	1	3	0	1.340482574
0	1.537	0.157	1	5	0	3.253090436
1	2.689	0.253	0	0	0	0
0	1.842	0.188	0	0	0	0
0	4.311	0.153	1	8	0	1.855717931
0	1.932	0.137	0	0	0	0
0	2.161	0.158	1	1	0	0.462748727
0	2.643	0.307	1	12	0	0
1	3.354	0.345	1	1	1	0.298151461
0	2.247	0.148	1	2	0	0.890075656
0	2.659	0.369	0	0	0	0
0	1.623	0.148	1	2	0	1.23228589
0	2.555	0.288	0	0	0	0
0	2.561	0.373	1	17	0	6.638032019
0	3.961	0.525	1	5	0	1.262307498
0	2.593	0.11	1	28	0	10.79830312
0	4.835	1.193	0	0	0	0
1	2.485	0.154	0	0	0	0
Total Area: 1220.12 μm^2 **Total CB1R Count:** 11,348						

Chapter 3: Results

3.1 Confocal microscopy

Immunofluorescent staining for TH revealed intense staining of neurons and neurites in the SNc and VTA, and little staining in the SNr (**Fig. 5-10**). To determine fluorescent staining intensity differences across the three regions, mean fluorescent intensity (MFI) values for TH were statistically analyzed. Shapiro-Wilk tests indicated normality for SNr and VTA ($p > 0.05$), while SNc showed a significant deviation ($p = 0.017$). However, visual inspection of Q-Q plots suggested the data was approximately normally distributed overall, and Mauchly's test showed that sphericity had not been violated for TH MFI ($\chi^2(2) = 2.951$, $p = 0.229$), so parametric testing was completed. The one-way repeated measures ANOVA for TH MFI showed an effect of brain area, $F(2, 16) = 26.58$, $p < 0.001$, $\eta^2 = 0.769$. In other words, there was a highly significant effect of brain region on TH MFI with an effect size indicating that nearly 77% of the variability in MFI was due to differences between brain regions. Decomposing this effect with post-hoc t-tests showed a larger TH MFI in the SNc compared to the SNr, $M_d = 36.194$ [22.751, 49.637], $p < 0.001$, $t(16) = 7.197$, $d = 3.411$, similar MFI in SNc and VTA, $M_d = 13.017$ [-0.427, 26.460], $p < 0.05$, $t(16) = 2.588$, $d = 1.227$, but smaller intensities in SNR compared to VTA $M_d = -23.177$ [-36.621, -9.734], $p < 0.001$, $t(16) = -4.609$, $d = -2.184$ (**Figs. 10, 11**). All reported p values are Bonferroni (*bonf*) corrected.

Immunofluorescent markers for GABAergic compartments (i.e. GAD67 and VGAT) showed intense punctate staining of neurites, synaptic terminals and cell bodies in the SNr, with somewhat lesser intensity observed in the SNc and VTA (**Figs. 5, 7-10**). For GAD67 MFI analysis, Shapiro-Wilk tests indicated normality for all three regions examined ($p > 0.05$) and visual inspection of Q-Q plots suggested the data was normally distributed overall as well. Mauchly's test indicated that the assumption of sphericity had been violated for GAD67 MFI ($\chi^2(2) = 6.391$, $p < 0.05$), therefore Greenhouse-Geisser corrected tests are reported ($\varepsilon = 0.626$). The one-way repeated measures ANOVA for GAD67 MFI showed an effect of brain region, $F(2, 16) = 23.770$, $p < 0.001$, $\eta^2 = 0.748$. Post-hoc tests showed smaller GAD67 MFI in the SNc compared to the SNr, $M_d = -9.926$ [-19.812, -0.040], $p_{bonf} < 0.05$, $t(16) = -2.684$, $d = -0.824$, larger GAD67 MFI in the SNc compared to the VTA, $M_d = 15.379$ [5.493, 25.264], $p_{bonf} < 0.05$, $t(16) = 4.158$, $d = 1.276$, and larger intensities of GAD67 in the SNr compared to the VTA, $M_d = 25.305$ [15.419, 35.191], $p_{bonf} < 0.001$, $t(16) = 6.842$, $d = 2.099$ (**Figs. 10, 11**).

Immunofluorescent labeled sagittal brain sections revealed four distinct intensely CB1R-labelled areas: the hippocampus, the globus pallidus, the cerebellum and midbrain. A closer examination of CB1R staining in the midbrain revealed its predominant localization in the SNr, with staining gradually diminishing towards the SNc, and sparse labeling observed in the VTA (**Figs, 5-10**). CB1R MFI data underwent similar tests as GAD67 and TH labelling. Shapiro-Wilk tests indicated normality for all three regions ($p > 0.05$), and visual inspection of Q-Q plots supported these results. Further, Mauchly's test indicated that the assumption of sphericity had been violated for CB1R MFI ($\chi^2(2) = 19.279$, $p < 0.001$), therefore the Greenhouse-Geisser corrected tests are reported ($\varepsilon = 0.516$). The one-way repeated measures ANOVA for CB1R MFI showed an effect of brain area, $F(2, 16) = 27.017$ $p < 0.001$, $\eta^2 = 0.772$. Following post-hoc t-tests showed a significantly smaller CB1R MFI in the SNc compared to the SNr, M_d = -76.433 [-116.712, -36.154], $p_{bonf} < 0.001$, $t(16) = -5.072$, $d = -2.009$, similar intensities in SNc and VTA, $M_d = 31.212$ [-9.067, 71.492], $p_{bonf} < 0.165$, $t(16) = 2.071$, $d = 0.820$, and larger CB1R MFI in the SNr compared to VTA, $M_d = 107.645$ [67.366, 147.925], $p_{bonf} < 0.001$, $t(16) = 7.144$, $d = 2.830$ (**Figs. 10, 11**).

To further examine the subcellular localization of CB1Rs within the midbrain and assess potential colocalization with major neurotransmitter systems, additional immunolabeling was conducted using the previously mentioned antibodies along with glutamatergic markers VGlut1 and VGlut2. CB1R colocalization with VGlut1 and VGlut2 was sparse, predominantly localized to the SNr and the SNr-SNc transition zone (**Figs. 5, 6**), with minimal colocalization observed in the VTA (**Fig. 9**). In contrast, CB1R colocalized more extensively with VGAT in the SNr and SNr-SNc boundary (**Figs. 7, 8**), while no meaningful colocalization was detected in the VTA (**Fig 9**). These findings suggest that CB1Rs are present at both excitatory and inhibitory terminals in the midbrain, with a preference for inhibitory terminals.

For further insights, analysis of confocal images in the hippocampus and cerebellum (positive controls) were examined. In the CA1 of the hippocampus, intense punctate CB1R labeling was observed in stratum pyramidale, where it predominantly colocalized with VGAT-positive neurites surrounding pyramidal cells and to a lesser extent with VGlut1, which is abundant in stratum oriens and radiatum (**Fig. 12**). In the cerebellum, CB1R was primarily localized in the molecular layer and surrounding Purkinje cell bodies. CB1R labelling preferentially colocalized with VGAT-positive compartments, especially basket cell pinceau terminals (**Figs. 13, 14**).

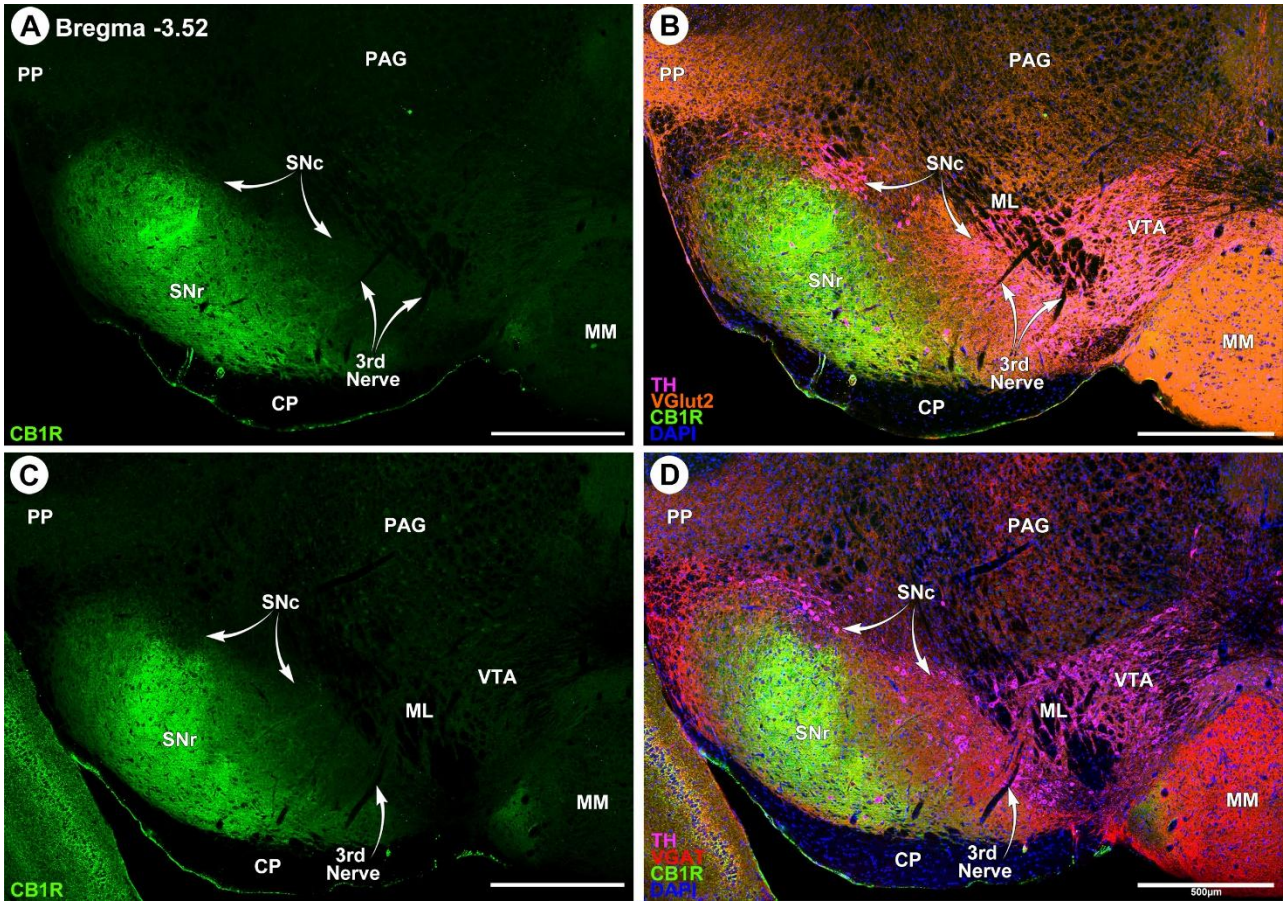

Figure 5. Coronal serial sections of the midbrain showing SNc, SNr and VTA. Panels A and C show single-labeling for CB1R corresponding to the same sections shown in Panels B and D, respectively. Panel B is triple immunolabelled with TH (magenta), CB1R (green) and VGlut2 (orange). Panel D is labelled similarly but with VGAT (red) instead of VGlut2. Nuclei are stained with DAPI (blue). Intense CB1R staining is present in the SNr and colocalization of CB1R with either VGlut2 or VGAT (yellow) is noticeable in the SNr and SNr-SNc transition zone. In both images, the third nerve and medial lemniscus (ML) are visible as a dark, unstained regions between the VTA and SNc. CP, cerebral peduncle; MM, medial mammillary nucleus; PAG, periaqueductal gray; PP, peripeduncular nucleus.

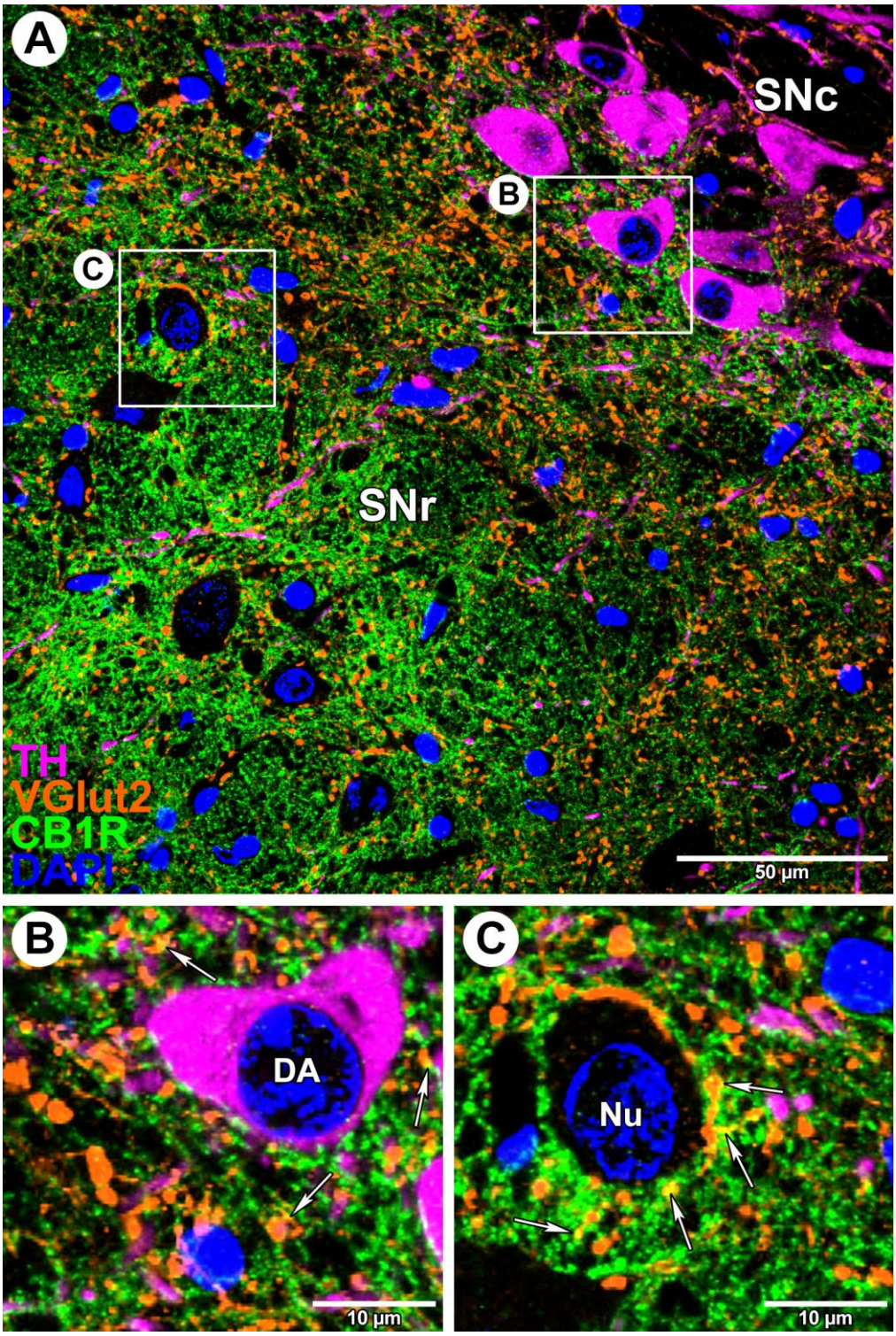

Figure 6. High magnification confocal image of the SNc and SNr with CB1R (green), TH (magenta) and VGlut2 (orange) showing little CB1R-VGlut2 colocalization. Intense CB1R labelling is seen in the SNr and gradually diminishes towards the SNc. Weak staining is found in the SNc. At the SNr-SNc transition zone, CB1R staining surrounds some TH-positive dopamine (DA) neurons. VGlut2 presents as punctate labeling consistent with presynaptic terminals, and DAPI (blue) highlights regional cell nuclei (Nu). B-C are enlarged images of the boxed regions in A. White arrows point to the sparse colocalization of CB1R and VGlut2 staining (yellow). Colocalization appears more prominent in the SNr near non-TH-positive cell bodies compared to co-staining adjacent to DA neurons.

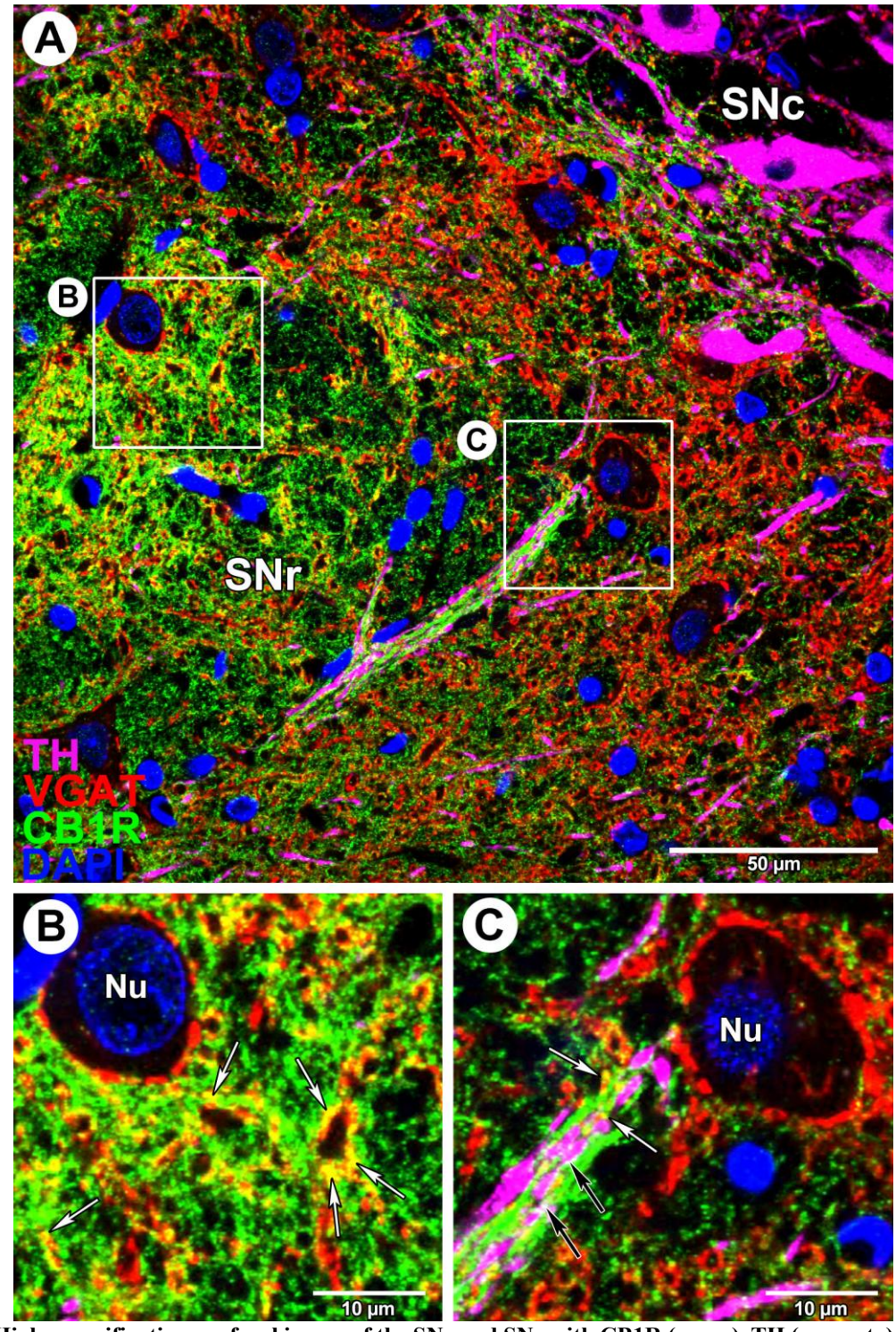

Figure 7. High magnification confocal image of the SNc and SNr with CB1R (green), TH (magenta) and VGAT (red) showing prominent CB1R-VGAT colocalization. Similar to Figure 6, Panel A shows intense CB1R labelling in the SNr that gradually decreases towards the SNc, where only weak signal remains. At the SNr-SNc transition zone CB1R labeling surrounds some DA neurons. VGAT staining reveals dense puncta and occasional neurite labelling throughout the region. DAPI (blue) stains regional nuclei (Nu). B-C are enlarged views of the boxed regions in A. White arrows point to the extensive colocalization of CB1R and VGAT staining (yellow), while black arrows point to faint overlap of TH and CB1R staining (white). Colocalization of CB1R and VGAT (yellow) is evident throughout the SNr (B). TH-positive and CB1R-positive processes appear to run parallel to one another with little overlap (C).

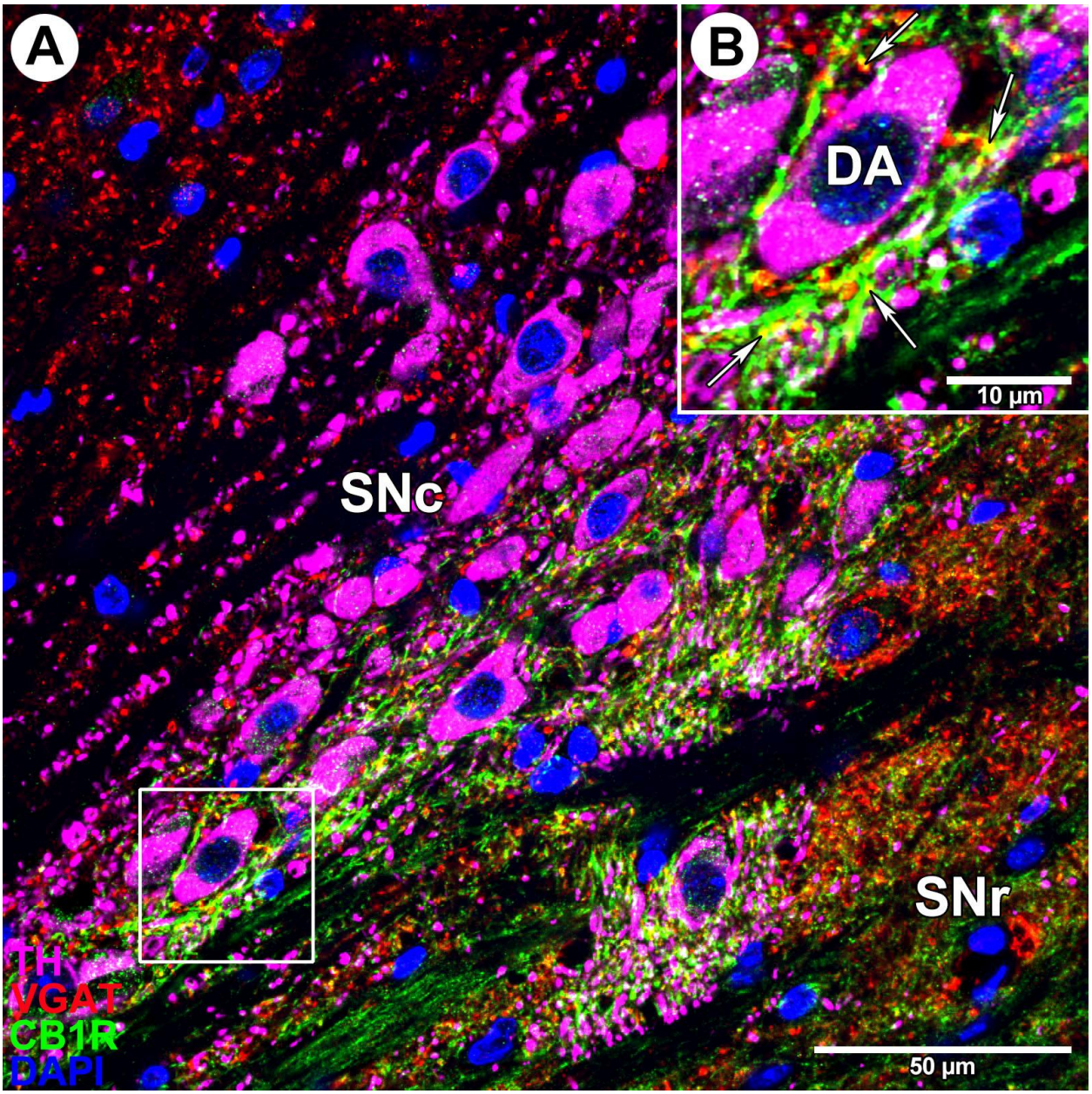

Figure 8. High magnification confocal image of the SNc-SNr transition zone triple immunolabelled with CB1R (green), TH (magenta) and VGAT (red) showing SNc CB1R presence. Intense CB1R signal is observed surrounding TH-positive DA neurons at the boundary between the SNc (top left, stained prominently with TH-positive cell bodies) and SNr (bottom right). CB1R and VGAT staining colocalization (yellow) is evident at this border. Inset shows an enlarged view of boxed region in A. CB1R-positive processes appear to envelop the dopamine (DA) neuron somata. White arrows denote CB1R-VGAT colocalization. DAPI (blue) stains regional nuclei.

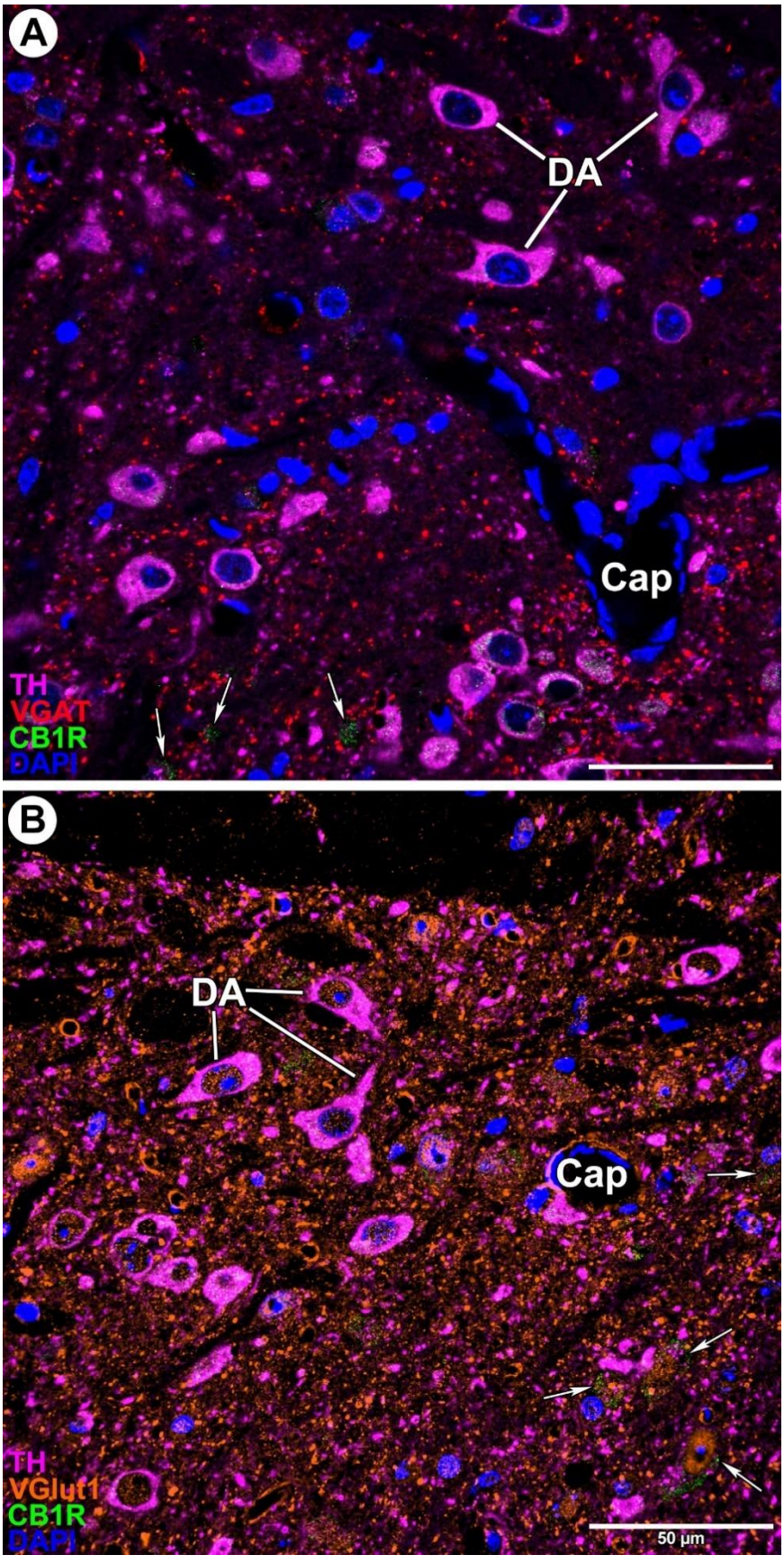

Figure 9. Confocal image of the VTA highlighting minimal CB1R expression. Both panel A and B show fluorescent labeling for CB1R (green), TH (magenta), and DAPI (blue). Panel A also shows staining for VGAT (red), while panel B includes VGlut1 (orange). Compared to the SN, the VTA exhibits sparse CB1R immuno-reactivity, indicated by white arrows. Minimal, if any, co-localization of CB1R with VGAT or VGlut1 is observed. Capillaries (Cap) are identified as unlabeled circular or tubular regions surrounded by flattened DAPI-stained nuclei of vascular cells. Representative TH-positive dopamine (DA) neuron somata are labeled, characterized by strong cytoplasmic TH signal.

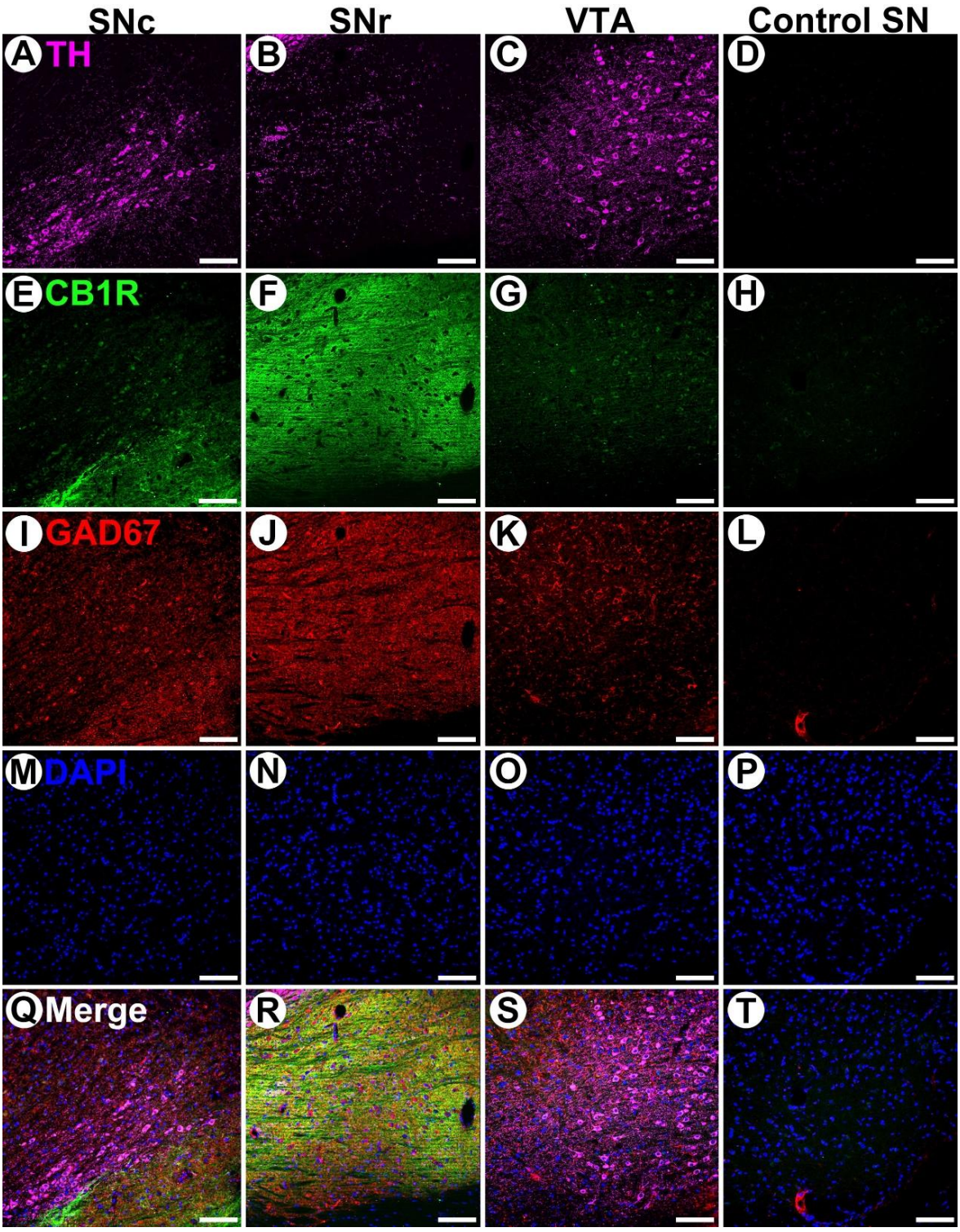

Figure 10. Triple immunolabelled sagittal sections of the SNc, SNr and VTA representative of images used in mean fluorescent intensity analysis. Across rows, images are grouped by fluorescent stain: TH (A-D, magenta), CB1R (E-H, green), GAD67 (I-L, red), and DAPI (M-P, blue). The bottom row shows all four channels merged (Q-T). A-P show fluorescent channels independently for SNc, SNr, VTA and control SN. Large TH-positive DA neurons are seen in the SNc and VTA and punctate staining in the SNr. CB1R and GAD67 showed intense staining in the SNr and less in the SNc and VTA. Secondary controls are shown in the right column. IgG reactivity was noted with the secondary antibody of GAD67 (L) and faint background staining in the CB1R channel (H). Scale bars = 100 μm.

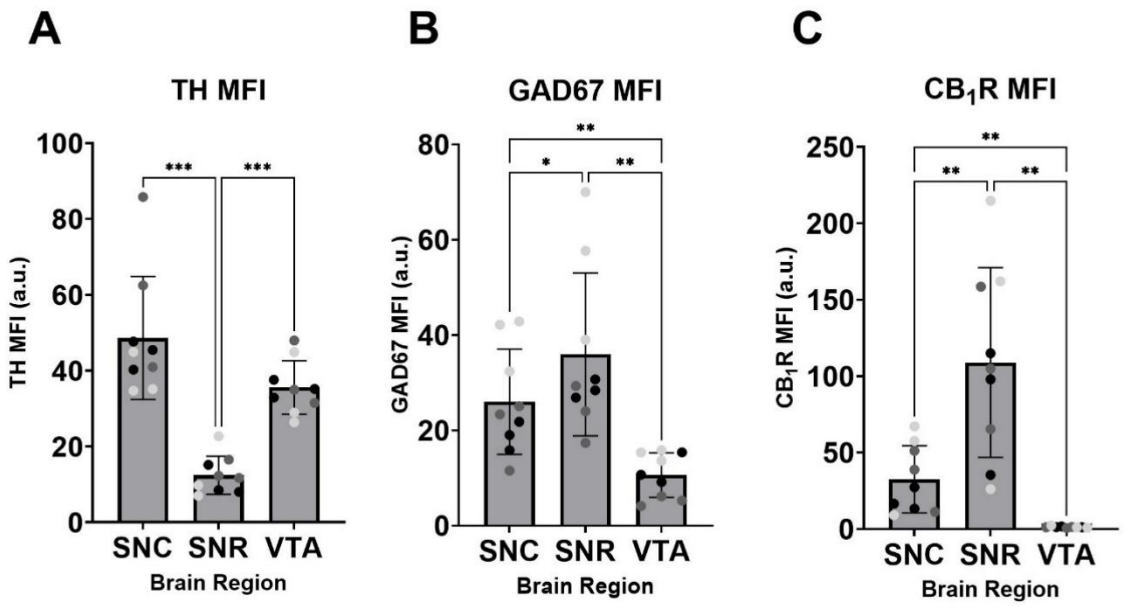

Figure 11. Graphical representation of mean fluorescent intensity (MFI) of TH, GAD67 and CB1R immunolabelling across the SNc, SNr and VTA. One-way ANOVA results indicated statistically significant differences in TH MFI between SNr and VTA, and SNr and SNc, with the SNc and VTA showing greater staining for TH than the SNr. There was no notable TH MFI difference between the SNc and VTA. GAD67 MFI statistically differed between all regions, with SNr presenting with the highest intensity of GAD67 immunolabelling and VTA with the least. CB1R MFI also statistically differed between all regions. The SNr had the most CB1R staining, followed by the SNc, and the VTA presented with the least. *, $p < 0.05$; **, $p < 0.01$; *** $p < 0.001$; a.u., arbitrary units. Data points are colour coated by animal: black = mouse 1, dark gray = mouse 2, light gray = mouse 3.

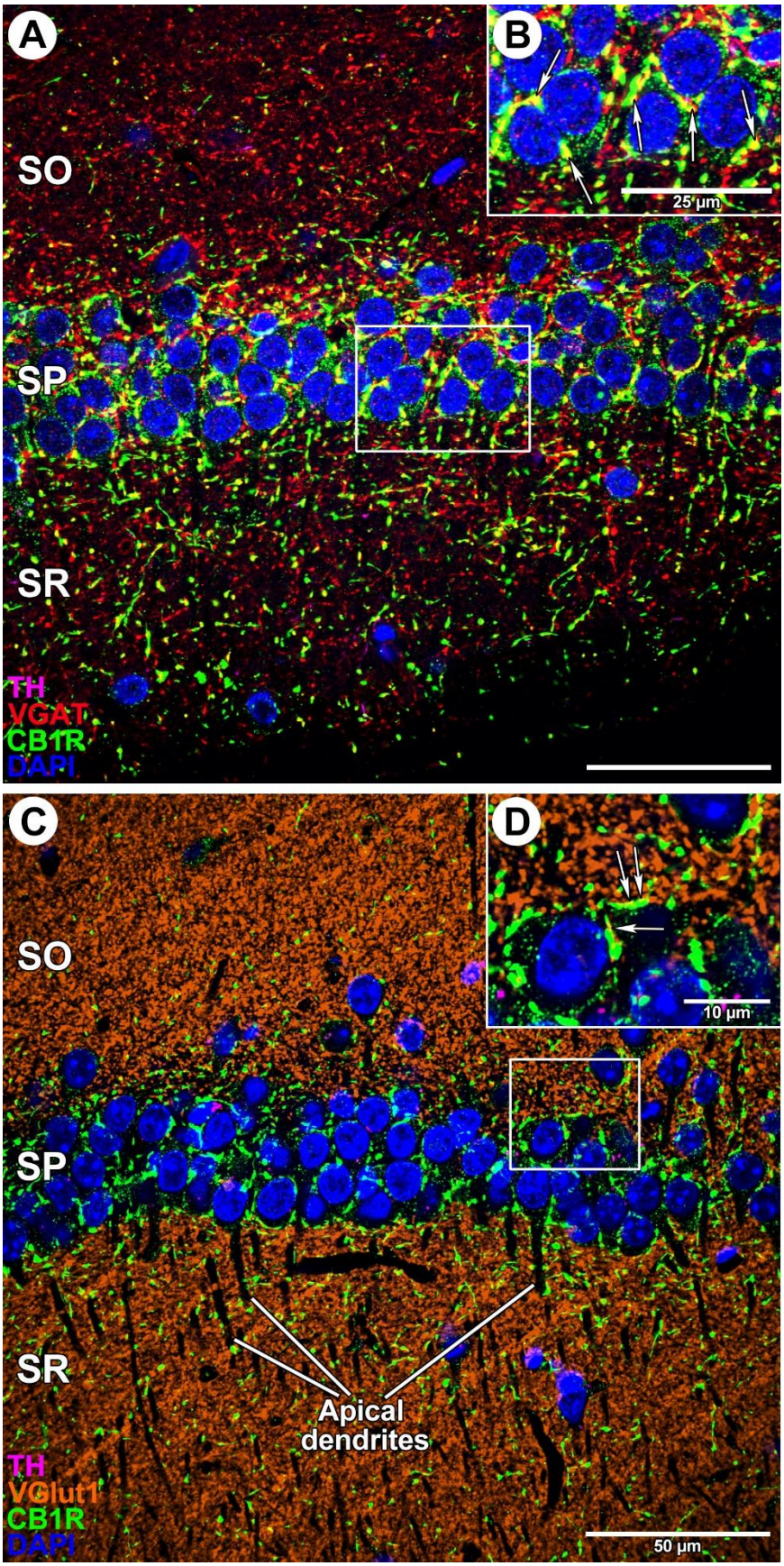

Figure 12. High magnification confocal images of the stratum pyramidale (SP) layer of the CA1 in the hippocampus highlighting predominant CB1R–VGAT over CB1R–VGlut2 colocalization. The SP contains densely packed pyramidal neurons, visible by DAPI (blue) nuclear staining. Intense CB1R (green) punctate staining is seen around the SP nuclei, and sparse staining in the stratum oriens (SO) and stratum radiatum (SR). Minor TH (magenta) staining is apparent in all panels. Panel A shows VGAT (red) immunolabelling. Inset (B) is an enlarged view of the boxed region in A. CB1R puncta exhibit substantial colocalization with VGAT-positive processes (yellow), indicated by white arrows. Panel C shows VGlut1 (orange) immunolabelling. Similarly, the inset (D) is an enlarged view of the boxed region in C. CB1R colocalization with VGlut1 is observed (yellow, indicated by white arrows), though to a lesser extent than with VGAT. SR unstained regions lined by CB1R-positive puncta are indicative of apical dendrites. VGlut1 labelling is noticeably more intense in the SO and SR with sparse staining in the SP, whereas VGAT labelling is more apparent in the SP compared to the SO and SR.

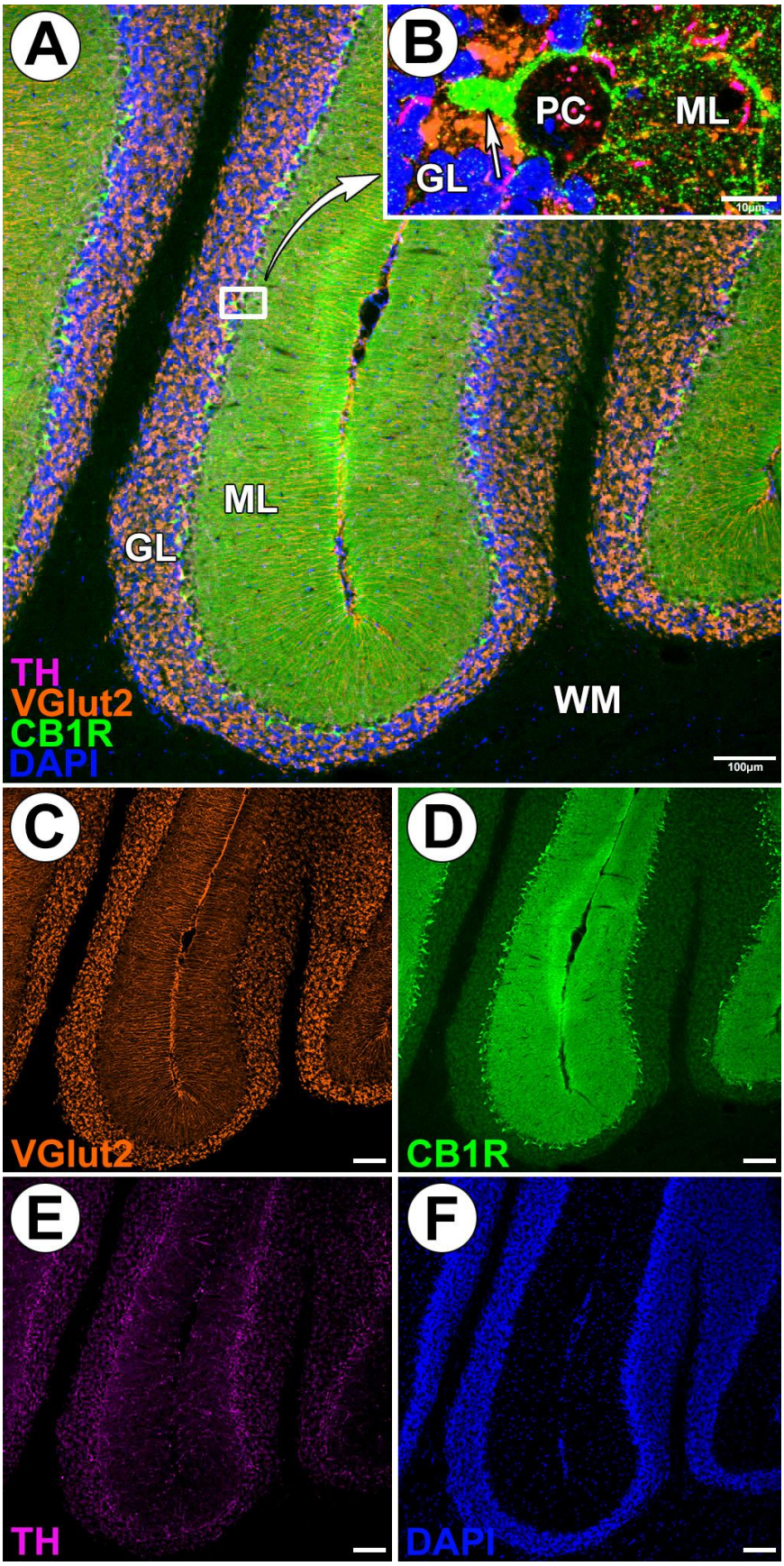

Figure 13. Confocal images of the cerebellum stained with CB1R (green), TH (magenta), VGlut2 (orange) and DAPI (blue) revealing minimal CB1R-VGlut2 colocalization. Panel A and B show low and high magnification images, respectively, with B representing the boxed region in A. Panels C–F display the individual fluorescence channels to clearly illustrate staining differences across cerebellar layers. CB1R signal is prominent at low magnification in the molecular (ML) and Purkinje cell layers. At high magnification (B), a white arrow points to a densely CB1R-labeled basket cell pinceau surrounding a Purkinje cell (PC), several of which are visible as characteristic "paintbrush-like" structures in D. Subtle co-localization between CB1R and VGlut2 (yellow) is observed in the ML. VGlut2 immuno-reactivity is most intense in the granule cell layer (GL), though VGlut2-positive processes extending into the ML are also visible, especially in C. TH labeling is present around and on PC somata. Scale bars = 100 µm unless otherwise indicated. WM, white matter.

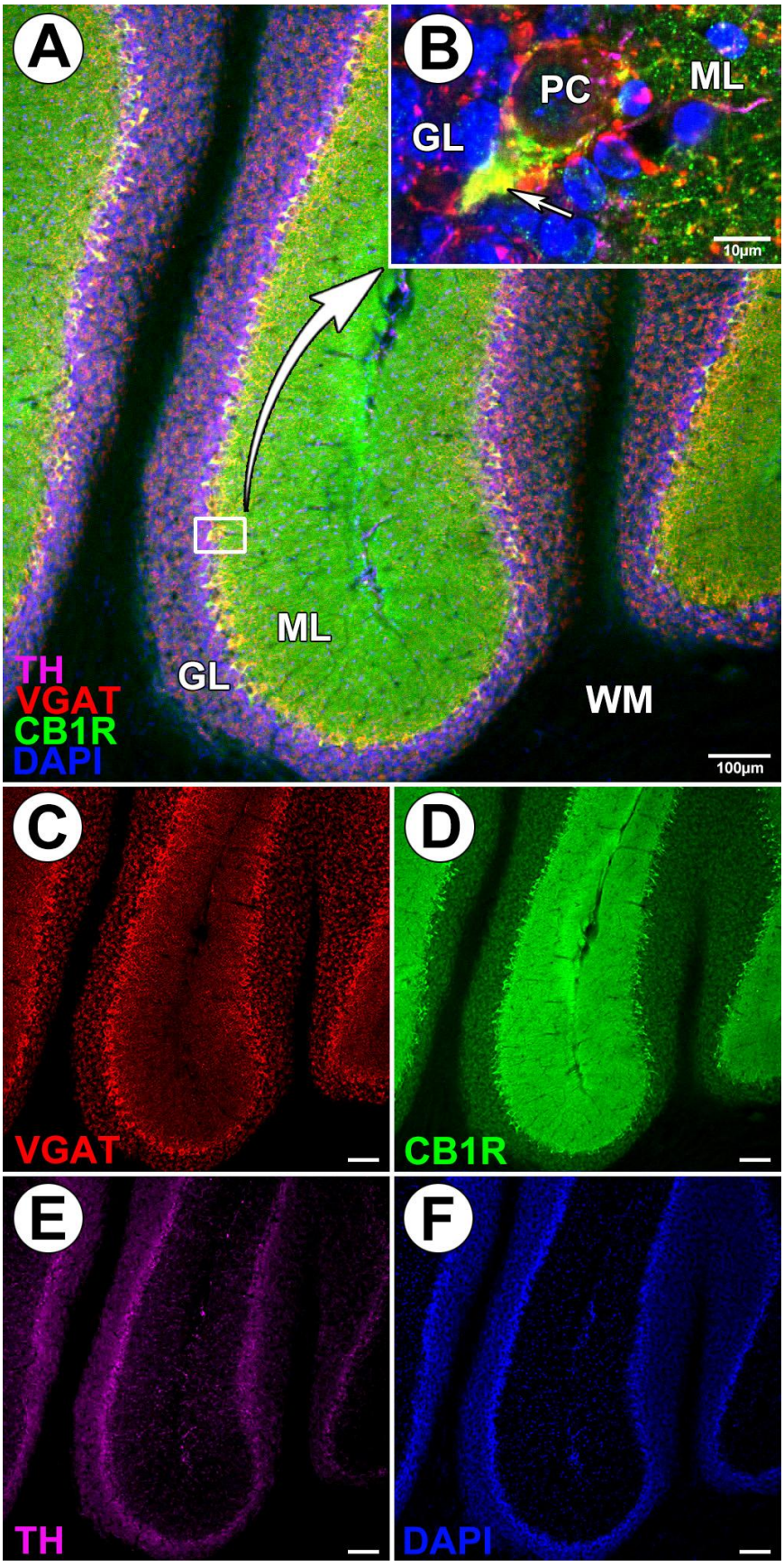

Figure 14. Confocal images of the cerebellum stained with CB1R (green), TH (magenta), VGAT (red) and DAPI (blue) demonstrating extensive CB1R-VGAT colocalization. Panels A and B show low and high magnification images, respectively, with B corresponding to the boxed region in A. Images C–F display each fluorescence channel individually to highlight differential staining across cerebellar layers. CB1R-positive labelling is observed intensely in the molecular layer (ML) and around Purkinje cells (PC) at low magnification. In B, a small white arrow indicates a basket cell pinceau exhibiting strong co-localization of CB1R and VGAT (yellow) around a PC. VGAT labeling is prominent on and surrounding PCs, as shown in C, and appears less intense in the ML and granule cell layer (GL). TH immunoreactivity is also evident on and around PC somata. Scale bars = 100 μm unless otherwise indicated. WM, white matter.

3.2 Immunoelectron microscopy

TEM results (raw data) from double immunolabeling for CB1R (gold) and TH (DAB) are summarized in **Table 6**. The total area analyzed was approximately 4,450 μm² for the SNc, 4,345 μm² for the SNr, and 5,735 μm² for the VTA. Variability in total area was due to differences in the number of images acquired for montage reconstruction (Gigapan) per block examined, which was influenced by tissue quality and staining consistency. In total, 272 presynaptic terminals forming synapses onto TH-positive DA compartments were analyzed, with 92, 67, and 113 terminals evaluated from the SNc, SNr, and VTA, respectively. Among the three regions, the highest number of CB1R-positive synapses were observed in the SNc, followed closely by the SNr. When classified by synapse type, the majority of CB1R-positive terminals were identified as inhibitory. All analyzed TEM montages from this study are available in high-resolution here:

1. SNr Mouse 1: https://www.gigapan.com/gigapans/9f4473738962fcba308a2d40542450d1
2. SNr Mouse 2: https://www.gigapan.com/gigapans/95815aec5a180e8cd5b38d7fedee0f9c
3. SNr Mouse 3: https://www.gigapan.com/gigapans/fecf851e4cf5f7a1a308c6b993412347
4. SNc Mouse 1: https://www.gigapan.com/gigapans/237235
5. SNc Mouse 2: https://www.gigapan.com/gigapans/c8bb2505edfecf30601fd89cd3b8980f
6. SNc Mouse 3: https://www.gigapan.com/gigapans/8630693670c25eba3df2492a4e2a6874
7. VTA Mouse 1: https://www.gigapan.com/gigapans/4f20752d61709e867813e8174db4a3fe
8. VTA Mouse 2: https://www.gigapan.com/gigapans/66322165060c84e9af4bed36aa589d9f
9. VTA Mouse 3: https://www.gigapan.com/gigapans/7af894ecc55639e4df0427d9b23d674d

The following results describe regional differences in CB1R density, variations in CB1R terminal positivity across brain regions and synapse types, and immunogold particle density within CB1R-positive presynaptic terminals.

Table 6. Summary of TEM Double CB1R-TH Immunolabelling Results

Measure	SNc	SNr	VTA
Total area analyzed (μm^2)	4450.043	4344.869	5734.318
Total synapses	92	67	113
Excitatory synapses	27	13	55
CB1R-positive	8	3	6
Inhibitory synapses	65	54	58
CB1R-positive	41	40	25

3.2.1 CB1R regional density

Double immunolabeling with CB1R-gold (silver-enhanced) and TH-DAB produced results consistent with confocal findings (**Figs. 15, 16, 19**). CB1R-gold labeling was densely localized to the SN, globus pallidus, and—as expected—within the positive control regions, the cerebellum and hippocampus. TH-DAB immunoreactivity was observed in the SNc, VTA, caudate-putamen, and locus coeruleus. At higher magnification, CB1R-gold labeling was predominantly localized to the SNr within the SN, the molecular and Purkinje cell layers of the cerebellum, and the pyramidal cell layer of CA1–CA3 as well as the granule cell layer of the dentate gyrus (DG) in the hippocampus (**Fig. 16**). Negative control conditions confirmed the specificity of the immunolabeling (**Figs. 15C, 16C, F, J**).

Serial semithin sections obtained from ultramicrotome slicing following TEM processing of double-labeled midbrain regions revealed high-magnification TH-DAB staining of DA neuron somata and processes within the SN and VTA (**Figs. 18, 19**). At this magnification, CB1R-gold labeling is difficult to discern without comparison to unstained regions. Parallel serial sections were stained with toluidine blue (aq), a basic dye that binds acidic tissue components, to assess tissue integrity prior to TEM imaging. This staining highlights nuclei, cell membranes, and overall cellular architecture. In contrast to the unstained sections, the toluidine blue-stained sections allowed for clearer visualization of non-DA cell populations, additional axons, and well-defined capillary boundaries. Notably, tissue blocks were cut at an oblique angle so grazing-plane sections

could be obtained (**Fig. 18**) to ensure double immunolabeling was sufficiently captured to acquire quality TEM micrographs for analysis.

Due to the small sample size (n = 9; one Gigapan image per region per mouse across three mice), the statistical power was insufficient to reliably assess normality in CB1R density measurements (counts/μm²). Therefore, a non-parametric approach was used by default. A Friedman test was conducted to compare CB1R density across the three brain regions, as the data consisted of repeated measures from three mice (i.e. related samples). The Friedman test revealed a significant difference in CB1R density across brain regions $\chi^2(2) = 6.00$, $p = 0.0278$. Post hoc Dunn's tests (Bonferroni-corrected) showed that CB1R density was significantly higher in the SNr compared to the VTA (p = 0.043), but no significant differences were found between the SNc and VTA (p = 0.662), or SNr and SNc (p = 0.662). The mean CB1R density was highest in SNr (M = 6.838), followed by SNc (M = 1.304) and lowest in VTA (M = 0.450) (**Fig. 19**).

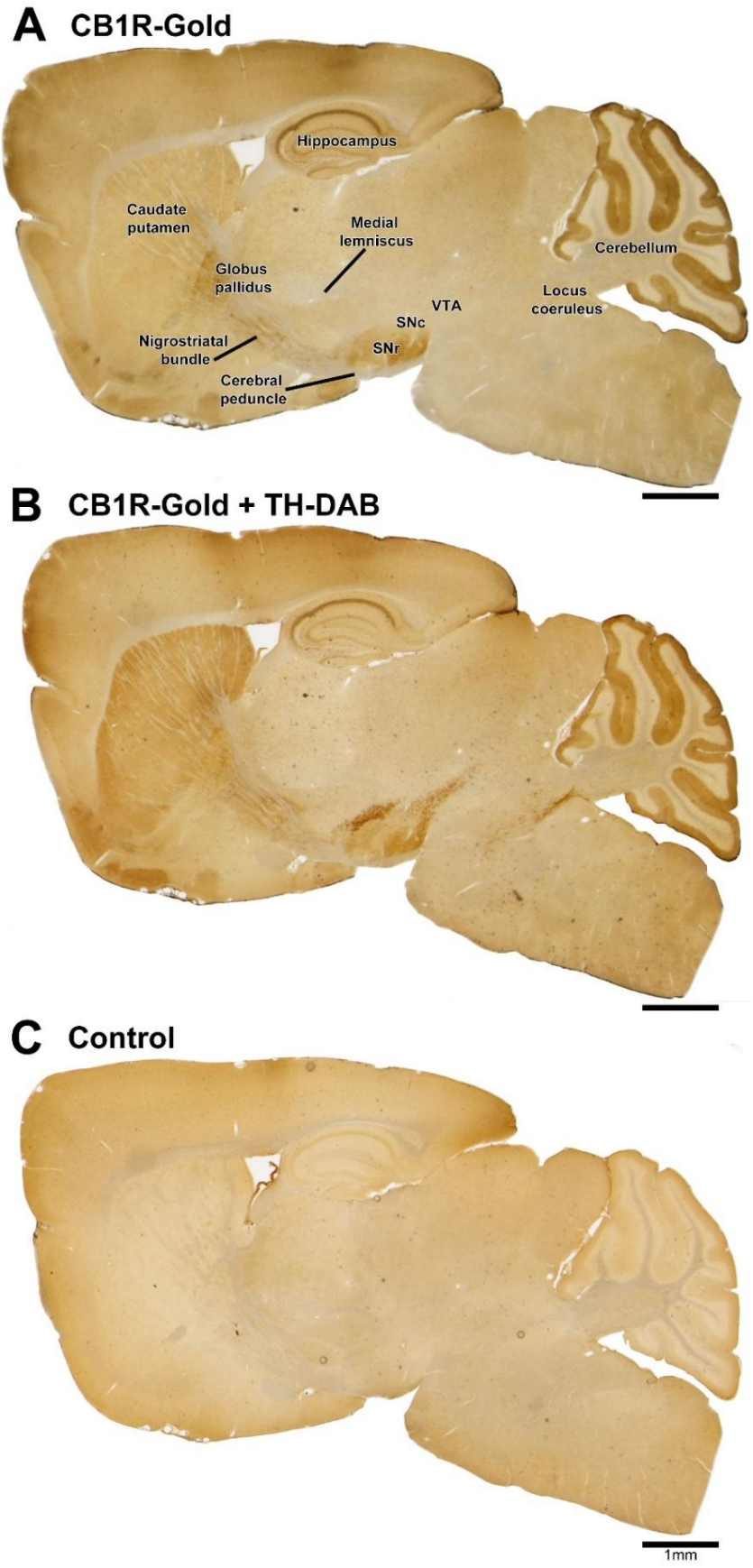

Figure 15. Stereoscopic light micro-graphs of sagittal sections immune-labelled with CB1R-gold and TH-DAB. (A) CB1R 1.4 nm gold immunoparticle staining with silver enhancement is observed in the SNr, globus pallidus, and faintly along the nigrostriatal bundle projecting from the SN to the striatum. Robust CB1R signal is also present in the positive control regions—the hippocampus and cerebellum. As expected, heavily myelinated fiber tracts such as the medial lemniscus and cerebral peduncle remain unstained. (B) The same section shown in A, additionally labeled for TH using 3,3'-diaminobenzidine (DAB). CB1R staining remains consistent with panel A, while TH-DAB labeling is evident in the caudate-putamen, locus coeruleus, SNc, and VTA. Speckled DAB precipitate is visible across the section. (C) Serial section from the same mouse processed under negative control conditions. Apart from some DAB precipitate, no TH labeling is present. CB1R staining is largely absent, with only faint background signal near the cortical surface. Note: Anatomical regions labeled in panel A are applicable to panels B and C, though labeling was omitted to enhance visualization of staining patterns.

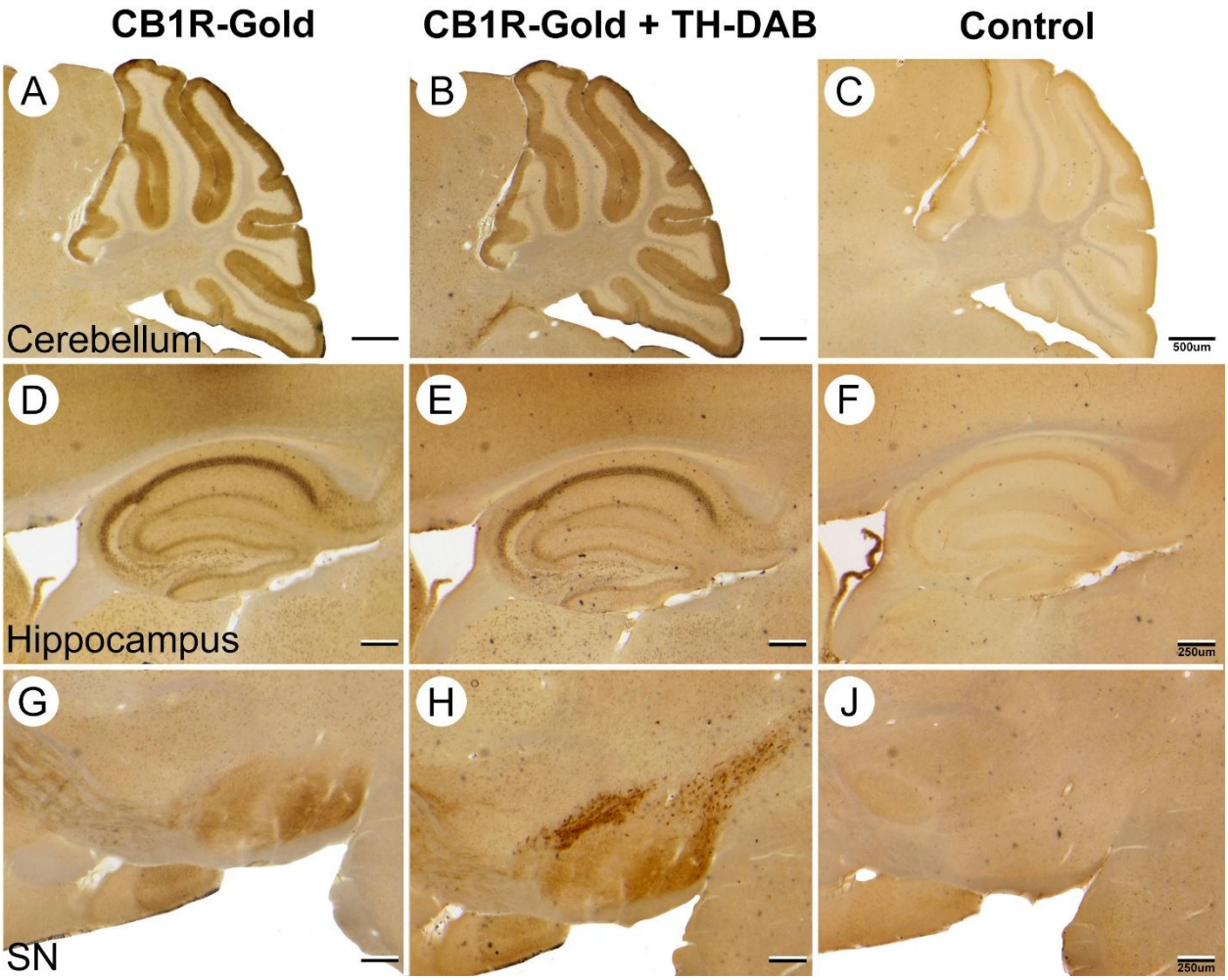

Figure 16. High-magnification images of the cerebellum (A–C), hippocampus (D–F), and SN (G–J) corresponding to sagittal sections shown in Figure 15. Columns from left to right show CB1R immunogold staining with silver enhancement, double labeling with CB1R-gold and TH-DAB, and negative control conditions. (A) In the cerebellum, CB1R-gold labeling is localized predominantly to the molecular and Purkinje cell layers. (B) TH-DAB staining is localized to the locus coeruleus, situated anterior to the lateral recess of the fourth ventricle and ventral to the vestibulocerebellar nucleus. (D) In the hippocampus, CB1R-gold staining is most prominent in the pyramidal cell layer and lacunosum moleculare of CA1–CA3, as well as the granule cell layer and, to a lesser extent, the hilus of the dentate gyrus (DG). (E) TH-DAB labeling is minimal, with no distinct signal discernible beyond scattered DAB precipitate. (G) In the SN, CB1R-gold labeling is clearly visible in the SNr and along the nigrostriatal bundle projecting toward the striatum. Signal is also present ventral to the cerebral peduncle (a heavily myelinated tract beneath the SNr) in the DG. (H) TH-DAB staining localizes to the SNc and VTA (dorsal to the SNr), and also follows the trajectory of the nigrostriatal bundle. Mild nonspecific DAB precipitate is also visible. (C, F, J) All control sections exhibit minimal background CB1R-gold staining and only subtle DAB precipitate, confirming labeling specificity.

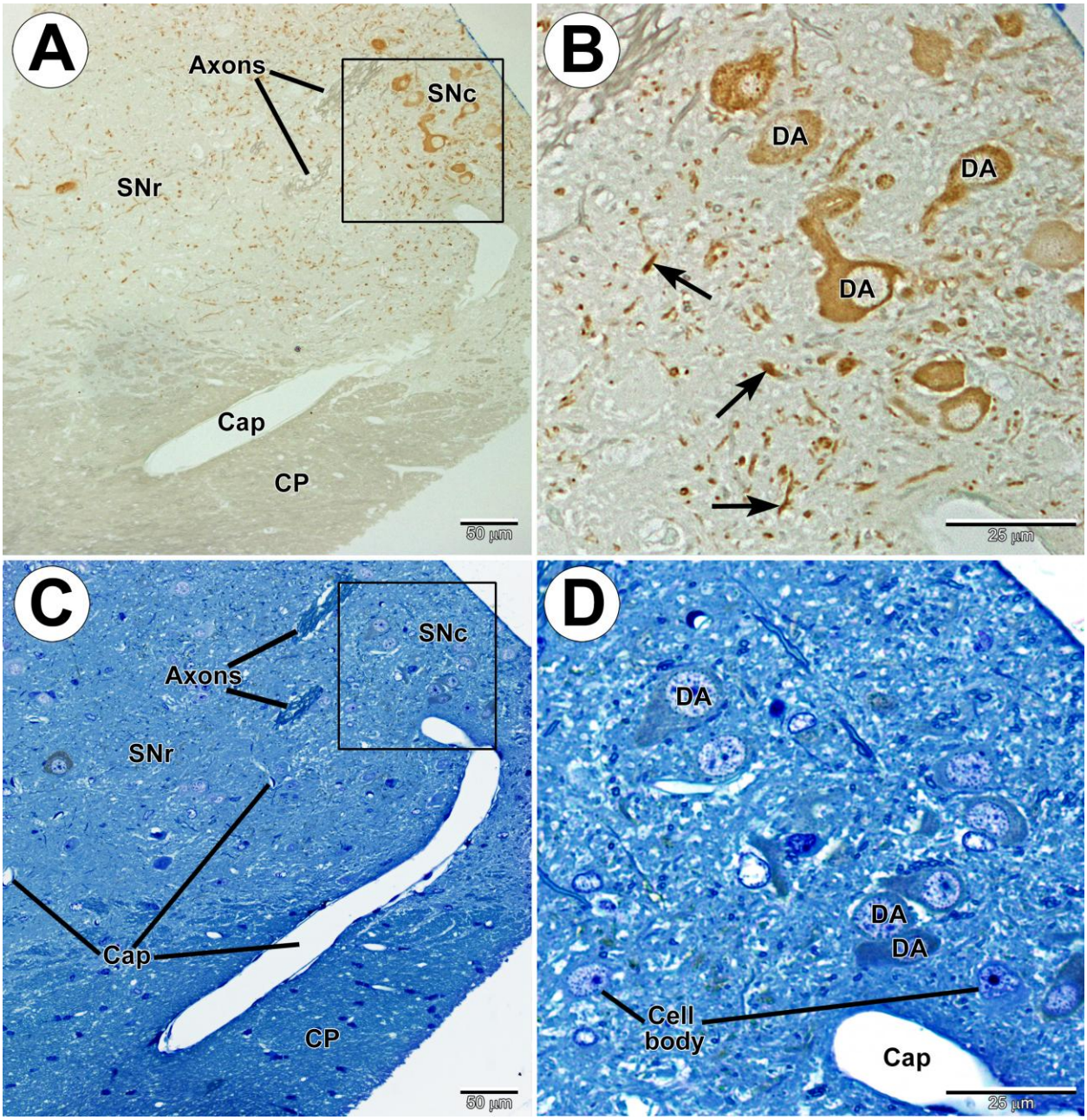

Figure 17. Low and high magnification light micrographs of double pre-embedding methods for localization of CB1R and TH in the SN, with and without toluidine blue staining. (A–B) Low and high magnification images of the same section, with B representing the boxed region in A. Panel A includes both the SNr, containing TH-positive DA processes and a single visible DA neuron, and the SNc, which is dominated by TH-labeled DA neuron somata. The heavily myelinated cerebral peduncle (CP) is visible ventral to the SNr. A large capillary (Cap) is also seen traversing the CP and extending into the SN region. In B, three centrally located TH-positive DA neuron somata are clearly labeled, with additional unlabeled neurons surrounding them. Black arrows indicate TH-positive neuronal processes. (C–D) Serial sections corresponding to A–B, stained with toluidine blue for structural contrast, with D representing the boxed region in C. Toluidine blue staining enhances visualization of capillary walls, non-DA cell bodies, and myelinated fiber tracts.

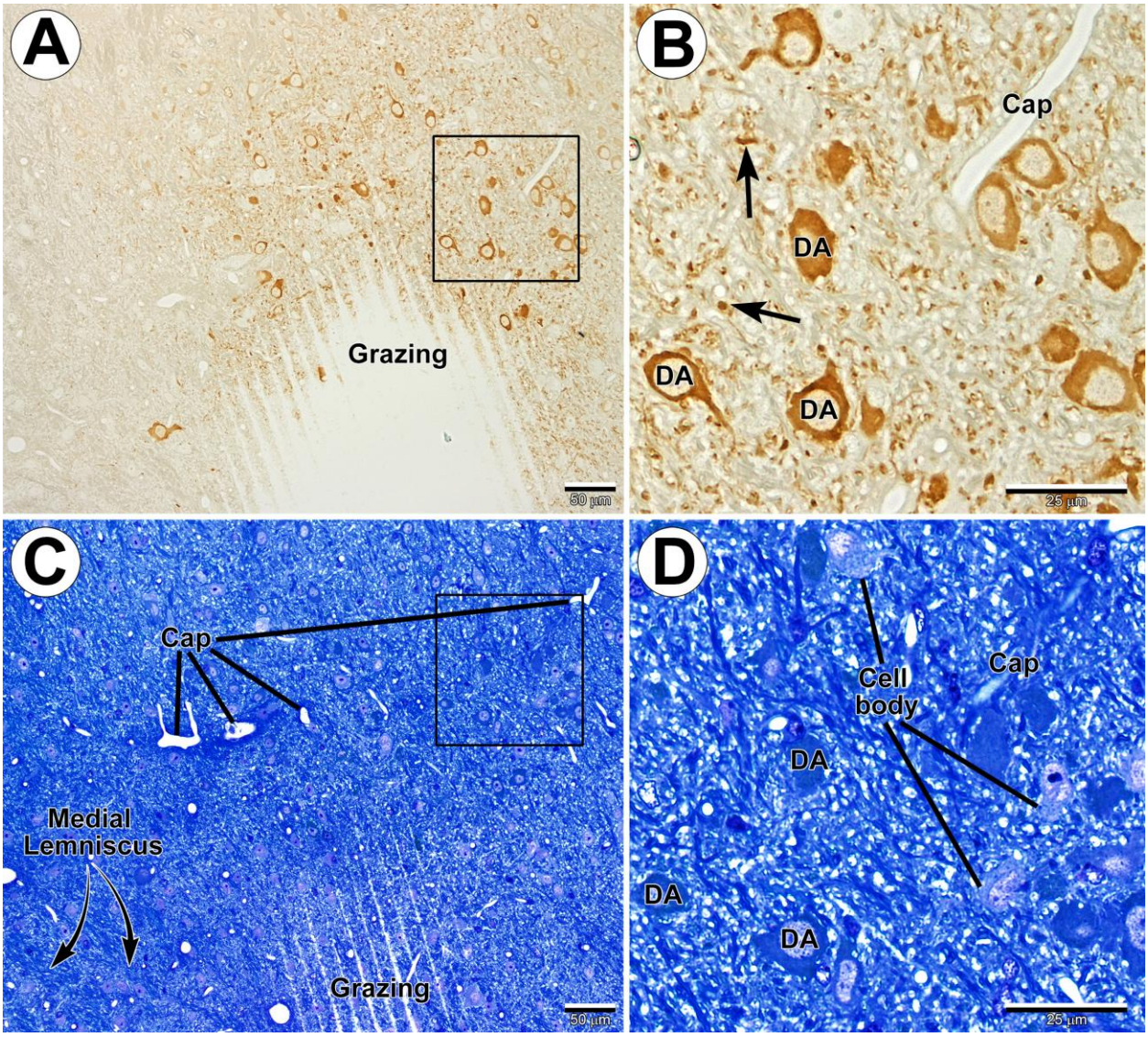

Figure 18. Low and high magnification light micrographs of double pre-embedding methods for localization of CB1R and TH in the VTA, with and without toluidine blue staining. (A–B) Low and high magnification images of the same section, with B corresponding to the boxed region in A. Panel A shows a grazing section through the TH-positive DA neuron-rich VTA, representative of those selected for TEM imaging to confirm staining quality prior to analysis. In B, three TH-positive DA neuron somata are clearly labeled, surrounded by additional unlabeled DA neurons. A capillary (Cap) is visible in the upper right corner. Black arrows indicate TH-positive neuronal processes. (C–D) Serial sections corresponding to A–B, stained with toluidine blue for enhanced structural contrast, with D representing the boxed region in C. In C, the medial lemniscus appears as a dense, toluidine blue-stained fiber tract in the lower left corner, and several capillaries are clearly outlined (examples marked). At higher magnification (D), toluidine blue improves visualization of non-DA cell bodies (labeled), in contrast to DA neurons. The same DA neuron somata labeled in B are also indicated in D.

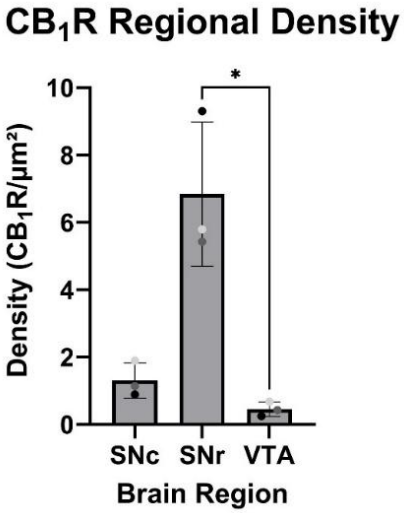

Figure 19. Graphical representation of CB1R immunoparticle densities in the SNc, SNr, and VTA. CB1R immunoparticles were manually counted per region for each mouse, and results are expressed as particle count per µm². A Friedman test followed by Dunn's post hoc comparisons with Bonferroni correction revealed a statistically significant difference between the SNr and VTA ($p < 0.05$), while no significant differences were observed between the SNc and SNr or SNc and VTA. Notably, mean CB1R densities followed trends consistent with confocal MFI data. Data points are color-coded by animal: black = mouse 1, dark gray = mouse 2, light gray = mouse 3.

3.2.2 Differences in CB1R-positive synapses across regions and synapse type

When examining morphology-prepared TEM sections of adult male mouse midbrain, large dopaminergic neurons are readily identifiable, surrounded by numerous presynaptic terminals, which appear to be primarily cholinergic, GABAergic, glutamatergic, or mixed in phenotype. Compared to other neuron populations in the region, DA neurons are characterized by large somata, prominent euchromatic nuclei, and cytoplasm densely packed with organelles—features indicative of high metabolic activity (**Fig. 20**). Myelinated axons and dendrites containing microtubules (visible as light-gray, straw-like structures in longitudinal section) are also abundant in the region (**Fig. 20**). In addition, the midbrain contains glial cells, including astrocytes, microglia, and oligodendrocytes, as well as vascular-associated cells such as pericytes and endothelial cells, around capillaries (not shown).

Upon examining the ultrastructure of midbrain presynaptic terminals, morphological features characteristic of glutamatergic, GABAergic, and cholinergic phenotypes are apparent (**Fig. 21**). Glutamatergic terminals typically contain numerous small (~30–50 nm in diameter), spherical synaptic vesicles and form asymmetric synapses, defined by a prominent postsynaptic density (PSD). GABAergic terminals exhibit small, pleomorphic, often oblong vesicles (~20 nm wide and 80 nm long) and form symmetric synapses where the pre- and postsynaptic membranes display comparable electron density under TEM. This symmetrical appearance can make GABAergic synapses more difficult to identify with certainty. Cholinergic terminals also form symmetric synapses, but are distinguished by their larger, spherical synaptic vesicles (~50–60 nm

in diameter) which are notably larger than those of glutamatergic terminals. All three terminal types are observed to synapse onto TH-positive dopaminergic compartments (**Fig. 21**).

In TEM-based classification, glutamatergic terminals are typically defined as excitatory, whereas GABAergic and cholinergic terminals are grouped together as inhibitory (despite the fact that cholinergic terminals typically deliver excitatory input). This way of classifying was used throughout the study as tissue integrity decreased with additional staining methods (observable across **Figs. 21 and 22**). TEM blocks of the DG (hippocampus) were also prepared as a positive control for CB1R-gold and TH-DAB staining. As expected, the granule cell layer of the DG showed a high concentration of CB1R-positive axons and terminals (**Fig. 23**), confirming immunoparticle labeling.

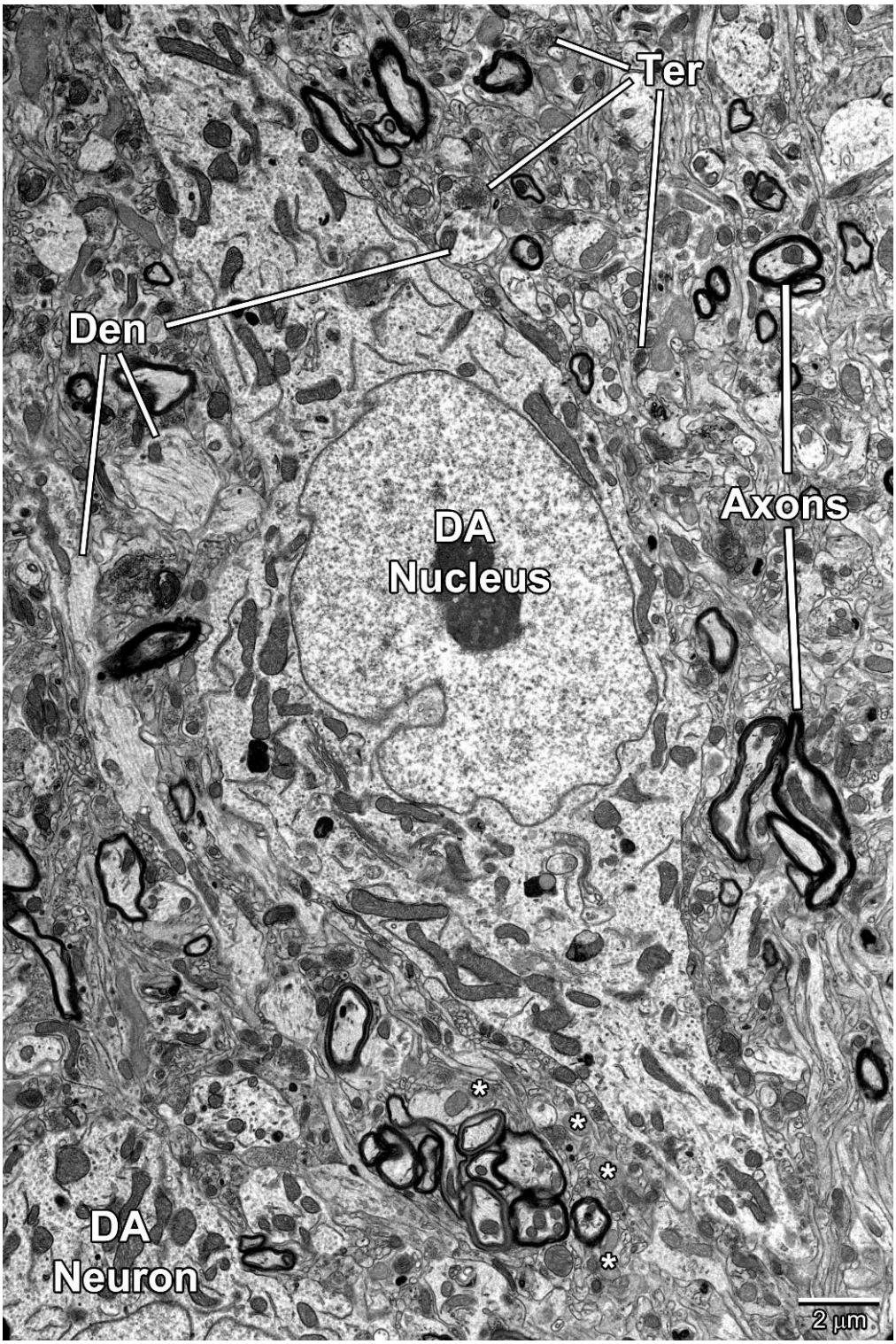

Figure 20. TEM morphological imaging of a DA neuron in the SN of an adult mouse brain. The DA neuron contains a large euchromatic nucleus with a prominent nucleolus and cytoplasm populated with organelles—mitochondria, Golgi bodies, lysosomes, and endoplasmic reticulum—indicative of high metabolic activity. The surrounding neuropil contains dendrites (Den), myelinated axons, and pre-synaptic terminals (Ter) apparent by vesicles and synaptic densities. Asterisks (*) indicate pale mitochondria characteristic of astrocytic processes, although astrocyte boundaries are difficult to delineate. Tissue blocks were provided by Dr. Patrick Nahirney.

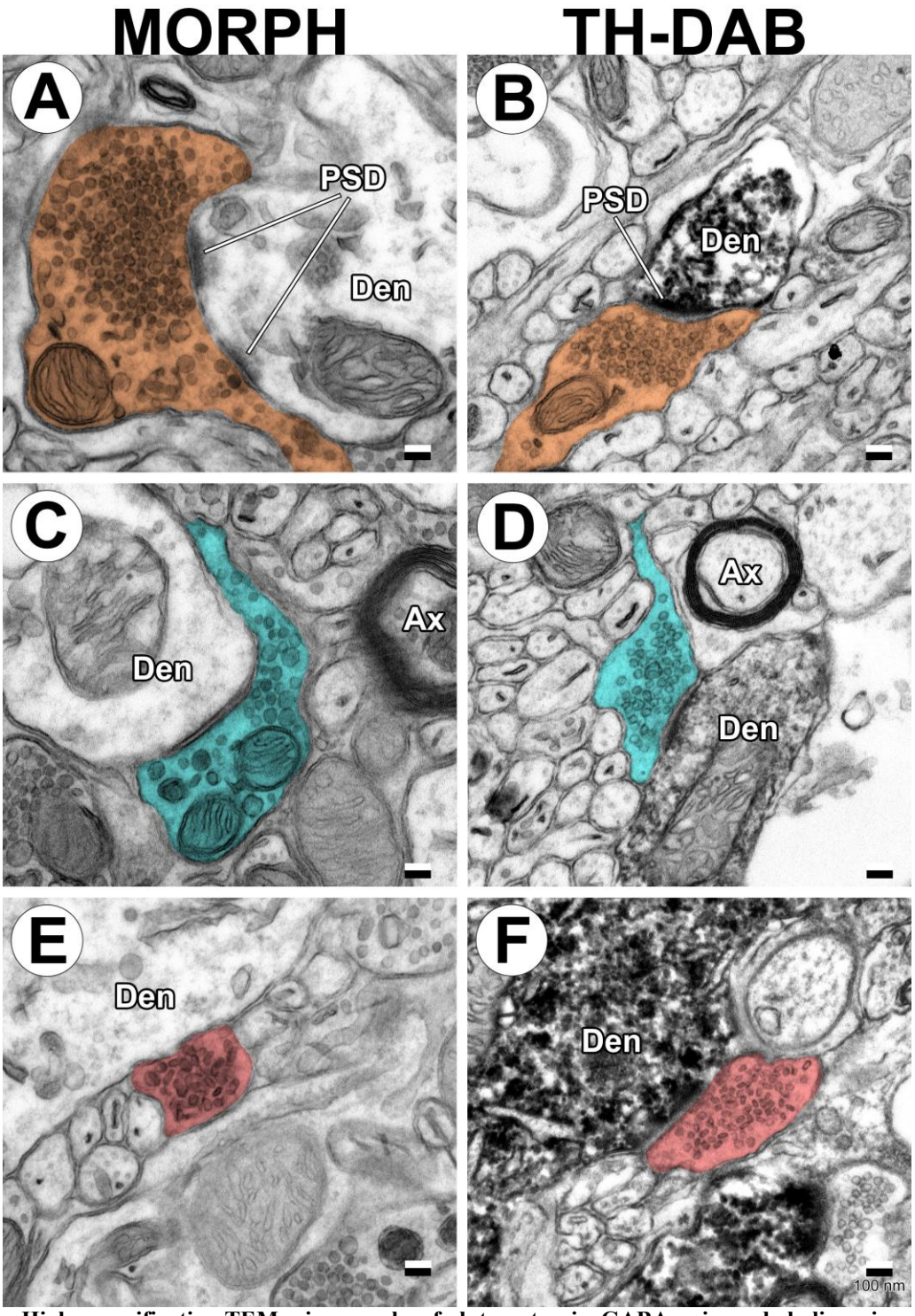

Figure 21. High-magnification TEM micrographs of glutamatergic, GABAergic, and cholinergic synapses in unstained and TH-DAB stained tissue. (A-B) Glutamatergic presynaptic terminals (orange) display small, spherical vesicles (~30-50 nm diameter) and prominent postsynaptic densities (PSD). (C–D) Two (likely) cholinergic terminals (cyan) containing large, spherical vesicles (~50-60 nm diameter) forming symmetric synapses are seen. (E–F) GABAergic terminals (red) exhibit pleomorphic vesicles (~20 nm wide and ~80 nm long) and symmetric synaptic densities. All synapse phenotypes form synapses onto TH-positive compartments, indicating input to DA neurons. Morphology-prepared tissue blocks were provided by Dr. Patrick Nahirney; TH-DAB–only blocks were provided by Charlotte Copas. Den, dendrite; Ax, axon.

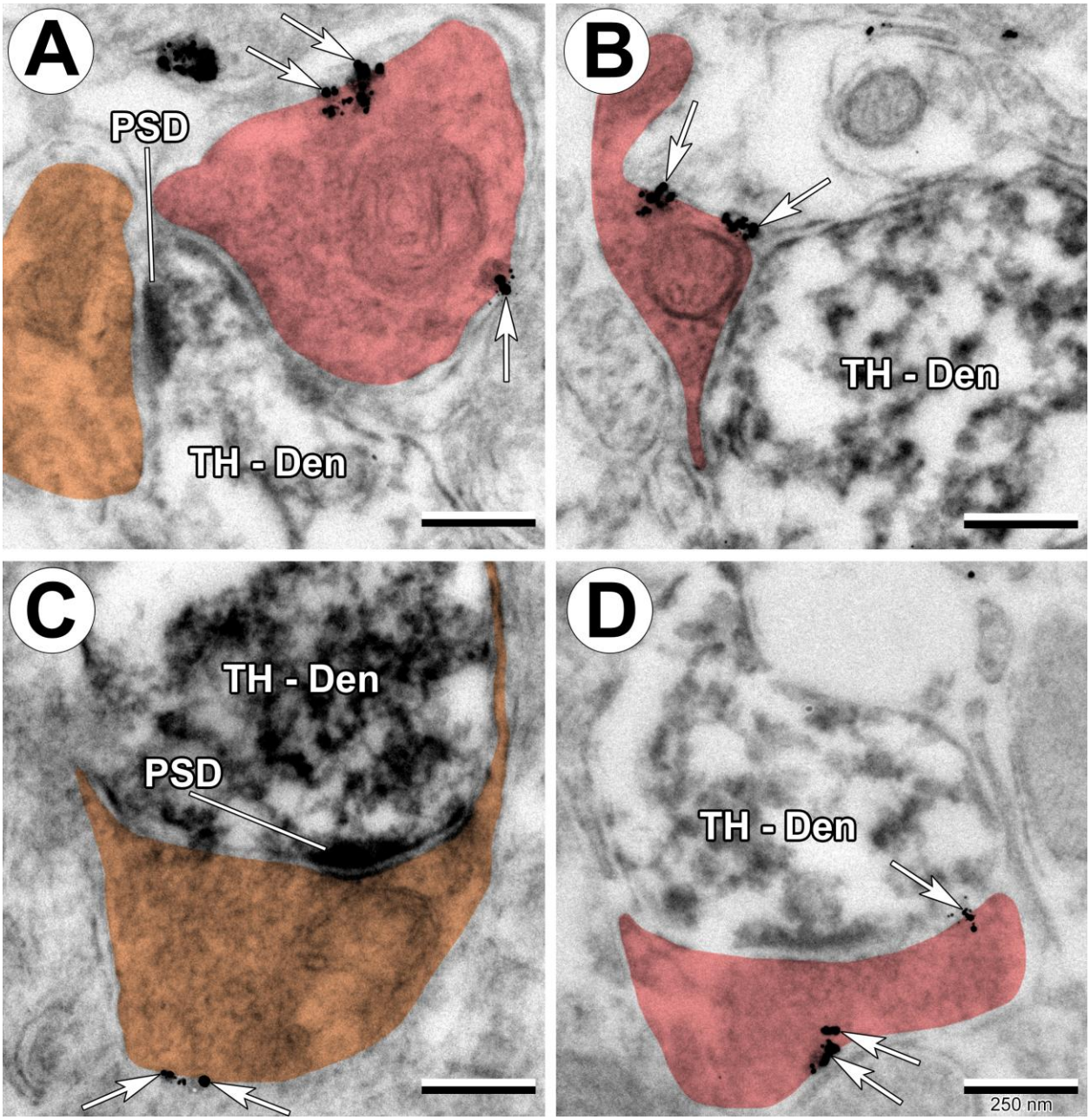

Figure 22. High-magnification TEM micrographs of excitatory and inhibitory synapses in CB1R-gold (silver-enhanced) and TH-DAB double-labeled tissue from the SNr, representative of synapses analyzed throughout the study. TH-positive DA compartments are filled with amorphous DAB reaction product, while CB1R immunogold particles appear as dense black puncta along plasma membranes (indicated by white arrows). (A) Both an excitatory (orange) and inhibitory (red) presynaptic terminal synapse onto a TH-positive dendrite. (B–D) both show inhibitory terminals, which more frequently contained CB1R immunoparticles, while (C) displays an excitatory terminal with a prominent post-synaptic density (PSD) visible through the DAB staining. Double labeling reduced overall tissue integrity, making vesicle morphology more difficult to resolve. As a result, terminal phenotypes were classified more broadly as excitatory or inhibitory rather than specifically as glutamatergic, GABAergic, or cholinergic. Den, dendrite.

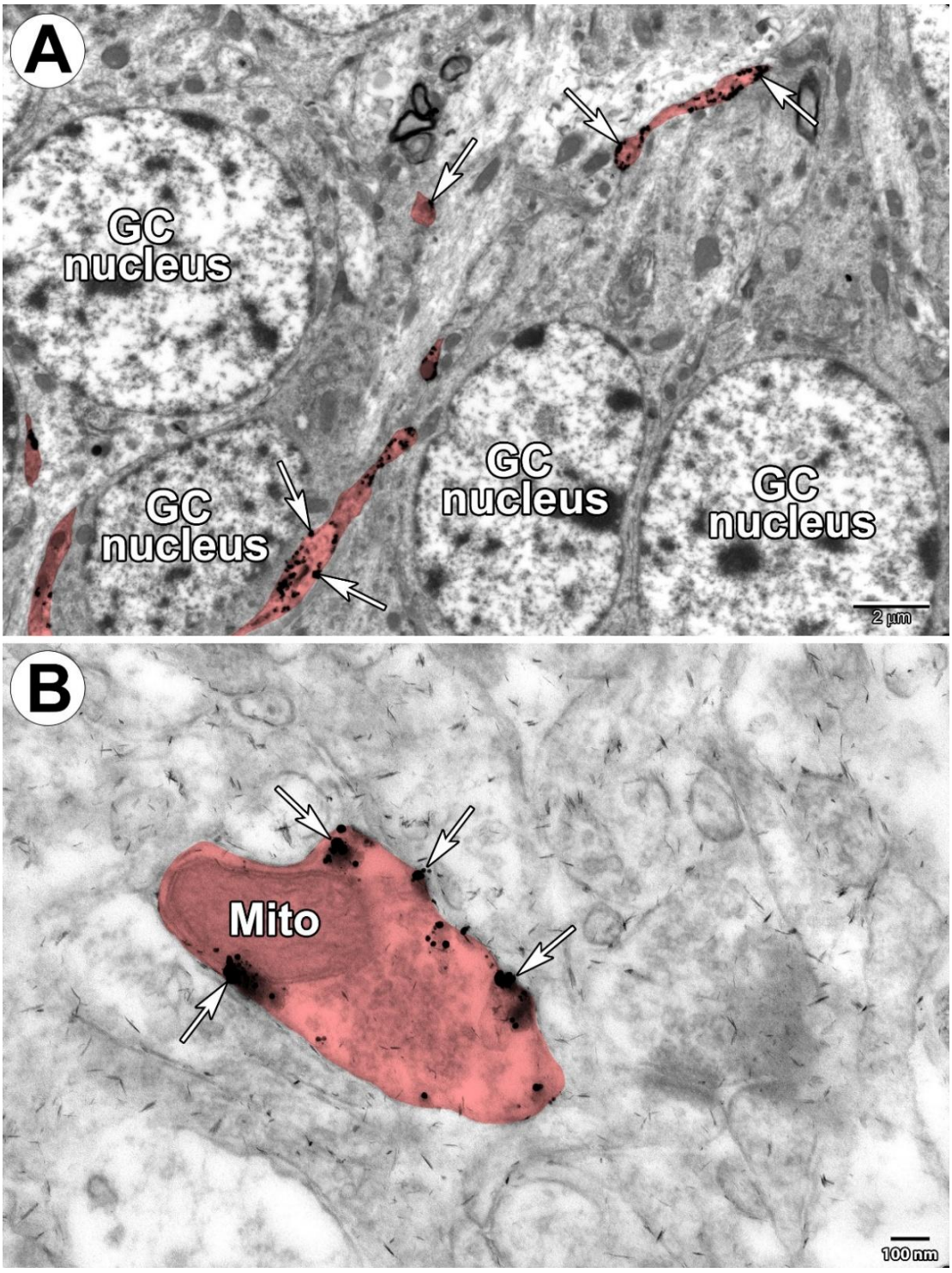

Figure 23. Low and high magnification TEM micrographs of the granule cell layer of the DG (hippocampus), serving as a positive control for CB1R labeling. A) Low-magnification image showing four labeled granule cells (GC) with euchromatic nuclei and adjacent CB1R-immunopositive unmyelinated axonal tracts. CB1R immunogold particles are densely clustered within presumptive inhibitory (red) compartments. (B) High-magnification image of the same region highlights a presynaptic inhibitory terminal with numerous CB1R particles localized to the plasma membrane. A mitochondrion (Mito) is in the terminal. Scattered electron-dense flecks consistent with non-specific uranyl acetate precipitate are present. White arrows to CB1R particles.

Statistical analyses were conducted to assess differences in CB1R terminal positivity across brain regions and synapse types. Initially, the percentage of CB1R-positive synapses was calculated separately for each mouse and brain region, for total synapses, excitatory synapses, and inhibitory synapses (n = 9 per condition). Given the small sample size and potential deviation from normality, non-parametric Friedman tests were first used to evaluate regional differences. These tests did not yield statistically significant results in any category, likely due to limited statistical power, despite observable trends in the data (**Fig. 24A**). To overcome these limitations, a generalized linear mixed model (GLMM) was implemented. GLMMs are well-suited for hierarchical data structures and can detect subtle effects and interactions that non-parametric tests may miss. This approach allowed inclusion of all raw data points, with CB1R terminal positivity as the dependent variable, and region and synapse type entered as fixed effects in separate models. Mouse ID was modeled as a random effect to account for repeated measures. The GLMM, conducted using JASP, revealed that CB1R terminal positivity was significantly predicted by brain region, with the SNr showing the highest proportion of CB1R-positive terminals and the VTA the lowest (**Fig. 24B**). Synapse type also significantly predicted CB1R terminal positivity, with inhibitory terminals displaying higher levels of CB1R expression compared to excitatory terminals (**Fig. 24C**). Raw data corresponding to these results are presented in **Table 6** above, and GLMM plotted data is visible in **Tables 7-9**. Note that p-values reported are Holm-adjusted for multiple comparisons.

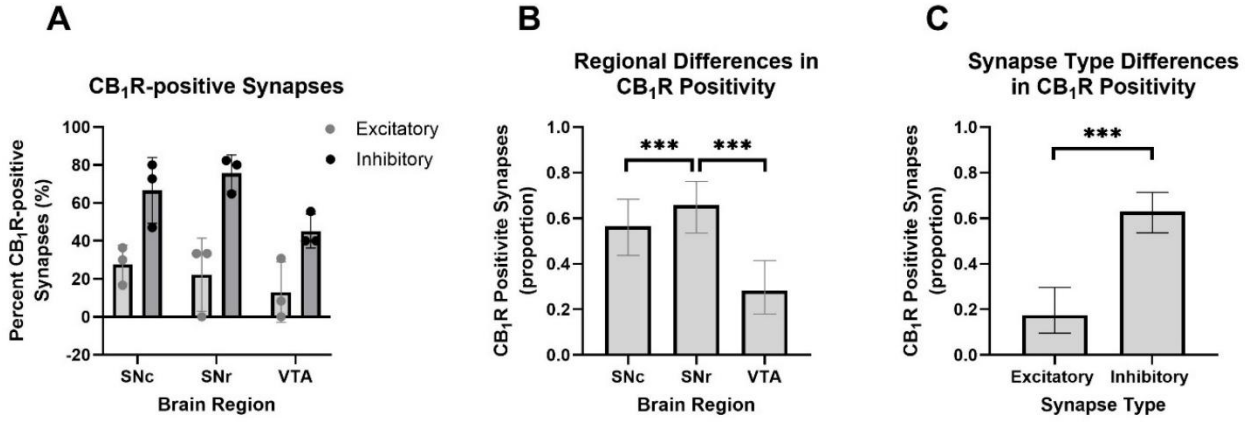

Figure 24. Graphical representation of trends in CB1R terminal positivity across brain regions and synapse types. Graph A shows the percentage of CB1R-positive synapses per region (both inhibitory or excitatory). Graph B displays estimated marginal means (EMMs) from the GLMM conducted in JASP, with region as the fixed effect, CB1R positivity as the dependent variable, and Mouse ID included as a random factor. Post hoc comparisons (Holm-adjusted p-values) revealed significant differences between the SNc and SNr, and the SNr and VTA. Graph C presents EMMs from a second GLMM in which synapse type was the fixed effect, with all other model parameters identical CB1R positivity significantly differed between excitatory and inhibitory synapses. $p < 0.001$.

The GLMM conducted to assess whether predicted CB1R terminal positivity differed across brain regions had the following inputs: CB1R terminal positivity (binary) was set as the dependent variable, region (SNc, SNr, VTA) was set as a fixed effect; Mouse ID was set as a random factor to account for repeated measures. The model revealed a statistically significant main effect of region, $\chi^2(2) = 8.060$, $p = 0.018$, indicating that CB1R terminal positivity significantly differed across the SNc, SNr, and VTA. Post hoc pairwise comparisons revealed no significant difference between the SNc and SNr, however, predicted CB1R terminal positivity was significantly higher in the SNc compared to the VTA (Estimate = 0.282, 95% CI [0.142, 0.422], $Z = 3.938$, $p < 0.001$), and in the SNr compared to the VTA (Estimate = 0.374, 95% CI [0.205, 0.543], $Z = 4.348$, $p < 0.001$). Full results are presented in **Tables 7 and 8**.

A second GLMM was conducted under the same conditions, with synapse type (excitatory or inhibitory) specified as the fixed effect instead of region. This model revealed a statistically significant main effect of synapse type, $\chi^2(1) = 9.359$, $p = 0.002$, indicating that CB1R terminal positivity differed significantly between excitatory and inhibitory synapses. Post hoc contrasts showed significantly lower predicted CB1R terminal positivity at excitatory terminals compared to inhibitory ones (Estimate = –0.455, 95% CI [–0.561, –0.348], $Z = –8.384$, $p < 0.001$). The negative estimate reflects reduced CB1R labeling at excitatory terminals relative to inhibitory counterparts. Full results are presented in **Table 9**.

Table 7. GLMM Estimated Marginal Means of CB1R-Positive Terminals by Brain Region.

Region	Estimate	95% CI	Z-value	P adjusted Holm
SNc	0.565	[0.437, 0.684]	0.994	0.32
SNr	0.657	[0.535, 0.761]	2.509	0.012
VTA	0.283	[0.18, 0.415]	-3.099	0.002

Table 8. GLMM Contrast Results: Brain Region Comparisons

Region	Estimate	95% CI	Z-value	P adjusted Holm
SNc vs. SNr	-0.092	[-0.265, 0.081]	-1.043	0.297
SNc vs. VTA	0.282	[0.142, 0.422]	3.938	< .001
SNr vs. VTA	0.374	[0.205, 0.543]	4.348	< .001

Table 9. GLMM Estimated Marginal Means of CB1R-Positive Terminals by Synapse Type

Synapse Type	Estimate	95% CI	Z-value	P adjusted holm
Excitatory	0.175	[0.096, 0.296]	-4.427	<0.001
Inhibitory	0.629	[0.536, 0.714]	2.693	0.007

3.2.3 CB1R density on CB1R-positive synaptic terminals

CB1R density of traced pre-synaptic terminal membranes varied across brain regions and between excitatory and inhibitory synapses. Density was first calculated for each positively labelled synapse as CB1R immunoparticle count per μm^2. To determine the appropriate statistical approach, normality was then assessed using Shapiro–Wilk tests for CB1R-positive terminal densities in the SNc, SNr, and VTA for each mouse, separately for inhibitory and excitatory synapses (nine independent tests per synapse type; 18 in total). For inhibitory synapses, the results were as follows: in the SNc, $W = 0.8138$, $p = 0.0008$ (mouse 1); $W = 0.8147$, $p < 0.0571$ (mouse 2); $W = 0.9585$, $p = 0.7629$ (mouse 3). In the SNr, $W = 0.7174$, $p = 0.0014$ (mouse 1); $W = 0.8680$, $p = 0.0394$ (mouse 2); $W = 0.5335$, $p < 0.0001$ (mouse 3). In the VTA, $W = 0.8799$, $p = 0.2259$ (mouse 1); $W = 0.7928$, $p = 0.0239$ (mouse 2); $W = 0.8575$, $p = 0.0713$ (mouse 3). For excitatory synapses, sample sizes were insufficient to reliably assess normality. Given that some inhibitory data met the assumptions of normality while others did not, and excitatory data could not be tested, nonparametric statistical methods were used for subsequent analyses.

Kruskal–Wallis tests were conducted within each brain region to assess differences between mice for both excitatory and inhibitory terminal data. For inhibitory terminals, no significant differences were found: SNc, $H(2) = 5.19$, $p = 0.075$; SNr, $H(2) = 3.37$, $p = 0.155$; VTA, $H(2) = 1.99$, $p = 0.370$. Similarly, for excitatory terminals, no notable differences were observed: SNc, $H(2) = 0.88$, $p = 0.743$; SNr, $H(2) = 2.70$, $p = 0.500$; VTA, $H(2) = 2.41$, $p = 0.400$. As no statistically significant between-mouse differences were detected in any case, data were pooled across animals for subsequent analyses.

Once data was pooled for each region, two final Kruskal-Wallis tests were completed to check for regional differences between receptor density on CB1R-positive excitatory and inhibitory terminals. A significant difference was observed between regions for inhibitory synapses, $H(2) = 21.78$, $p < 0.0001$. Dunn's post-hoc comparisons with Bonferroni correction

revealed inhibitory terminal CB1R density was greater in the SNr than the VTA ($Z = 4.644$, $p < 0.0001$), and in the SNc than the VTA ($Z = 3.236$, $p = 0.004$), but no difference was observed between the SNc and SNr ($Z = 1.633$, $p = 0.308$). No difference was detected between regions for excitatory synapses $H(2) = 1.064$, $p = 0.6122$ (**Fig. 25**).

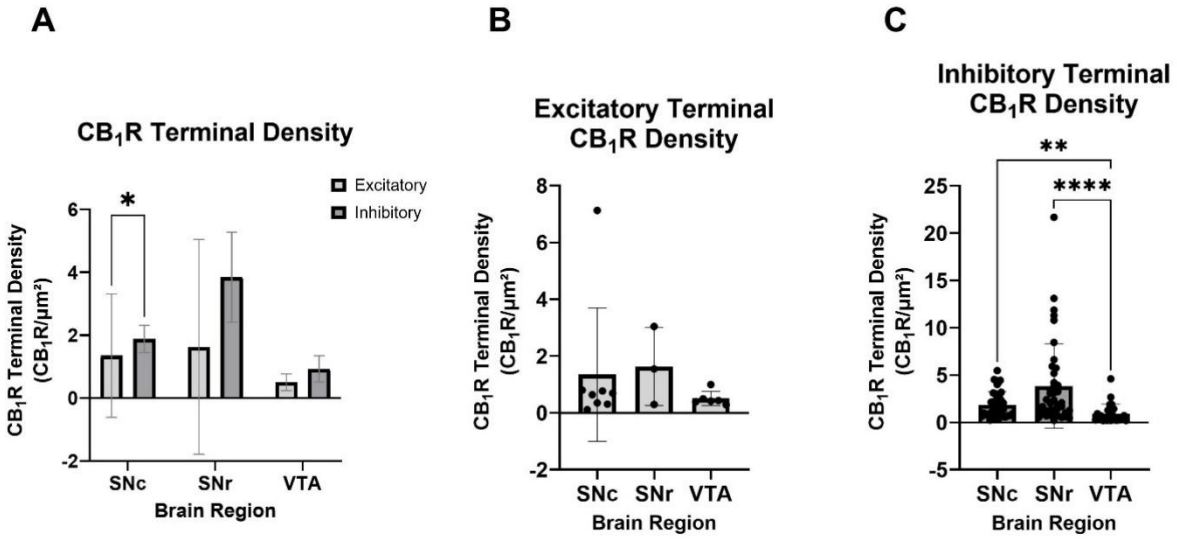

Figure 25. Graphical representation of CB1R immunoparticle density in excitatory and inhibitory presynaptic terminals across brain regions. (A) CB_1R particle densities in excitatory and inhibitory terminals are shown across the SNc, SNr, and VTA. Most terminals displayed densities ranging from 1 to 4 particles per µm². Mann–Whitney U tests were used to assess statistical differences within each region, revealing a significant difference between inhibitory and excitatory terminals in the SNc ($p < 0.05$) only. (B) CB_1R particle densities in excitatory terminals are shown across regions. A Kruskal–Wallis test indicated no significant regional differences, although the limited number of excitatory terminals constrained the ability to detect differences. (C) CB_1R particle densities in inhibitory terminals are shown across regions. A Kruskal–Wallis test revealed significant differences between the SNc and VTA ($p < 0.01$), and between the SNr and VTA ($p < 0.0001$).

To assess differences in CB1R density between excitatory and inhibitory synapses within each brain region, three separate Mann–Whitney U tests were conducted for the SNc, SNr, and VTA. A significant difference in CB1R density between inhibitory and excitatory synapses was observed in the SNc ($U = 76$, $p = 0.016$, $q = 0.047$), after controlling for multiple comparisons. However, no significant differences were found in the SNr ($U = 40$, $p = 0.37$, $q = 0.555$) or the VTA ($U = 69$, $p = 0.789$, $q = 0.789$) (**Fig. 25**).

Chapter 4: Discussion

4.1 CB1Rs rarely colocalize with TH-positive structures in the midbrain

Confocal microscopy findings presented here indicate that CB1Rs do not colocalize with TH-positive dopaminergic neurons or their processes in the SNc, SNr, or VTA. While low-magnification fluorescent micrographs appeared to show some CB1R signal overlapping with TH-positive cell bodies (**Fig. 10**), this apparent colocalization was not maintained under high-magnification imaging (**Figs. 6-9**). At higher resolution, the CB1R signal failed to localize to defined TH-positive structures, suggesting that the initial observation likely reflected optical artifacts rather than true colocalization. This discrepancy could be attributed to the increased exposure times and higher laser power typically required at low magnification to detect fluorescent signals, which can result in spectral bleed-through from adjacent channels. Additionally, low-magnification imaging collects signal from a comparatively thicker optical section, increasing the likelihood of out-of-plane fluorescence contaminating the image and producing the illusion of CB1R presence in TH-positive regions. Optical resolution limitations and signal dilution may also contribute to such false-positive appearances.

Corroborating these high-resolution confocal findings, ultrastructural data from immunoelectron microscopy revealed that CB1R immunoparticles were rarely associated with TH-DAB-labeled compartments. The term "rarely" is used instead of "never" because isolated CB1R-labeled particles were occasionally observed within DAB-positive regions; however, these did not clearly localize to identifiable membranes or subcellular compartments, suggesting possible non-specific labeling. It is important to note that due to the electron-dense nature of DAB, which appears as amorphous dark material under TEM, the distinction between CB1R immunoparticles (also electron dense) and the DAB signal can be obscured. Therefore, while co-localization cannot be ruled out entirely due to these technical limitations, the overall pattern strongly suggests that CB1Rs are not substantially expressed on dopaminergic neurons within these midbrain regions. This interpretation is consistent with prior reports indicating minimal or absent CB1R expression in dopaminergic populations (García et al., 2016; Herkenham et al., 1991).

4.2 Regional fluorescent and CB1R immunoparticle density findings align with established functional roles of midbrain structures

Fluorescent intensity analyses from the present study suggest that the SNr is predominantly composed of GABAergic interneurons, with relatively sparse dopaminergic cell bodies and processes. In contrast, both the SNc and VTA exhibit a higher density of dopaminergic neurons and a lower proportion of GABAergic neurons. These observations are consistent with previous electrophysiological and immunohistochemical studies characterizing neuronal populations in the rodent midbrain. Specifically, Margolis and colleagues (2006, 2012) reported that approximately 71%, 13%, and 23% of neurons in the SNr, SNc, and VTA, respectively, are GABAergic, while 8%, 88%, and 55% are dopaminergic. CB1R fluorescent and immunoelectron microscopy regional density analyses revealed that CB1R density was highest in the SNr, followed by the SNc, and lowest in the VTA. This distribution pattern is also consistent with prior characterizations of midbrain CB1R expression in rodents (Han et al., 2017; Walsh et al., 2010) and humans (Glass et al., 1993; Hurley et al., 2003). Interpretation of CB1R, TH and GAD67 immunolabeling data requires consideration of the distinct afferent and efferent connectivity patterns of each midbrain subregion.

The SN comprises complex circuitry, though its principal efferent projection is the nigrostriatal dopaminergic pathway. The SNc receives GABAergic afferents from the dorsal striatum (i.e. caudate-putamen, CPu) and globus pallidus (GP), in addition to excitatory glutamatergic and cholinergic inputs arising from the pedunculopontine tegmental nucleus (PPT) and laterodorsal tegmental nucleus (LDT). Dopaminergic neurons of the SNc project to medium spiny neurons within the CPu and ventral striatum (nucleus accumbens), thereby modulating basal ganglia activity underlying motor execution, motivational salience, and reinforcement learning. In turn, these striatal neurons contribute to either the direct pathway, projecting monosynaptically to the internal GP (GPi) and SNr, or the indirect pathway, which involves sequential synapses to the external GP (GPe) and subthalamic nucleus (STN) before converging on the GPi and SNr. The SNr thus integrates inhibitory input from the striatum and GPe, and excitatory drive from the STN, allowing for finely regulated SNr output. Efferents from the SNr target the thalamus (Quik & Wonnacott, 2011), superior colliculus, and PPT—structures critically involved in sensorimotor integration and motor control. Additionally, GABAergic outputs from the SNr synapse locally onto

dopaminergic neurons of the SNc and, to a lesser extent, the VTA, thereby modulating dopaminergic excitability within both the nigrostriatal and mesolimbic systems.

The VTA constitutes the origin of the mesolimbic and mesocortical pathways and integrates diverse afferent inputs. It receives glutamatergic projections from the PPT, LDT, superior colliculus, periaqueductal gray (PAG), hypothalamus, and bed nucleus of the stria terminalis (BNST), along with GABAergic afferents from the rostromedial tegmental nucleus (RMT), nucleus accumbens, and local interneurons. VTA dopaminergic neurons project to a broad array of limbic and cortical structures, including the nucleus accumbens, prefrontal cortex, amygdala, and hippocampus, thereby mediating functions related to reward processing, motivational drive, affective learning, and executive control. Notably, the SNc exhibits partial target overlap with the VTA, also sending dopaminergic projections to the nucleus accumbens, however, its contribution to this pathway is comparatively limited (He et al., 2023; Poulin et al., 2018).

Given that the SNc and VTA are primarily involved in dopaminergic projections to the striatum and cortical regions—both of which strongly influence motor control and reward-related processing—while the SNr functions predominantly as a modulatory output structure, the relative distribution of TH and GAD67 immunofluorescence observed across these regions is consistent with their known functional specializations. Subsequently, a key question arises: how does the CB1R distribution observed in the present study relate to these established regional roles? The finding that CB1R expression is greatest in the SNr, followed by the SNc and VTA suggests a regionally specific functional role of CB1Rs, with the greatest modulatory potential in the SNr. As CB1Rs are found on presynaptic terminals and are known to suppress neurotransmitter release when localized on plasmalemma, their elevated expression in the SNr could correspond to decreased synaptic output from this region. Given that the SNr is predominantly composed of GABAergic neurons, this implies that CB1Rs may exert significant inhibitory control over GABAergic transmission from the SNr to its downstream targets. In contrast, the decreased CB1R expression in the SNc and even more limited presence in the VTA—regions dominated by dopaminergic neurons—combined with evidence suggesting that CB1Rs are unlikely to be expressed directly on DA neurons, points toward an indirect modulatory role in these regions. Here, CB1Rs may influence synaptic input to DA neurons rather than the dopaminergic cells themselves. The nature of this input—whether primarily inhibitory, excitatory, or both—remains

an open question. To further elucidate this, a closer examination of the ultrastructural data is warranted.

4.3 CB1Rs localize to inhibitory terminals synapsing onto DA neurons in the midbrain

Focusing specifically on CB1R-positive terminals synapsing onto dopaminergic neurons, ultrastructural analyses revealed that CB1Rs were predominantly localized to inhibitory presynaptic membranes within the SNr, somewhat in the SNc and minimally the VTA. These semi-quantitative findings were corroborated by confocal imaging, which demonstrated strong colocalization of VGAT and CB1R within the SNr and the SNr–SNc transition zone (**Figs. 7, 8**). Interestingly, the dopaminergic processes present in the SNr are presumed to originate primarily from the SNc, with minor contributions from the VTA (Prensa et al., 2009). Accordingly, CB1R activation on inhibitory terminals targeting dopaminergic elements in any of these regions would be expected to attenuate GABAergic input onto SNc and VTA DA neurons. Given that midbrain dopaminergic neurons exhibit pacemaker-like tonic firing under basal conditions, such disinhibition would likely enhance dopaminergic excitability and increase DA release in downstream targets, most notably the dorsal and ventral striatum. Functionally, in a healthy organism, CB1R activation could therefore manifest as enhanced motor output, increased motivational drive, or greater reward-seeking behaviour.

Given that CB1R density as well as overall CB1R presence on inhibitory DA-inputs was greater in the SNr and SNc compared to the VTA, it is more plausible that CB1R-mediated modulation in the midbrain would preferentially influence motor initiation and control (dorsal striatum), rather than reward-based behaviours (ventral striatum). However, preclinical and clinical investigations of CB1R function have yielded mixed results—an issue addressed in more detail in **Section 4.6**. One potential explanation for the discrepancy between the current study and results form behavioural studies may lie in regional heterogeneity. The VTA, in particular, displays considerable anatomical and functional heterogeneity, reportedly greater than that observed in the SNc (Margolis et al., 2006, 2012). Given the limited sample size of the current study, it is possible that subregions of the VTA with more pronounced CB1R expression were underrepresented or missed entirely. This could mean that there is in fact more CB1R input to the VTA than this study predicts, which could account for the observed CB1R influence on VTA-related behaviours.

It is important to acknowledge that the current study was limited in its ability to precisely classify synapse types beyond broad categorization as inhibitory or excitatory, due to the resolution

and quality constraints of the immunoelectron micrographs. Accurate identification of synapse type based on vesicle morphology—such as vesicle shape and size—was not consistently feasible, and categorization relied predominantly on the appearance of pre- and postsynaptic densities. Consequently, it is likely that many cholinergic terminals were classified as inhibitory, as they often lack the prominent postsynaptic densities characteristic of glutamatergic synapses (**Fig. 21**).

Previous work from our laboratory examining synaptic inputs to TH-positive DA neurons in the SNcM, SNcL, and VTA revealed that, in the SNc, approximately 20% of terminals were cholinergic, 30% were glutamatergic, and 51% were either purely GABAergic or exhibited mixed GABAergic content. In contrast, the VTA displayed a higher proportion of glutamatergic inputs (49%), followed by cholinergic (23%) and mixed GABAergic (28%), with no purely GABAergic terminals observed (Copas, 2023). Given the considerable presence of both cholinergic and GABAergic or GABA-mixed terminals in these regions, it is highly plausible that CB1Rs are also expressed on cholinergic terminals within the midbrain. Assuming this to be the case, the downstream functional effects of CB1R activation may differ from above interpretations focused solely on GABAergic (inhibitory) transmission.

Although cholinergic signaling can be complex, cholinergic inputs predominantly excite DA neurons via nicotinic acetylcholine receptors (nAChRs) and muscarinic receptors (Durand-de Cuttoli et al., 2018; Mena-Segovia et al., 2008). Activation of these receptors is associated with sustained depolarization, increased baseline (tonic) and burst firing, and enhanced dopamine release (Mena-Segovia et al., 2008). While acetylcholine (ACh) alone does not typically induce phasic firing, it can modulate the occurrence in conjunction with glutamatergic or GABAergic input (Le Gratiet et al., 2022). However, overall ACh release is characteristically slower and more prolonged, suggesting it plays a modulatory role in dopaminergic excitability over longer temporal scales (Le Gratiet et al., 2022). In this context, CB1R activation on cholinergic terminals would be expected to suppress excitatory cholinergic input to DA neurons, potentially diminishing firing and reducing dopaminergic output to downstream targets. Such a reduction in DA signaling could manifest functionally as impaired motor control, reduced motivational drive, or attenuated reward-seeking behaviour. However, it is important to note that cholinergic excitation of SNc DA neurons produces different behavioural outcomes depending on the neurons' anatomical location (Estakhr et al., 2017), suggesting that the precise positioning of cholinergic CB1R-expressing terminals may ultimately influence behavioural effects.

4.4 CB1Rs are rarely localized to excitatory DA-neuron inputs in the midbrain

TEM analyses revealed that CB1R immunoparticles localized to excitatory DA input terminals significantly less frequently than to inhibitory terminals. Among the three regions examined, the VTA displayed the lowest proportion of CB1R-positive excitatory terminals overall. Additionally, within each region, the density of CB1Rs on excitatory terminals appeared lower than on inhibitory terminals; however, unlike inhibitory terminals, no statistically significant differences in excitatory terminal density were observed across regions. This lack of significance may be attributed to the limited number of CB1R-positive excitatory terminals identified, which may have been insufficient for robust statistical comparison. These findings were further supported by qualitative confocal microscopy data. At high magnification, colocalization between VGlut2 and CB1R appeared substantially reduced compared to colocalization between VGAT and CB1R in the SN. The limited VGlut2–CB1R colocalization that was observed was primarily restricted to the SNr and, to a lesser extent, the SNr–SNc transition zone (**Fig. 6**), with no detectable colocalization in the VTA (**Fig. 9**).

Collectively, these data suggest that CB1Rs exert comparatively less influence over glutamatergic input to dopaminergic neurons than over inhibitory input. However, the presence of CB1Rs on excitatory terminals, albeit limited, implies a functional role in modulating glutamatergic transmission. Assuming CB1Rs located on the presynaptic membrane act to suppress neurotransmitter release, their presence on glutamatergic afferents would be expected to reduce excitatory drive onto dopaminergic neurons, thereby decreasing dopamine neuron excitability and attenuating dopamine release in downstream targets. Glutamatergic afferents to midbrain dopaminergic neurons are known to enhance firing rates, often promoting burst firing through activation of NMDA and AMPA receptors. Such phasic firing is critical for reward processing through the mesolimbic pathway and for facilitating habit learning via the nigrostriatal pathway. Therefore, even limited CB1R-mediated modulation of these inputs may carry important implications for behavioural outcomes related to reward processing and motor learning. **Figure 26** represents a visual summary of this study's findings.

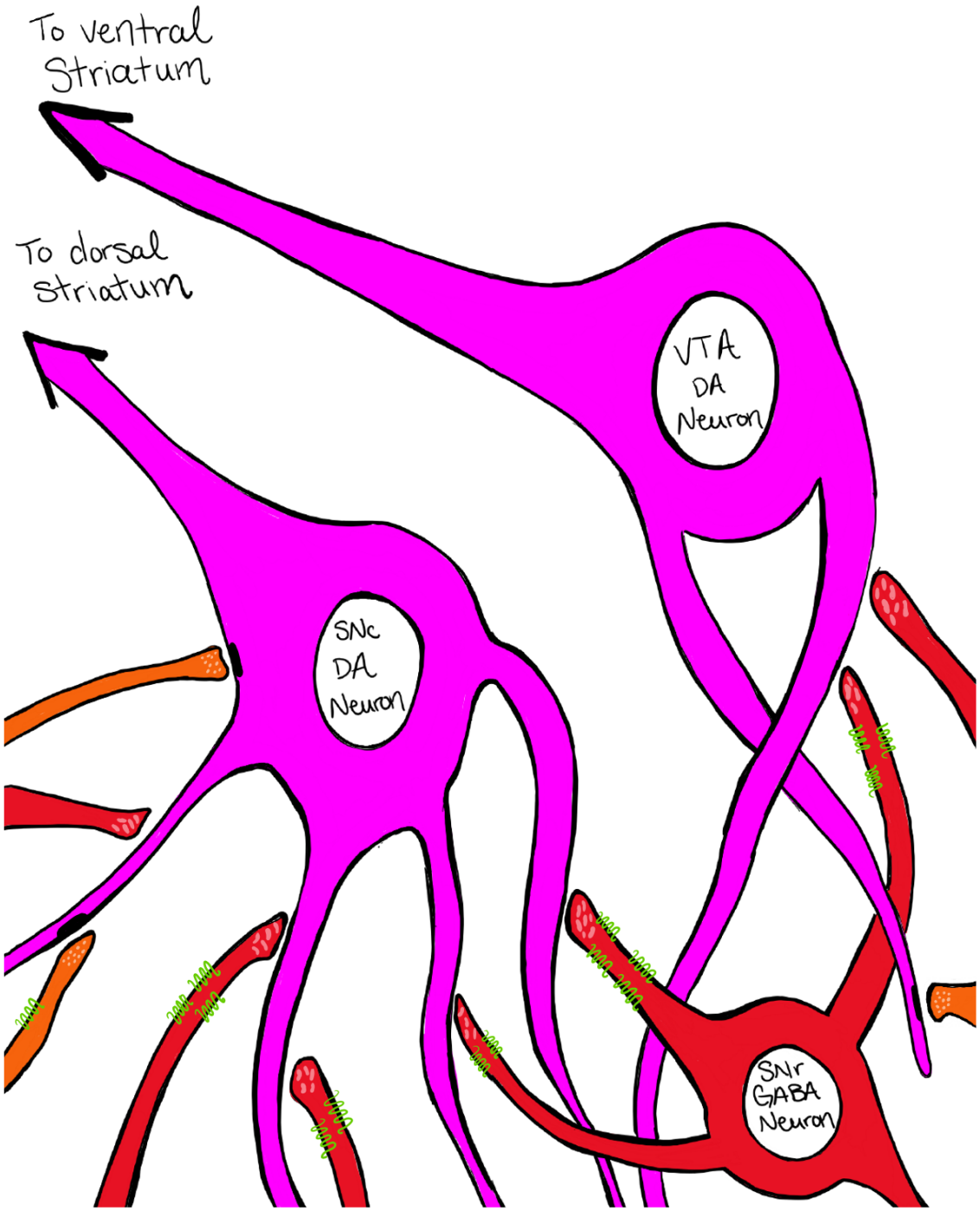

Figure 26. Visual summary. This study investigated CB1R (green) distribution within the SNc, SNr, and VTA, specifically examining CB1R localization and density on excitatory (orange) and inhibitory (red) presynaptic terminals opposing TH-positive DA neurons (magenta). Using immunoelectron and confocal microscopy techniques, we found that across all regions, CB1Rs were predominantly localized to inhibitory terminals contacting DA neurons. In terms of regional distribution, the highest number of CB1R-positive synapses was observed in the SNr, followed by the SNc, and then the VTA. By advancing our understanding of CB1R distribution within the midbrain, we can better elucidate how these receptors—and the broader endocannabinoid system—modulate neural pathways, ultimately contributing to a deeper understanding of DA-related diseases.

4.5 CB1R immunolabelling of positive control regions support midbrain findings

Confocal and electron microscopy analyses of hippocampal and cerebellar tissue, processed using the same staining protocols as midbrain samples, were examined throughout this study to (1) confirm the reliability and specificity of CB1R labeling (positive control), and (2) provide a comparative framework for interpreting CB1R localization patterns in the midbrain. Consistent with midbrain findings, the stratum pyramidale of the CA1 region and the Purkinje cell and molecular layers of the cerebellum exhibited dense colocalization of CB1R with VGAT immunofluorescence at the confocal level (**Figs. 12, 14**), while colocalization with VGlut1 or VGlut2 was markedly lower (**Figs. 12, 13**). At the light microscopy level, CB1R-gold labeling was similarly observed in these layers, and at the ultrastructural level, CB1R immunoparticles were densely localized to inhibitory terminals surrounding granule cells in the DG (**Fig. 23**). These observations are consistent with previous reports demonstrating prominent CB1R expression on GABAergic terminals in these regions (Bonilla-Del Río et al., 2021; Gutiérrez-Rodríguez et al., 2017; Kawamura et al., 2006).

Taken together, these findings reinforce the interpretation that CB1Rs are predominantly expressed on inhibitory terminals, and support the validity of this conclusion for the midbrain as well. Interestingly, when compared to CB1R-positive terminal densities identified with immunoelectron microscopy observed in other brain regions such as the basal lateral amygdala and CA1 (Bonilla-Del Río et al., 2021), all midbrain regions examined in this study displayed relatively lower densities of CB1Rs on inhibitory terminals. This suggests that the ECS may exert a comparatively weaker modulatory influence over synaptic activity in the midbrain than in regions more traditionally associated with synaptic plasticity and learning.

Further insight can be gained by examining CB1R function in these positive control regions. Notably, in the cerebellum, high-magnification confocal imaging revealed strong colocalization of CB1R and VGAT in GABAergic basket cell pinceaux surrounding Purkinje cell bodies (**Fig 14**). In this synaptic arrangement, CB1Rs modulate GABA release by inhibiting presynaptic calcium channels and thus reducing vesicle fusion (Diana et al., 2002). Additionally, depolarization of Purkinje cells can trigger the retrograde release of endocannabinoids, which act on CB1Rs located on basket cell terminals to further suppress inhibition (Szabo et al., 2004; Yoshida et al., 2002). This disinhibition contributes to cerebellum-dependent motor learning (Kishimoto & Kano, 2006). In the hippocampus the role of CB1Rs on GABAergic interneurons is

complex, but it is thought that CB1Rs influence certain types of memory through mediating communication between regions of the hippocampus and cortical structures (Robledo-Menendez et al., 2022).

4.6 Implications for DA-related disease states

Considering that CB1Rs can modulate inputs to DA neurons and thereby influence DA neurotransmission, they have been a focus of research aimed at both advancing the understanding of, and developing treatments for DA-related disorders such as Parkinson disease (PD), schizophrenia, and substance use disorders (SUDs).

4.6.1 Implications for Parkinson disease

The core pathologies of PD include the neurodegeneration of DA neurons in the SNc and the abnormal aggregation of α-synuclein, resulting in Lewy body formation (Morris et al., 2024; Parent & Parent, 2010). Recent theories regarding PD pathobiology propose that dopaminergic neuronal loss arises from a convergence of factors, including genetic predisposition, mitochondrial dysfunction, impaired proteasomal and lysosomal degradation leading to α-synuclein accumulation, and heightened immune responses (Morris et al., 2024). Regardless of the underlying mechanism, the progressive loss of DA neurons that disrupts DA input to the dorsal striatum remains central to the motor impairments observed in PD. Within the context of this study, a key therapeutic question emerges: could enhancing DA output from surviving neurons—specifically by activating CB1Rs to inhibit GABAergic input onto midbrain DA neurons and thereby disinhibit their activity—help alleviate PD-related motor symptoms?

Preclinical evidence suggests that CB1R agonists may alleviate motor impairments associated with PD. A recent meta-analysis examining the effects of cannabinoids in rodent models of PD found an overall improvement in motor behaviour, as demonstrated by enhanced performance in rotarod and pole tests compared to untreated PD animals (Urbi, Lee, et al., 2022). For instance, locomotor deficits induced by the mitochondrial toxin 1-methyl-4-phenyl-1,2,3,6-tetrahydropyridine (MPTP)—a widely used PD model—were mitigated by both URB597 (a FAAH inhibitor that increases levels of the endogenous CB1R agonist AEA) and WIN55,212-2 (a synthetic CB1R agonist) (Escamilla-Ramírez et al., 2017). These compounds also attenuated striatal and nigral DA depletion and reduced MPTP-induced downregulation of TH (Escamilla-Ramírez et al., 2017), suggesting that motor improvements may result from the preservation of

DA neurons rather than their increased activation. Notably, it has been proposed that cannabinoid-induced DA neuron preservation in rodent PD models may stem from a reduction in excitotoxicity and neuroinflammation (Fernández-Ruiz, 2009; More & Choi, 2015; Sheng et al., 2005). Nonetheless, the precise mechanisms underlying these neuroprotective effects remain to be fully elucidated.

Unfortunately, despite promising preclinical evidence, the therapeutic benefits of cannabinoids have not consistently translated into clinical success. A meta-analysis examining outcomes of cannabinoid treatments for PD patients revealed mixed results regarding motor symptom improvement (Urbi, Corbett, et al., 2022). This inconsistency may be due to variability in the type of cannabinoid administered, dosage, treatment duration, or disease stage. Interestingly, although results for overall motor improvements remain inconclusive, several studies reported encouraging outcomes for the treatment of specific symptoms such as tremors and dyskinesia using CB1R agonists (Kibret et al., 2023; Urbi, Corbett, et al., 2022). It is known that glutamatergic input to DA neurons increases following DA degeneration in PD (Campanelli et al., 2022). While the current study observed CB1R localization predominantly on inhibitory terminals, it is plausible that disease progression alters the balance between excitatory and inhibitory inputs to DA neurons, along with changes in CB1R distribution. Under such conditions, CB1R agonists might preferentially suppress excessive excitatory transmission, thereby reducing tremors and dyskinetic movements (Kibret et al., 2023; Urbi, Corbett, et al., 2022). Conversely, such suppression may also exacerbate bradykinesia. Ultimately, a clearer understanding of CB1R localization and function in PD is essential to consider cannabinoids for effective PD treatments, especially given the conflicting findings reported by post-mortem analyses and in vivo radiotracer imaging studies regarding CB1R expression and bioavailability (Hurley et al., 2003; Van Laere et al., 2012).

4.6.2 Implications for schizophrenia and psychosis-related disorders

Preclinical and clinical studies have consistently demonstrated a strong association between elevated midbrain dopaminergic activity and the manifestation of psychosis, as well as the positive and cognitive symptoms of schizophrenia (Abi-Dargham et al., 2009; Conn et al., 2020; Kesby et al., 2018; McCutcheon et al., 2019; Steeds et al., 2015). Moreover, first-generation (typical) antipsychotic medications, which primarily act as a post-synaptic blockade to D2 receptors, have been effective in alleviating positive symptoms (i.e. hallucinations, delusions etc.) and second-generation (atypical) antipsychotics, which antagonize both DA and serotonin

receptors, have shown efficacy in reducing both positive and negative symptoms (Aringhieri et al., 2018; Ayano, 2016; Richelson & Souder, 2000; Weston-Green, 2022). These findings suggest that modulation of dopaminergic signaling—particularly via alternative neural mechanisms—may hold therapeutic potential for mitigating positive symptoms of schizophrenia, while potentially minimizing the adverse side effects commonly associated with conventional antipsychotics (Stroup & Gray, 2018). Given the idea that the ECS regulates dopaminergic neuron excitability, it is plausible that targeted ECS modulation could represent a novel avenue for therapeutic intervention in schizophrenia.

Meta-analyses examining the relationship between cannabis use and the development of psychotic symptoms and schizophrenia have consistently concluded that cannabis use is associated with an increased risk of psychotic illness, with greater frequency and quantity of use correlating with higher risk (Henquet et al., 2005; Moore et al., 2007). However, it remains unclear which specific component of cannabis—known to contain hundreds of biologically active compounds—is primarily responsible for these effects. Cannabis products sold for recreational use often have high concentrations of THC, a CB1R agonist. Based on the rationale presented in this study, elevated THC intake may enhance dopaminergic neuron firing and increase dopamine release in target regions, thereby exacerbating psychotic symptoms. Supporting this, THC-induced psychotic-like symptoms have been demonstrated in controlled human studies (D'Souza et al., 2004, 2005, 2009). Conversely, it follows that a compound with CB1R antagonist properties could counteract this effect by enhancing inhibitory input to dopaminergic neurons, thereby reducing DA activity and potentially mitigating psychotic symptoms. This suggests that CB1R antagonism may represent a promising pharmacological strategy for modulating dopamine dysregulation in psychosis.

Rodent studies employing CBD (a partial CB1R antagonist), rimonabant (SR141716; a potent CB1R antagonist), as well as other CB1R antagonists such as AVE1625 and AM251, have demonstrated reductions in both positive and cognitive deficits characteristic of schizophrenia in preclinical models (Ballmaier et al., 2007; Black et al., 2011; Poncelet et al., 1999). These findings support the potential therapeutic relevance of CB1R antagonism in modulating schizophrenia-related symptomatology. In the clinical domain, there have also been encouraging results. For example, Leweke and coworkers (2012) conducted a double-blind, randomized clinical trial administering CBD to patients with acute schizophrenia, reporting significant reductions in

psychotic symptoms. Interestingly, this clinical improvement was accompanied by elevated serum levels of anandamide—an endogenous CB1R agonist—suggesting that the therapeutic effects observed may not be solely attributable to CB1R antagonism, but potentially involve modulation of endocannabinoid metabolism or other signaling pathways. These clinical outcomes, along with mixed results from other studies (Leweke et al., 2016; Roser et al., 2010), underscore both the complexity of schizophrenia and the multifaceted role of the endocannabinoid system, reinforcing the need for continued investigation into ECS mechanisms if cannabinoid-based therapies are to be effectively developed for this disorder.

4.6.3 Implications for substance use disorders

Major drugs of abuse have been extensively shown to increase dopaminergic firing from the VTA to the nucleus accumbens, a pathway that strongly influences reward-seeking behaviour (Di Chiara et al., 2004; Maldonado, 2003). While promising treatments for SUDs are emerging—such as opioid agonist therapies for opioid addiction—effective pharmacological interventions remain limited for substances like alcohol, nicotine, cannabis, and psychostimulants. Although the present study indicates that CB1R density is relatively lower in the VTA compared to the SNc and SNr, CB1Rs are nonetheless present within the VTA. Moreover, given the likelihood that dopaminergic processes from the VTA extend into the SNr, where they may be influenced by CB1R-positive inputs, it remains plausible that the ECS modulates mesolimbic and mesocortical DA circuits that are critically involved in addiction.

The findings of this study suggest that CB1Rs localize to both excitatory and inhibitory synaptic terminals. In the context of SUDs, CB1R activation on glutamatergic terminals would be expected to suppress excitatory input to dopaminergic neurons, potentially resulting in decreased dopaminergic activity and a corresponding reduction in addictive behaviours. In contrast, CB1R activation on GABAergic terminals would reduce inhibitory input onto dopaminergic neurons, leading to disinhibition, increased firing, and elevated dopamine release—mechanisms commonly associated with reinforcement and addiction. Given that the predominant synaptic tone onto midbrain dopamine neurons was found to be inhibitory, it follows that CB1R antagonism may be particularly effective in treating SUDs by restoring inhibitory control and reducing dopamine output to the striatum and cortical regions. This rationale has been previously proposed (Parsons & Hurd, 2015) and has been validated by preclinical studies. In rodent models of addiction, in which substances such as nicotine and alcohol elicit elevations in DA signaling, both genetic and

pharmacological blockade of CB1Rs have been shown to reduce drug-seeking and addictive behaviours (Cohen et al., 2002; Hungund et al., 2003; Soria et al., 2005). Similarly, in self-administration models involving substances such as morphine, heroin, and ethanol, CB1R antagonism—particularly with rimonabant—led to reduced drug intake and self-administration behaviour by animals (Arnone et al., 1997; Navarro et al., 2001, 2004). Conversely, administration of CB1R agonists has been shown to increase drug-seeking behaviour and substance preference, such as enhanced ethanol consumption (Colombo et al., 2002; Gallate et al., 1999), further supporting the role of CB1R signaling in the modulation of addictive behaviours.

It is important to acknowledge that the neuroscience of addiction is far more complex than the preceding discussion may suggest; it cannot be reduced to simply decreasing global dopamine output. In chronic drug users, for example, there is often a downregulation of dopamine receptors, blunted dopamine release, and a general desensitization of the reward system (Koob & Volkow, 2010; Volkow et al., 2007, 2010, 2011). This raises an important question: why would CB1R antagonists—which further reduce dopamine signaling—be effective in reducing addictive behaviours? One explanation is that CB1R antagonists help by blunting drug-induced dopamine surges particularly during periods of active use, thereby reducing the reinforcing and rewarding effects of substance use, although this has not explicitly been explored. Furthermore, CB1Rs—shown in this study to be highly concentrated in the hippocampus, a region critically involved in memory—may weaken drug-cue associations when blocked. This in turn could support a reduction in craving and relapse.

An additional layer of complexity is that CB1Rs themselves can become less available with chronic drug use (Ceccarini et al., 2014; Hirvonen et al., 2012). This raises a conceptual concern: if CB1R signaling is already diminished, what benefit is gained by further antagonizing the system? One idea is that decreased CB1R availability is likely uneven across brain regions and synapse types, demonstrated in the case of chronic cannabis use by Hirvonen and coworkers (2012). For example, CB1Rs on glutamatergic and GABAergic terminals may be differentially affected, and residual CB1R activity—particularly in regions critical to reward and habit—may still contribute to maladaptive signaling. In this context, CB1R antagonism may be beneficial by disrupting what remains of a dysregulated system, thereby aiding in the restoration of neural balance and reducing compulsive drug-seeking behaviour.

In clinical trials, rimonabant initially showed promising results in the treatment of SUDs and obesity, and was even approved and commercialized in several countries (Sam et al., 2011). However, it was later withdrawn from the market due to severe adverse effects, including depression and increased risk of suicidality (Manzanares et al., 2018; Soler-Cedeno & Xi, 2022). One proposed explanation for these effects is that rimonabant acts not only as a receptor antagonist, but as an inverse agonist—meaning it actively suppresses the baseline activity of CB1Rs, which are known to exhibit low-level signaling even in the absence of endogenous cannabinoids (Soler-Cedeno & Xi, 2022). In response to these issues, neutral CB1R antagonists and allosteric modulators have been investigated as alternative strategies. Compounds such as PIMSR, AM4113, and AM6527 have demonstrated encouraging results, appearing to preserve the therapeutic benefits of rimonabant while minimizing adverse psychological side effects (Soler-Cedeño et al., 2024; Soler-Cedeno & Xi, 2022). Nonetheless, the rise and fall of rimonabant as a potential treatment underscores the intricate nature of the endocannabinoid system and the broader neural circuits involved in addiction. It highlights the need for a more nuanced understanding of CB1R pharmacology before the development and widespread adoption of cannabinoid-based therapeutics for SUDs can be realized.

4.7 Limitations and future directions

Although this study provides novel contributions to our understanding of CB1R distribution in dopamine-rich regions of the midbrain, it is important to acknowledge limitations in study methodology, data interpretation, and generalizability. A major challenge encountered was balancing immunohistochemical techniques to achieve both sufficient and specific staining while preserving tissue integrity for ultrastructural analysis. Visualizing tyrosine hydroxylase (TH), an enzyme localized within cell bodies and neurites, required permeabilization of plasma membranes to allow antibody access. However, because CB1Rs are predominantly localized to the external plasma membrane, preserving membrane integrity was critical, creating a degree of conflict between staining needs. To address this, saponin—a milder permeabilizing agent—was employed instead of harsher agents like Triton X, which had been previously used in the laboratory. Nonetheless, the extensive treatment required to achieve optimal staining unfavorably contributed to tissue fragility and morphological degradation. This effect was particularly pronounced in the SNr, where the tissue is composed primarily of a delicate meshwork of neurites, in contrast to the neuron body-dense regions of the SNc and VTA. Although co-incubation of antibodies was

initially trialed during protocol optimization to reduce the duration of immunohistochemical processing, the combination of silver enhancement and DAB staining resulted in stain crossover, compromising specificity. Consequently, sequential antibody incubations and staining steps were adopted. The progressive loss of tissue integrity throughout staining procedures is evident when comparing morphological TEM micrographs, TH-DAB staining alone, and TH-DAB combined with CB1R-gold and silver enhancement techniques (**Figs. 21, 22**).

When considering the confocal microscopy data, although staining appeared specific when compared to negative controls processed simultaneously without primary antibody, some background staining was evident for CB1R at low magnification, as well as capillary staining visible with GAD67 (Fig. 2). As previously noted, the absence of background staining at higher magnifications suggests that the observed artifacts were optical in origin, potentially arising from increased signal integration across a thicker optical section, elevated exposure times, greater laser power requirements, or resolution constraints inherent to lower magnifications. The GAD67-positive staining observed in capillaries can be attributed to the antibody selection: the GAD67 primary antibody was raised in mouse, necessitating the use of an anti-mouse secondary antibody. Since this study was conducted in mice, endogenous immunoglobulins which are particularly abundant in blood vessels, were also targeted by the secondary antibody, leading to nonspecific capillary staining. Although this issue could potentially have been avoided by selecting a different antibody combination, antibodies were chosen based on careful consideration of prior successful protocols in the laboratory and commercial availability at the time of the study.

When considering these limitations, it is important to note that both immunoelectron microscopy and confocal micrograph data collection had inherent challenges. First, the loss of tissue integrity observed in TEM images invariably made it more difficult to accurately trace terminals and distinguish synapse types. Furthermore, given that immunoelectron microscopy is typically limited to two labels—discrete immunogold particles and the diffuse staining characteristic of DAB—incorporating an additional stain to definitively identify presynaptic terminal type (e.g., VGAT or VGlut2) was not feasible. Although dual labeling with different-sized immunoparticles was initially trialed during protocol optimization, it was unsuccessful due to poor permeabilization of larger particles. In future work, it would be valuable to cross-validate CB1R immunoparticle localization by adapting the current protocol to incorporate VGAT- or VGlut2-DAB staining in combination with CB1R-gold. Second, although ultrathin sectioning was

performed carefully and grazing sections were intentionally targeted, some variability in the depth of tissue sectioned likely occurred. As staining intensity is highest near the tissue surface, differences in cutting depth may have led to inconsistent detection of CB1R density, potentially creating the appearance of artificially higher or lower CB1R expression across regions. Third, as indicated by the confocal data, CB1R staining was most prominent in the SNr and at the border between the SNr and SNc. Consequently, regional selection could have influenced the results: if areas closer to the SNr-SNc boundary were chosen, CB1R-positive counts within the SNc would appear elevated compared to regions selected farther from the border.

Regarding confocal data collection specifically, MFI measurements were obtained at the low magnification shown in **Figure 10**, meaning background fluorescence and capillary-associated staining could have contributed to mean gray values obtained by FIJI software, potentially skewing results. Notably, some of the variability observed in MFI measurements across brain sections from the same animals may reflect true anatomical differences along the medial-to-lateral axis of each midbrain region, as sections were sampled from the beginning, middle, and end of each structure.

Finally, it is important to note that this study examined only male mice aged 3–6 months, corresponding to young to middle-aged adulthood in humans (Jackson et al., 2017). Consequently, potential differences in CB1R distribution in the midbrain across ages and sexes were not captured. Previous research has demonstrated that CB1R distribution varies significantly between sexes and across the lifespan in both rodents and humans across various brain regions (Laurikainen et al., 2019; Xing et al., 2014), making it highly plausible that similar variations exist within the midbrain. Understanding these differences would provide valuable insights into the role of the ECS in DA-related diseases. Furthermore, although substantial research has explored the function of CB1Rs in relation to dopaminergic systems and associated disease states, important gaps in knowledge remain, representing a promising direction for future investigation.

4.8 Conclusions

The ECS is a complex neuromodulatory network that exerts control over numerous neural systems, including the DA-rich nigrostriatal, mesocortical, and mesolimbic pathways of the midbrain. For the first time, this study employed immunoelectron microscopy, complemented by confocal microscopy, to semi-quantitatively assess the distribution of CB1Rs on synapses contacting DA neurons within the SNc, SNr, and VTA. Our findings indicate that among CB1R-positive terminals contacting DA compartments, CB1Rs are primarily localized to inhibitory

terminals and are most frequently found in the SNr, to a lesser extent in the SNc, and least in the VTA. Advancing our understanding of CB1R distribution and function within DA-rich brain regions offers valuable insights into how the ECS modulates DA neuron activity, ultimately contributing to our knowledge of DA-related diseases and informing the development of novel therapeutic strategies.

References

Abi-Dargham, A., van de Giessen, E., Slifstein, M., Kegeles, L. S., & Laruelle, M. (2009). Baseline and amphetamine-stimulated dopamine activity are related in drug-naïve schizophrenic subjects. *Biological Psychiatry*, *65*(12), 1091–1093. https://doi.org/10.1016/j.biopsych.2008.12.007

Aringhieri, S., Carli, M., Kolachalam, S., Verdesca, V., Cini, E., Rossi, M., McCormick, P. J., Corsini, G. U., Maggio, R., & Scarselli, M. (2018). Molecular targets of atypical antipsychotics: From mechanism of action to clinical differences. *Pharmacology & Therapeutics*, *192*, 20–41. https://doi.org/10.1016/j.pharmthera.2018.06.012

Arnone, M., Maruani, J., Chaperon, F., Thiébot, M. H., Poncelet, M., Soubrié, P., & Le Fur, G. (1997). Selective inhibition of sucrose and ethanol intake by SR 141716, an antagonist of central cannabinoid (CB1) receptors. *Psychopharmacology*, *132*(1), 104–106. https://doi.org/10.1007/s002130050326

Ayano, G. (2016). First Generation Antipsychotics: Pharmacokinetics, Pharmacodynamics, Therapeutic Effects and Side Effects: A Review. *Research & Reviews: Journal of Chemistry*, *5*(3), 53–63.

Bach, J.-P., Ziegler, U., Deuschl, G., Dodel, R., & Doblhammer-Reiter, G. (2011). Projected numbers of people with movement disorders in the years 2030 and 2050. *Movement Disorders: Official Journal of the Movement Disorder Society*, *26*(12), 2286–2290. https://doi.org/10.1002/mds.23878

Baddenhausen, S., Lutz, B., & Hofmann, C. (2024). Cannabinoid type-1 receptor signaling in dopaminergic Engrailed-1 expressing neurons modulates motivation and depressive-like behavior. *Frontiers in Molecular Neuroscience*, *17*. https://doi.org/10.3389/fnmol.2024.1379889

Ballmaier, M., Bortolato, M., Rizzetti, C., Zoli, M., Gessa, G., Heinz, A., & Spano, P. (2007). Cannabinoid Receptor Antagonists Counteract Sensorimotor Gating Deficits in the Phencyclidine Model of Psychosis. *Neuropsychopharmacology*, *32*(10), 2098–2107. https://doi.org/10.1038/sj.npp.1301344

Black, M. D., Stevens, R. J., Rogacki, N., Featherstone, R. E., Senyah, Y., Giardino, O., Borowsky, B., Stemmelin, J., Cohen, C., Pichat, P., Arad, M., Barak, S., De Levie, A., Weiner, I., Griebel, G., & Varty, G. B. (2011). AVE1625, a cannabinoid CB1 receptor antagonist, as a co-treatment with antipsychotics for schizophrenia: Improvement in cognitive function and reduction of antipsychotic-side effects in rodents. *Psychopharmacology*, *215*(1), 149–163. https://doi.org/10.1007/s00213-010-2124-0

Bonilla-Del Río, I., Puente, N., Mimenza, A., Ramos, A., Serrano, M., Lekunberri, L., Gerrikagoitia, I., Christie, B. R., Nahirney, P. C., & Grandes, P. (2021). Acute Δ9 - tetrahydrocannabinol prompts rapid changes in cannabinoid CB 1 receptor immunolabeling and subcellular structure in CA1 hippocampus of young adult male mice. *Journal of Comparative Neurology (1911)*, *529*(9), 2332–2346. https://doi.org/10.1002/cne.25098

Busquets-Garcia, A., Bains, J., & Marsicano, G. (2018). CB1 Receptor Signaling in the Brain: Extracting Specificity from Ubiquity. *Neuropsychopharmacology*, *43*(1), 4–20. https://doi.org/10.1038/npp.2017.206

Campanelli, F., Natale, G., Marino, G., Ghiglieri, V., & Calabresi, P. (2022). Striatal glutamatergic hyperactivity in Parkinson's disease. *Neurobiology of Disease*, *168*, 105697. https://doi.org/10.1016/j.nbd.2022.105697

Canada, P. H. A. of. (2020, July 6). *Schizophrenia in Canada* [Guidance]. https://www.canada.ca/en/public-health/services/publications/diseases-conditions/schizophrenia-canada.html

Carlsson, A. (2002). Treatment of Parkinson's with L-DOPA. The early discovery phase, and a comment on current problems. *Journal of Neural Transmission*, *109*(5), 777–787. https://doi.org/10.1007/s007020200064

Ceccarini, J., Hompes, T., Verhaeghen, A., Casteels, C., Peuskens, H., Bormans, G., Claes, S., & Laere, K. V. (2014). Changes in Cerebral CB1 Receptor Availability after Acute and Chronic Alcohol Abuse and Monitored Abstinence. *Journal of Neuroscience*, *34*(8), 2822–2831. https://doi.org/10.1523/JNEUROSCI.0849-13.2014

Cohen, C., Perrault, G., Voltz, C., Steinberg, R., & Soubrié, P. (2002). SR141716, a central cannabinoid (CB1) receptor antagonist, blocks the motivational and dopamine-releasing effects of nicotine in rats. *Behavioural Pharmacology*, *13*(5), 451.

Colombo, G., Serra, S., Brunetti, G., Gomez, R., Melis, S., Vacca, G., Carai, M. A., & Gessa, G. (2002). Stimulation of voluntary ethanol intake by cannabinoid receptor agonists in ethanol-preferring sP rats. *Psychopharmacology*, *159*(2), 181–187. https://doi.org/10.1007/s002130100887

Conn, K.-A., Burne, T. H. J., & Kesby, J. P. (2020). Subcortical Dopamine and Cognition in Schizophrenia: Looking Beyond Psychosis in Preclinical Models. *Frontiers in Neuroscience*, *14*. https://doi.org/10.3389/fnins.2020.00542

Copas, C. (2023). *Ultrastructural analysis of synaptic inputs to dopamine neurons in the substantia nigra pars compacta and the ventral tegmental area*. University of Victoria.

Dahlstroem, A., & Fuxe, K. (1964). Evidence For the Existence of Monoamine-Containing Neurons in the Central Nervous System. I. Demonstration of Monoamines in the Cell Bodies of Brain Stem Neurons. *Acta Physiologica Scandinavica. Supplementum*, SUPPL 232:1-55.

Daubner, S. C., Le, T., & Wang, S. (2011). Tyrosine hydroxylase and regulation of dopamine synthesis. *Archives of Biochemistry and Biophysics*, *508*(1), 1–12. https://doi.org/10.1016/j.abb.2010.12.017

Deniau, J. M., Kitai, S. T., Donoghue, J. P., & Grofova, I. (1982). Neuronal interactions in the substantia nigra pars reticulata through axon collaterals of the projection neurons. *Experimental Brain Research*, *47*(1), 105–113. https://doi.org/10.1007/BF00235891

Deniau, J. M., Mailly, P., Maurice, N., & Charpier, S. (2007). The pars reticulata of the substantia nigra: A window to basal ganglia output. *Progress in Brain Research*, *160*, 151–172. https://doi.org/10.1016/S0079-6123(06)60009-5

Di Chiara, G., Bassareo, V., Fenu, S., De Luca, M. A., Spina, L., Cadoni, C., Acquas, E., Carboni, E., Valentini, V., & Lecca, D. (2004). Dopamine and drug addiction: The nucleus accumbens shell connection. *Neuropharmacology*, *47*, 227–241. https://doi.org/10.1016/j.neuropharm.2004.06.032

Diana, M. A., Levenes, C., Mackie, K., & Marty, A. (2002). Short-Term Retrograde Inhibition of GABAergic Synaptic Currents in Rat Purkinje Cells Is Mediated by Endogenous Cannabinoids. *Journal of Neuroscience*, *22*(1), 200–208. https://doi.org/10.1523/JNEUROSCI.22-01-00200.2002

D'Souza, D. C., Abi-Saab, W. M., Madonick, S., Forselius-Bielen, K., Doersch, A., Braley, G., Gueorguieva, R., Cooper, T. B., & Krystal, J. H. (2005). Delta-9-tetrahydrocannabinol effects in schizophrenia: Implications for cognition, psychosis, and addiction. *Biological Psychiatry*, *57*(6), 594–608. https://doi.org/10.1016/j.biopsych.2004.12.006

D'Souza, D. C., Perry, E., MacDougall, L., Ammerman, Y., Cooper, T., Wu, Y.-T., Braley, G., Gueorguieva, R., & Krystal, J. H. (2004). The psychotomimetic effects of intravenous delta-9-tetrahydrocannabinol in healthy individuals: Implications for psychosis. *Neuropsychopharmacology: Official Publication of the American College of Neuropsychopharmacology*, *29*(8), 1558–1572. https://doi.org/10.1038/sj.npp.1300496

D'Souza, D. C., Sewell, R. A., & Ranganathan, M. (2009). Cannabis and psychosis/schizophrenia: Human studies. *European Archives of Psychiatry and Clinical Neuroscience*, *259*(7), 413–431. https://doi.org/10.1007/s00406-009-0024-2

Durand-de Cuttoli, R., Mondoloni, S., Marti, F., Lemoine, D., Nguyen, C., Naudé, J., d'Izarny-Gargas, T., Pons, S., Maskos, U., Trauner, D., Kramer, R. H., Faure, P., & Mourot, A. (2018). Manipulating midbrain dopamine neurons and reward-related behaviors with light-controllable nicotinic acetylcholine receptors. *eLife*, *7*, e37487. https://doi.org/10.7554/eLife.37487

Escamilla-Ramírez, A., García, E., Palencia-Hernández, G., Colín-González, A. L., Galván-Arzate, S., Túnez, I., Sotelo, J., & Santamaría, A. (2017). URB597 and the Cannabinoid WIN55,212-2 Reduce Behavioral and Neurochemical Deficits Induced by MPTP in Mice: Possible Role of Redox Modulation and NMDA Receptors. *Neurotoxicity Research*, *31*(4), 532–544. https://doi.org/10.1007/s12640-016-9698-1

Estakhr, J., Abazari, D., Frisby, K., McIntosh, J. M., & Nashmi, R. (2017). Differential Control of Dopaminergic Excitability and Locomotion by Cholinergic Inputs in Mouse Substantia Nigra. *Current Biology: CB*, *27*(13), 1900-1914.e4. https://doi.org/10.1016/j.cub.2017.05.084

Fernández-Ruiz, J. (2009). The endocannabinoid system as a target for the treatment of motor dysfunction. *British Journal of Pharmacology*, *156*(7), 1029–1040. https://doi.org/10.1111/j.1476-5381.2008.00088.x

Filion, M. (1979). Effects of interruption of the nigrostriatal pathway and of dopaminergic agents on the spontaneous activity of globus pallidus neurons in the awake monkey. *Brain Research*, *178*(2), 425–441. https://doi.org/10.1016/0006-8993(79)90704-2

Fitzgerald, M. L., Shobin, E., & Pickel, V. M. (2012). Cannabinoid modulation of the dopaminergic circuitry: Implications for limbic and striatal output. *Progress in Neuro-Psychopharmacology and Biological Psychiatry*, *38*(1), 21–29. https://doi.org/10.1016/j.pnpbp.2011.12.004

Gallate, J. E., Saharov, T., Mallet, P. E., & McGregor, I. S. (1999). Increased motivation for beer in rats following administration of a cannabinoid CB1 receptor agonist. *European Journal of Pharmacology*, *370*(3), 233–240. https://doi.org/10.1016/s0014-2999(99)00170-3

Gantz, S. C., Ford, C. P., Morikawa, H., & Williams, J. T. (2018). The Evolving Understanding of Dopamine Neurons in the Substantia Nigra and Ventral Tegmental Area. *Annual Review of Physiology*, *80*(Volume 80, 2018), 219–241. https://doi.org/10.1146/annurev-physiol-021317-121615

García, C., Palomo-Garo, C., Gómez-Gálvez, Y., & Fernández-Ruiz, J. (2016). Cannabinoid–dopamine interactions in the physiology and physiopathology of the basal ganglia. *British Journal of Pharmacology*, *173*(13), 2069–2079. https://doi.org/10.1111/bph.13215

Glass, M., Faull, R. L. M., & Dragunow, M. (1993). Loss of cannabinoid receptors in the substantia nigra in huntington's disease. *Neuroscience*, *56*(3), 523–527. https://doi.org/10.1016/0306-4522(93)90352-G

Grace, A. A. (1991). Phasic versus tonic dopamine release and the modulation of dopamine system responsivity: A hypothesis for the etiology of schizophrenia. *Neuroscience*, *41*(1), 1–24. https://doi.org/10.1016/0306-4522(91)90196-U

Gutiérrez-Rodríguez, A., Puente, N., Elezgarai, I., Ruehle, S., Lutz, B., Reguero, L., Gerrikagoitia, I., Marsicano, G., & Grandes, P. (2017). Anatomical characterization of the cannabinoid CB1 receptor in cell-type–specific mutant mouse rescue models. *Journal of Comparative Neurology*, *525*(2), 302–318. https://doi.org/10.1002/cne.24066

Han, X., He, Y., Bi, G.-H., Zhang, H.-Y., Song, R., Liu, Q.-R., Egan, J. M., Gardner, E. L., Li, J., & Xi, Z.-X. (2017). CB1 Receptor Activation on VgluT2-Expressing Glutamatergic Neurons Underlies Δ9-Tetrahydrocannabinol (Δ9-THC)-Induced Aversive Effects in Mice. *Scientific Reports*, *7*, 12315. https://doi.org/10.1038/s41598-017-12399-z

He, C.-B., Jin, Y., Li, Y., Zhang, Q., Yang, B., Xu, M., Yang, J., Yi, X.-N., Dong, Y.-L., Wang, J., & Li, Y.-Q. (2023). Collateral projections from the ventral tegmental area/substantia nigra pars compacta to the nucleus accumbens and insular cortex in the rat. *Anatomical Science International*, *98*(4), 580–592. https://doi.org/10.1007/s12565-023-00728-4

Henquet, C., Murray, R., Linszen, D., & van Os, J. (2005). The environment and schizophrenia: The role of cannabis use. *Schizophrenia Bulletin*, *31*(3), 608–612. https://doi.org/10.1093/schbul/sbi027

Herkenham, M., Lynn, A. B., de Costa, B. R., & Richfield, E. K. (1991). Neuronal localization of cannabinoid receptors in the basal ganglia of the rat. *Brain Research*, *547*(2), 267–274. https://doi.org/10.1016/0006-8993(91)90970-7

Hirvonen, J., Goodwin, R. S., Li, C.-T., Terry, G. E., Zoghbi, S. S., Morse, C., Pike, V. W., Volkow, N. D., Huestis, M. A., & Innis, R. B. (2012). Reversible and regionally selective downregulation of brain cannabinoid CB1 receptors in chronic daily cannabis smokers. *Molecular Psychiatry*, *17*(6), 642–649. https://doi.org/10.1038/mp.2011.82

Hornykiewicz, O. (2008). Basic research on dopamine in Parkinson's disease and the discovery of the nigrostriatal dopamine pathway: The view of an eyewitness. *Neuro-Degenerative Diseases*, *5*(3–4), 114–117. https://doi.org/10.1159/000113678

Hungund, B. L., Szakall, I., Adam, A., Basavarajappa, B. S., & Vadasz, C. (2003). Cannabinoid CB1 receptor knockout mice exhibit markedly reduced voluntary alcohol consumption and lack alcohol-induced dopamine release in the nucleus accumbens. *Journal of Neurochemistry*, *84*(4), 698–704. https://doi.org/10.1046/j.1471-4159.2003.01576.x

Hurley, M. J., Mash, D. C., & Jenner, P. (2003). Expression of cannabinoid CB1 receptor mRNA in basal ganglia of normal and parkinsonian human brain. *Journal of Neural Transmission*, *110*(11), 1279–1288. https://doi.org/10.1007/s00702-003-0033-7

Ikemoto, S. (2007). Dopamine reward circuitry: Two projection systems from the ventral midbrain to the nucleus accumbens–olfactory tubercle complex. *Brain Research Reviews*, *56*(1), 27–78. https://doi.org/10.1016/j.brainresrev.2007.05.004

Jackson, S. J., Andrews, N., Ball, D., Bellantuono, I., Gray, J., Hachoumi, L., Holmes, A., Latcham, J., Petrie, A., Potter, P., Rice, A., Ritchie, A., Stewart, M., Strepka, C., Yeoman, M., & Chapman, K. (2017). Does age matter? The impact of rodent age on study outcomes. *Laboratory Animals*, *51*(2), 160–169. https://doi.org/10.1177/0023677216653984

Julian, M. D., Martin, A. B., Cuellar, B., Rodriguez De Fonseca, F., Navarro, M., Moratalla, R., & Garcia-Segura, L. M. (2003). Neuroanatomical relationship between type 1 cannabinoid receptors and dopaminergic systems in the rat basal ganglia. *Neuroscience*, *119*(1), 309–318. https://doi.org/10.1016/S0306-4522(03)00070-8

Katona, I., Sperlágh, B., Sík, A., Käfalvi, A., Vizi, E. S., Mackie, K., & Freund, T. F. (1999). Presynaptically located CB1 cannabinoid receptors regulate GABA release from axon terminals of specific hippocampal interneurons. *The Journal of Neuroscience: The Official Journal of the Society for Neuroscience*, *19*(11), 4544–4558. https://doi.org/10.1523/JNEUROSCI.19-11-04544.1999

Kawamura, Y., Fukaya, M., Maejima, T., Yoshida, T., Miura, E., Watanabe, M., Ohno-Shosaku, T., & Kano, M. (2006). The CB1 cannabinoid receptor is the major cannabinoid receptor at excitatory presynaptic sites in the hippocampus and cerebellum. *The Journal of Neuroscience: The Official Journal of the Society for Neuroscience*, *26*(11), 2991–3001. https://doi.org/10.1523/JNEUROSCI.4872-05.2006

Kesby, J. P., Eyles, D. W., McGrath, J. J., & Scott, J. G. (2018). Dopamine, psychosis and schizophrenia: The widening gap between basic and clinical neuroscience. *Translational Psychiatry*, *8*(1), 1–12. https://doi.org/10.1038/s41398-017-0071-9

Kibret, B. G., Canseco-Alba, A., Onaivi, E. S., & Engidawork, E. (2023). Crosstalk between the endocannabinoid and mid-brain dopaminergic systems: Implication in dopamine dysregulation. *Frontiers in Behavioral Neuroscience*, *17*. https://www.frontiersin.org/articles/10.3389/fnbeh.2023.1137957

Kishimoto, Y., & Kano, M. (2006). Endogenous cannabinoid signaling through the CB1 receptor is essential for cerebellum-dependent discrete motor learning. *The Journal of Neuroscience: The Official Journal of the Society for Neuroscience*, *26*(34), 8829–8837. https://doi.org/10.1523/JNEUROSCI.1236-06.2006

Koob, G. F., & Volkow, N. D. (2010). Neurocircuitry of Addiction. *Neuropsychopharmacology*, *35*(1), 217–238. https://doi.org/10.1038/npp.2009.110

Laurikainen, H., Tuominen, L., Tikka, M., Merisaari, H., Armio, R.-L., Sormunen, E., Borgan, F., Veronese, M., Howes, O., Haaparanta-Solin, M., Solin, O., & Hietala, J. (2019). Sex difference in brain CB1 receptor availability in man. *NeuroImage*, *184*, 834–842. https://doi.org/10.1016/j.neuroimage.2018.10.013

Le Gratiet, K. L., Anderson, C. K., Puente, N., Grandes, P., Copas, C., Nahirney, P. C., Delaney, K. R., & Nashmi, R. (2022). Differential Subcellular Distribution and Release Dynamics of Cotransmitted Cholinergic and GABAergic Synaptic Inputs Modify Dopaminergic Neuronal Excitability. *The Journal of Neuroscience: The Official Journal of the Society for Neuroscience*, *42*(46), 8670–8693. https://doi.org/10.1523/JNEUROSCI.2514-21.2022

Leweke, F. M., Mueller, J. K., Lange, B., & Rohleder, C. (2016). Therapeutic Potential of Cannabinoids in Psychosis. *Biological Psychiatry*, *79*(7), 604–612. https://doi.org/10.1016/j.biopsych.2015.11.018

Leweke, F. M., Piomelli, D., Pahlisch, F., Muhl, D., Gerth, C. W., Hoyer, C., Klosterkötter, J., Hellmich, M., & Koethe, D. (2012). Cannabidiol enhances anandamide signaling and alleviates psychotic symptoms of schizophrenia. *Translational Psychiatry*, *2*(3), e94–e94. https://doi.org/10.1038/tp.2012.15

Lu, H.-C., & Mackie, K. (2016). An Introduction to the Endogenous Cannabinoid System. *Biological Psychiatry*, *79*(7), 516–525. https://doi.org/10.1016/j.biopsych.2015.07.028

Maldonado, R. (2003). The neurobiology of addiction. In W. W. Fleischhacker & D. J. Brooks (Eds.), *Addiction Mechanisms, Phenomenology and Treatment* (pp. 1–14). Springer. https://doi.org/10.1007/978-3-7091-0541-2_1

Manzanares, J., Cabañero, D., Puente, N., García-Gutiérrez, M. S., Grandes, P., & Maldonado, R. (2018). Role of the endocannabinoid system in drug addiction. *Biochemical Pharmacology*, *157*, 108–121. https://doi.org/10.1016/j.bcp.2018.09.013

Margolis, E. B., Lock, H., Hjelmstad, G. O., & Fields, H. L. (2006). The ventral tegmental area revisited: Is there an electrophysiological marker for dopaminergic neurons? *The Journal of Physiology*, *577*(3), 907–924. https://doi.org/10.1113/jphysiol.2006.117069

Margolis, E. B., Toy, B., Himmels, P., Morales, M., & Fields, H. L. (2012). Identification of Rat Ventral Tegmental Area GABAergic Neurons. *PLOS ONE*, *7*(7), e42365. https://doi.org/10.1371/journal.pone.0042365

McCutcheon, R. A., Abi-Dargham, A., & Howes, O. D. (2019). Schizophrenia, Dopamine and the Striatum: From Biology to Symptoms. *Trends in Neurosciences*, *42*(3), 205–220. https://doi.org/10.1016/j.tins.2018.12.004

McElvain, L. E., Chen, Y., Moore, J. D., Brigidi, G. S., Bloodgood, B. L., Lim, B. K., Costa, R. M., & Kleinfeld, D. (2021). Specific populations of basal ganglia output neurons target distinct brain stem areas while collateralizing throughout the diencephalon. *Neuron*, *109*(10), 1721-1738.e4. https://doi.org/10.1016/j.neuron.2021.03.017

Mena-Segovia, J., Winn, P., & Bolam, J. P. (2008). Cholinergic modulation of midbrain dopaminergic systems. *Brain Research Reviews*, *58*(2), 265–271. https://doi.org/10.1016/j.brainresrev.2008.02.003

Mielnik, C. A., Sugamori, K. S., Finlay, D. B., Thorpe, H. H. A., Schapira, M., Sivananthan, N., Li, C. K., Lam, V. M., Harrington, S., Abdelrahman, M. H., Trembleau, L. A., McIntyre Burnham, W., Khokhar, J. Y., Salahpour, A., Ramsey, A. J., Glass, M., Greig, I. R., & Ross, R. A. (2021). A novel allosteric modulator of the cannabinoid CB1 receptor ameliorates hyperdopaminergia endophenotypes in rodent models. *Neuropsychopharmacology*, *46*(2), 413–422. https://doi.org/10.1038/s41386-020-00876-5

Misgeld, U. (2004). Innervation of the substantia nigra. *Cell and Tissue Research*, *318*(1), 107–114. https://doi.org/10.1007/s00441-004-0918-2

Moore, T. H., Zammit, S., Lingford-Hughes, A., Barnes, T. R., Jones, P. B., Burke, M., & Lewis, G. (2007). Cannabis use and risk of psychotic or affective mental health outcomes: A systematic review. *The Lancet*, *370*(9584), 319–328. https://doi.org/10.1016/S0140-6736(07)61162-3

Morales, M., & Margolis, E. B. (2017). Ventral tegmental area: Cellular heterogeneity, connectivity and behaviour. *Nature Reviews Neuroscience*, *18*(2), 73–85. https://doi.org/10.1038/nrn.2016.165

More, S. V., & Choi, D.-K. (2015). Promising cannabinoid-based therapies for Parkinson's disease: Motor symptoms to neuroprotection. *Molecular Neurodegeneration*, *10*(1), 17. https://doi.org/10.1186/s13024-015-0012-0

Morris, H. R., Spillantini, M. G., Sue, C. M., & Williams-Gray, C. H. (2024). The pathogenesis of Parkinson's disease. *The Lancet*, *403*(10423), 293–304. https://doi.org/10.1016/S0140-6736(23)01478-2

Nauta, W. J. H. (1958). Hippocampal Projections and Related Neural Pathways to the Mid-Brain in the Cat. *Brain*, *81*(3), 319–340. Https://Doi.Org/10.1093/Brain/81.3.319

Navarro, M., Carrera, M. R. A., del Arco, I., Trigo, J. M., Koob, G. F., & Rodríguez de Fonseca, F. (2004). Cannabinoid receptor antagonist reduces heroin self-administration only in dependent rats. *European Journal of Pharmacology*, *501*(1), 235–237. https://doi.org/10.1016/j.ejphar.2004.08.022

Navarro, M., Carrera, M. R. A., Fratta, W., Valverde, O., Cossu, G., Fattore, L., Chowen, J. A., Gómez, R., Arco, I. del, Villanúa, M. A., Maldonado, R., Koob, G. F., & Fonseca, F. R. de. (2001). Functional Interaction between Opioid and Cannabinoid Receptors in Drug Self-Administration. *Journal of Neuroscience*, *21*(14), 5344–5350. https://doi.org/10.1523/JNEUROSCI.21-14-05344.2001

Nazarenus, C., & Cox, J. (2019). The Discovery of the Endocannabinoid System. In *Medical Cannabis Handbook* (pp. 28–37). Springer Publishing Company. https://doi.org/10.1891/9780826135735.0003

Olds, J., Killam, K. F., & Bach-y-Rita, P. (1956). Self-Stimulation of the Brain Used as a Screening Method for Tranquilizing Drugs. *Science*, *124*(3215), 265–266. https://doi.org/10.1126/science.124.3215.265

Olds, J., & Milner, P. (1954). Positive reinforcement produced by electrical stimulation of septal area and other regions of rat brain. *Journal of Comparative and Physiological Psychology*, *47*(6), 419–427. https://doi.org/10.1037/h0058775

Olds, J., & Olds, M. E. (1958). Positive reinforcement produced by stimulating hypothalamus with iproniazid and other compounds. *Science (New York, N.Y.)*, *127*(3307), 1175–1176. https://doi.org/10.1126/science.127.3307.1175

Pardo-Garcia, T. R., Garcia-Keller, C., Penaloza, T., Richie, C. T., Pickel, J., Hope, B. T., Harvey, B. K., Kalivas, P. W., & Heinsbroek, J. A. (2019). Ventral Pallidum Is the Primary Target for Accumbens D1 Projections Driving Cocaine Seeking. *The Journal of Neuroscience: The Official Journal of the Society for Neuroscience*, *39*(11), 2041–2051. https://doi.org/10.1523/JNEUROSCI.2822-18.2018

Parent, M., & Parent, A. (2010). Substantia nigra and Parkinson's disease: A brief history of their long and intimate relationship. *The Canadian Journal of Neurological Sciences. Le Journal Canadien Des Sciences Neurologiques*, *37*(3), 313–319. https://doi.org/10.1017/s0317167100010209

Parsons, L. H., & Hurd, Y. L. (2015). Endocannabinoid signalling in reward and addiction. *Nature Reviews Neuroscience*, *16*(10), 579–594. https://doi.org/10.1038/nrn4004

Partanen, J., & Achim, K. (2022). Neurons gating behavior—Developmental, molecular and functional features of neurons in the Substantia Nigra pars reticulata. *Frontiers in Neuroscience*, *16*. https://doi.org/10.3389/fnins.2022.976209

Paxinos, G., & Franklin, K. B. J. (2001). *The Mouse Brain in Stereotaxic Coordinates* (2 edition). Academic Press.

Poncelet, M., Barnouin, M. C., Brelière, J. C., Le Fur, G., & Soubrié, P. (1999). Blockade of cannabinoid (CB1) receptors by 141716 selectively antagonizes drug-induced

reinstatement of exploratory behaviour in gerbils. *Psychopharmacology*, *144*(2), 144–150. https://doi.org/10.1007/s002130050987

Poulin, J.-F., Caronia, G., Hofer, C., Cui, Q., Helm, B., Ramakrishnan, C., Chan, C. S., Dombeck, D. A., Deisseroth, K., & Awatramani, R. (2018). Mapping projections of molecularly defined dopamine neuron subtypes using intersectional genetic approaches. *Nature Neuroscience*, *21*(9), 1260–1271. https://doi.org/10.1038/s41593-018-0203-4

Prensa, L., Giménez-Amaya, J. M., Parent, A., Bernácer, J., & Cebrián, C. (2009). The Nigrostriatal Pathway: Axonal Collateralization and Compartmental Specificity. In G. Giovanni, V. Di Matteo, & E. Esposito (Eds.), *Birth, Life and Death of Dopaminergic Neurons in the Substantia Nigra* (pp. 49–58). Springer. https://doi.org/10.1007/978-3-211-92660-4_4

Puente, N., Río, I. B.-D., Achicallende, S., Nahirney, P. C., & Grandes, P. (2019). High-resolution Immunoelectron Microscopy Techniques for Revealing Distinct Subcellular Type 1 Cannabinoid Receptor Domains in Brain. *Bio-Protocol*, *9*(2), e3145. https://doi.org/10.21769/BioProtoc.3145

Qian, W. (2023). *First Electron Microscope Is Constructed | EBSCO Research Starters*. https://www.ebsco.com/research-starters/history/first-electron-microscope-constructed

Quik, M., & Wonnacott, S. (2011). A6β2* and α4β2* Nicotinic Acetylcholine Receptors As Drug Targets for Parkinson's Disease. *Pharmacological Reviews*, *63*(4), 938–966. https://doi.org/10.1124/pr.110.003269

Ramón y Cajal, S. (1899). *Textura del sistema nervioso del hombre y de los vertebrados: Estudios sobre el plan estructural y composición histológica de los centros nerviosos adicionados de consideraciones fisiológicas fundadas en los nuevos descubrimientos*. https://www.cervantesvirtual.com/obra/textura-del-sistema-nervioso-del-hombre-y-de-los-vertebrados-estudios-sobre-el-plan-estructural-y-composicion-histologica-de-los-centros-nerviosos-adicionados-de-consideraciones-1150918/

Richelson, E., & Souder, T. (2000). Binding of antipsychotic drugs to human brain receptors focus on newer generation compounds. *Life Sciences*, *68*(1), 29–39. https://doi.org/10.1016/s0024-3205(00)00911-5

Ritchie, H., Arriagada, P., & Roser, M. (2022). Opioids, Cocaine, Cannabis, and Other Illicit Drugs. *Our World in Data*. https://ourworldindata.org/illicit-drug-use

Robledo-Menendez, A., Vella, M., Grandes, P., & Soria-Gomez, E. (2022). Cannabinoid control of hippocampal functions: The where matters. *The FEBS Journal*, *289*(8), 2162–2175. https://doi.org/10.1111/febs.15907

Roser, P., Vollenweider ,Franz X., & and Kawohl, W. (2010). Potential antipsychotic properties of central cannabinoid (CB1) receptor antagonists. *The World Journal of Biological Psychiatry*, *11*(2–2), 208–219. https://doi.org/10.3109/15622970801908047

Roth, J. (1996). The silver anniversary of gold: 25 years of the colloidal gold marker system for immunocytochemistry and histochemistry. *Histochemistry and Cell Biology*, *106*(1), 1–8. https://doi.org/10.1007/BF02473197

Sam, A. H., Salem, V., & Ghatei, M. A. (2011). Rimonabant: From RIO to Ban. *Journal of Obesity*, *2011*, 432607. https://doi.org/10.1155/2011/432607

Seamans, J. K., & Yang, C. R. (2004). The principal features and mechanisms of dopamine modulation in the prefrontal cortex. *Progress in Neurobiology*, *74*(1), 1–58. https://doi.org/10.1016/j.pneurobio.2004.05.006

Sheng, W. S., Hu, S., Min, X., Cabral, G. A., Lokensgard, J. R., & Peterson, P. K. (2005). Synthetic cannabinoid WIN55,212-2 inhibits generation of inflammatory mediators by IL-1β-stimulated human astrocytes. *Glia*, *49*(2), 211–219. https://doi.org/10.1002/glia.20108

Skaper, S. D., & Di Marzo, V. (2012). Endocannabinoids in nervous system health and disease: The big picture in a nutshell. *Philosophical Transactions of the Royal Society B: Biological Sciences*, *367*(1607), 3193–3200. https://doi.org/10.1098/rstb.2012.0313

Smith, K. S., Tindell, A. J., Aldridge, J. W., & Berridge, K. C. (2009). Ventral pallidum roles in reward and motivation. *Behavioural Brain Research*, *196*(2), 155–167. https://doi.org/10.1016/j.bbr.2008.09.038

Soares-Cunha, C., Coimbra, B., David-Pereira, A., Borges, S., Pinto, L., Costa, P., Sousa, N., & Rodrigues, A. J. (2016). Activation of D2 dopamine receptor-expressing neurons in the nucleus accumbens increases motivation. *Nature Communications*, *7*(1), 11829. https://doi.org/10.1038/ncomms11829

Soler-Cedeño, O., Alton, H., Bi, G.-H., Linz, E., Ji, L., Makriyannis, A., & Xi, Z.-X. (2024). AM6527, a neutral CB1 receptor antagonist, suppresses opioid taking and seeking, as well as cocaine seeking in rodents without aversive effects. *Neuropsychopharmacology: Official Publication of the American College of Neuropsychopharmacology*, *49*(11), 1678–1688. https://doi.org/10.1038/s41386-024-01861-y

Soler-Cedeno, O., & Xi, Z.-X. (2022). Neutral CB1 Receptor Antagonists as Pharmacotherapies for Substance Use Disorders: Rationale, Evidence, and Challenge. *Cells*, *11*(20), Article 20. https://doi.org/10.3390/cells11203262

Soria, G., Mendizábal, V., Touriño, C., Robledo, P., Ledent, C., Parmentier, M., Maldonado, R., & Valverde, O. (2005). Lack of CB1 Cannabinoid Receptor Impairs Cocaine Self-Administration. *Neuropsychopharmacology*, *30*(9), 1670–1680. https://doi.org/10.1038/sj.npp.1300707

Soria-Gomez, E., Zottola, A. C. P., Mariani, Y., Desprez, T., Barresi, M., Río, I. B., Muguruza, C., Bon-Jego, M. L., Julio-Kalajzić, F., Flynn, R., Terral, G., Fernández-Moncada, I., Robin, L. M., Cruz, J. F. O. da, Corinti, S., Amer, Y. O., Goncalves, J., Varilh, M., Cannich, A., … Bellocchio, L. (2021). Subcellular specificity of cannabinoid effects in striatonigral circuits. *Neuron*, *109*(9), 1513-1526.e11. https://doi.org/10.1016/j.neuron.2021.03.007

Soti, M., Ranjbar, H., Kohlmeier, K. A., & Shabani, M. (2022). Parkinson's disease related alterations in cannabinoid transmission. *Brain Research Bulletin*, *178*, 82–96. https://doi.org/10.1016/j.brainresbull.2021.11.009

Steeds, H., Carhart-Harris, R. L., & Stone, J. M. (2015). Drug models of schizophrenia. *Therapeutic Advances in Psychopharmacology*, *5*(1), 43–58. https://doi.org/10.1177/2045125314557797

Stroup, T. S., & Gray, N. (2018). Management of common adverse effects of antipsychotic medications. *World Psychiatry*, *17*(3), 341–356. https://doi.org/10.1002/wps.20567

Su, D., Cui, Y., He, C., Yin, P., Bai, R., Zhu, J., Lam, J. S. T., Zhang, J., Yan, R., Zheng, X., Wu, J., Zhao, D., Wang, A., Zhou, M., & Feng, T. (2025). Projections for prevalence of Parkinson's disease and its driving factors in 195 countries and territories to 2050: Modelling study of Global Burden of Disease Study 2021. *The BMJ*, *388*, e080952. https://doi.org/10.1136/bmj-2024-080952

Szabo, B., Than, M., Thorn, D., & Wallmichrath, I. (2004). Analysis of the effects of cannabinoids on synaptic transmission between basket and Purkinje cells in the cerebellar cortex of the rat. *The Journal of Pharmacology and Experimental Therapeutics*, *310*(3), 915–925. https://doi.org/10.1124/jpet.104.066670

Tang, W., Kochubey, O., Kintscher, M., & Schneggenburger, R. (2020). A VTA to Basal Amygdala Dopamine Projection Contributes to Signal Salient Somatosensory Events during Fear Learning. *Journal of Neuroscience*, *40*(20), 3969–3980. https://doi.org/10.1523/JNEUROSCI.1796-19.2020

Tao-Cheng, J.-H., Crocker, V., Moreira, S. L., & Azzam, R. (2021). Optimization of protocols for pre-embedding immunogold electron microscopy of neurons in cell cultures and brains. *Molecular Brain*, *14*(1), 86. https://doi.org/10.1186/s13041-021-00799-2

Tsou, K., Brown, S., Sañudo-Peña, M. C., Mackie, K., & Walker, J. M. (1998). Immunohistochemical distribution of cannabinoid CB1 receptors in the rat central nervous system. *Neuroscience*, *83*(2), 393–411. https://doi.org/10.1016/s0306-4522(97)00436-3

Urbi, B., Corbett, J., Hughes, I., Owusu, M. A., Thorning, S., Broadley, S. A., Sabet, A., & Heshmat, S. (2022). Effects of Cannabis in Parkinson's Disease: A Systematic Review and Meta-Analysis. *Journal of Parkinson's Disease*, *12*(2), 495–508. https://doi.org/10.3233/JPD-212923

Urbi, B., Lee, Y., Hughes, I., Thorning, S., Broadley, S. A., Sabet, A., & Heshmat, S. (2022). Effects of cannabinoids in Parkinson's disease animal models: A systematic review and meta-analysis. *BMJ Open Science*, *6*(1). https://doi.org/10.1136/bmjos-2022-100302

Van Laere, K., Casteels, C., Lunskens, S., Goffin, K., Grachev, I. D., Bormans, G., & Vandenberghe, W. (2012). Regional changes in type 1 cannabinoid receptor availability in Parkinson's disease in vivo. *Neurobiology of Aging*, *33*(3), 620.e1-620.e8. https://doi.org/10.1016/j.neurobiolaging.2011.02.009

Vázquez-Vélez, G. E., & Zoghbi, H. Y. (2021). Parkinson's Disease Genetics and Pathophysiology. *Annual Review of Neuroscience*, *44*(Volume 44, 2021), 87–108. https://doi.org/10.1146/annurev-neuro-100720-034518

Vicq d'Azyr, F. (with Bibliothèque interuniversitaire de santé (Paris)). (1786). *Traité d'anatomie et de physiologie avec des planches coloriées représentant au naturel les divers organes de l'Homme et des Animaux / vol. I*. Paris : François Didot l'aîné. http://archive.org/details/BIUSante_00519x01

Volkow, N. D., & Blanco, C. (2023). Substance use disorders: A comprehensive update of classification, epidemiology, neurobiology, clinical aspects, treatment and prevention. *World Psychiatry*, *22*(2), 203–229.

Volkow, N. D., Fowler, J. S., Wang, G.-J., Swanson, J. M., & Telang, F. (2007). Dopamine in Drug Abuse and Addiction: Results of Imaging Studies and Treatment Implications. *Archives of Neurology*, *64*(11), 1575–1579. https://doi.org/10.1001/archneur.64.11.1575

Volkow, N. D., Wang, G.-J., Fowler, J. S., Tomasi, D., & Telang, F. (2011). Addiction: Beyond dopamine reward circuitry. *Proceedings of the National Academy of Sciences*, *108*(37), 15037–15042. https://doi.org/10.1073/pnas.1010654108

Volkow, N. D., Wang, G.-J., Fowler, J. S., Tomasi, D., Telang, F., & Baler, R. (2010). Addiction: Decreased reward sensitivity and increased expectation sensitivity conspire to overwhelm the brain's control circuit. *BioEssays : News and Reviews in Molecular, Cellular and Developmental Biology*, *32*(9), 748–755. https://doi.org/10.1002/bies.201000042

Walsh, S., Mnich, K., Mackie, K., Gorman, A. M., Finn, D. P., & Dowd, E. (2010). Loss of cannabinoid CB1 receptor expression in the 6-hydroxydopamine-induced nigrostriatal terminal lesion model of Parkinson's disease in the rat. *Brain Research Bulletin*, *81*(6), 543–548. https://doi.org/10.1016/j.brainresbull.2010.01.009

Weston-Green, K. (2022). Antipsychotic Drug Development: From Historical Evidence to Fresh Perspectives. *Frontiers in Psychiatry*, *13*. https://doi.org/10.3389/fpsyt.2022.903156

Xing, G., Carlton, J., Jiang, X., Wen, J., Jia, M., & Li, H. (2014). Differential Expression of Brain Cannabinoid Receptors between Repeatedly Stressed Males and Females may Play a Role in Age and Gender-Related Difference in Traumatic Brain Injury: Implications from Animal Studies. *Frontiers in Neurology*, *5*. https://doi.org/10.3389/fneur.2014.00161

Yoshida, T., Hashimoto, K., Zimmer, A., Maejima, T., Araishi, K., & Kano, M. (2002). The Cannabinoid CB1 Receptor Mediates Retrograde Signals for Depolarization-Induced Suppression of Inhibition in Cerebellar Purkinje Cells. *Journal of Neuroscience*, *22*(5), 1690–1697. https://doi.org/10.1523/JNEUROSCI.22-05-01690.2002

Young, C. B., Reddy, V., & Sonne, J. (2025). Neuroanatomy, Basal Ganglia. In *StatPearls*. StatPearls Publishing. http://www.ncbi.nlm.nih.gov/books/NBK537141/

Zhou, F.-M., & Lee, C. R. (2011). Intrinsic and integrative properties of substantia nigra pars reticulata neurons. *Neuroscience*, *198*, 69–94. https://doi.org/10.1016/j.neuroscience.2011.07.061

Zou, S., & Kumar, U. (2018). Cannabinoid Receptors and the Endocannabinoid System: Signaling and Function in the Central Nervous System. *International Journal of Molecular Sciences*, *19*(3), 833. https://doi.org/10.3390/ijms19030833

Appendix A: Antibodies List

Antibody	Species	Manufacturer	Catalog Number
Anti-cannabinoid receptor type-1 (CB1R)	Goat	Nittobo Medical Co. Ltd.	MSFR100610
Anti-cannabinoid receptor type-1 (CB1R)	Rabbit	Nittobo Medical Co. Ltd.	MSFR100590
Anti-glutamate decarboxylase 67 (GAD67)	Mouse	ThermoFisher Scientific	MA5-24909
Anti-tyrosine hydroxylase (TH)	Rabbit	Pel-Freeze Biologicals	P40101-150
Anti-Vesicular GABA Transporter (VGAT)	Mouse	Synaptic Systems	131011
Anti-Vesicular Glutamate Transporter 1 (VGlut1)	Guinea Pig	Synaptic Systems	135304
Anti-Vesicular Glutamate Transporter 2 (VGlut2)	Mouse	Synaptic Systems	135421
Anti-goat Alexa Fluor 488	Donkey	ThermoFisher Scientific Invitrogen	A11055
Anti-rabbit Alexa Fluor 594	Donkey	ThermoFisher Scientific Invitrogen	R37119
Anti-mouse Alexa Fluor 647	Donkey	ThermoFisher Scientific Invitrogen	A32787
Anti-goat Alexa Fluor 647	Donkey	ThermoFisher Scientific Invitrogen	A21447
Anti-guinea pig Cy5	Donkey	Jackson Immuno Research Laboratories Inc.	706175148
Anti-goat biotinylated	Donkey	ThermoFisher Scientific Invitrogen	A16003
Streptavidin 1.4 nm gold-conjugated		Nanoprobes	2016-1ML
Anti-rabbit horseradish peroxidase (HRP)	Donkey	ThermoFisher Scientific Invitrogen	A16029

Appendix B: Graphical protocol for immunoelectron microscopy methods

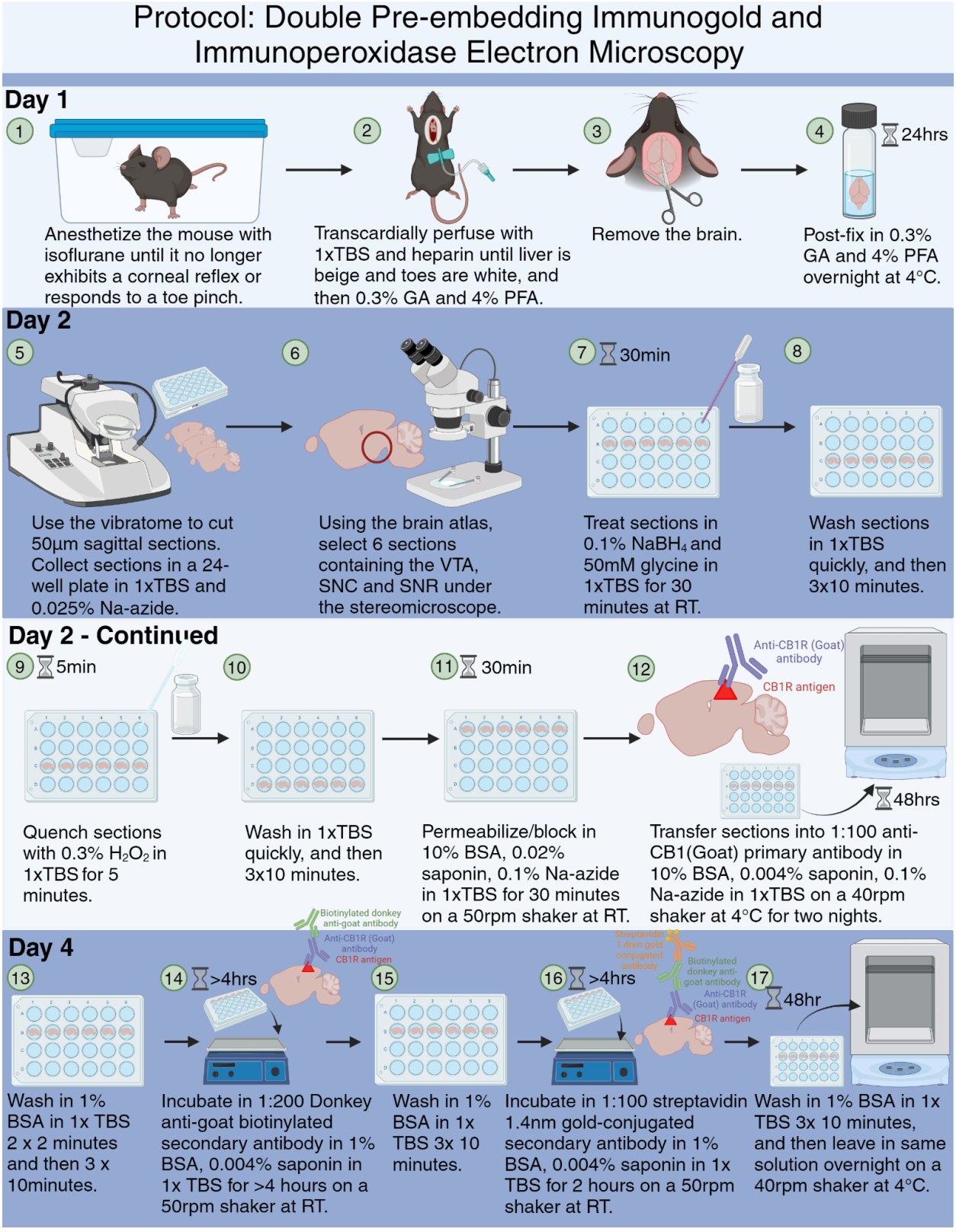

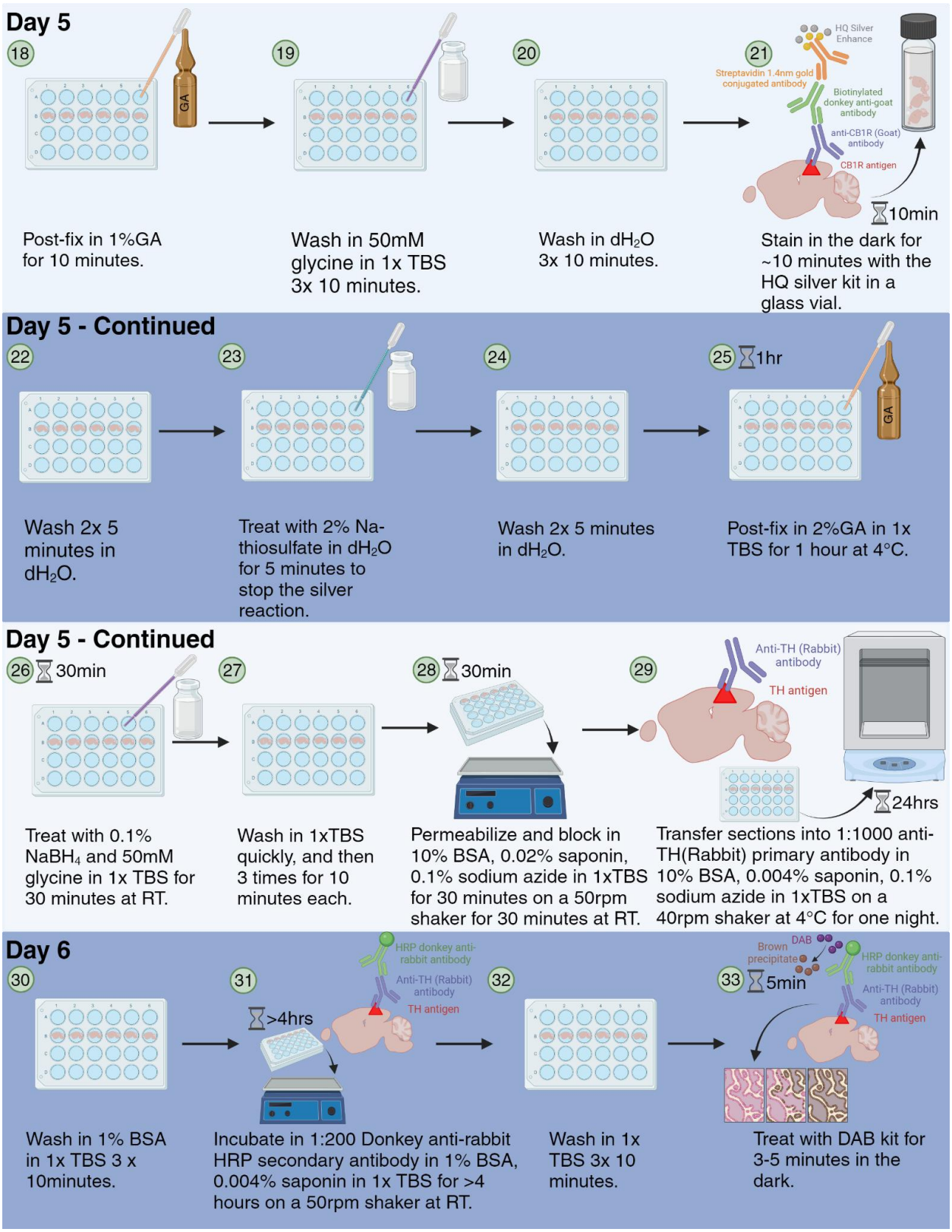
Day 5
18
GA
Post-fix in 1%GA for 10 minutes.
19
Wash in 50mM glycine in 1x TBS 3x 10 minutes.
20
Wash in dH2O 3x 10 minutes.
21
HQ Silver Enhance
Streptavidin 1.4nm gold conjugated antibody
Biotinylated donkey anti-goat antibody
anti-CB1R (Goat) antibody
CB1R antigen
10min
Stain in the dark for ~10 minutes with the HQ silver kit in a glass vial.
Day 5 - Continued
22
Wash 2x 5 minutes in dH2O.
23
Treat with 2% Na-thiosulfate in dH2O for 5 minutes to stop the silver reaction.
24
Wash 2x 5 minutes in dH2O.
25
1hr
GA
Post-fix in 2%GA in 1x TBS for 1 hour at 4°C.
Day 5 - Continued
26
30min
Treat with 0.1% NaBH4 and 50mM glycine in 1x TBS for 30 minutes at RT.
27
Wash in 1xTBS quickly, and then 3 times for 10 minutes each.
28
30min
Permeabilize and block in 10% BSA, 0.02% saponin, 0.1% sodium azide in 1xTBS for 30 minutes on a 50rpm shaker for 30 minutes at RT.
29
Anti-TH (Rabbit) antibody
TH antigen
24hrs
Transfer sections into 1:1000 anti-TH(Rabbit) primary antibody in 10% BSA, 0.004% saponin, 0.1% sodium azide in 1xTBS on a 40rpm shaker at 4°C for one night.
Day 6
30
Wash in 1% BSA in 1x TBS 3 x 10minutes.
31
>4hrs
HRP donkey anti-rabbit antibody
Anti-TH (Rabbit) antibody
TH antigen
Incubate in 1:200 Donkey anti-rabbit HRP secondary antibody in 1% BSA, 0.004% saponin in 1x TBS for >4 hours on a 50rpm shaker at RT.
32
Wash in 1x TBS 3x 10 minutes.
33
5min
Brown precipitate
DAB
HRP donkey anti-rabbit antibody
Anti-TH (Rabbit) antibody
TH antigen
Treat with DAB kit for 3-5 minutes in the dark.

Day 6 - Continued

34 Wash in 1x TBS 3x 10 minutes.

35 

Post-fix in 2%GA for 1 hour.

36 Wash in 1x TBS 3x 10 minutes.

37 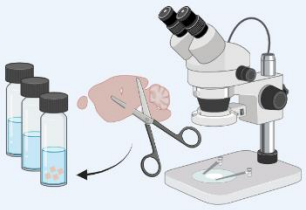
Microdissect the VTA, SNR and SNC into ~1mm^2 squares under the stereomicroscope and place in 4mL vials in 0.15M Na-cacodylate. Leave in fridge overnight.

Day 7: TEM Processing

38 1.25hrs 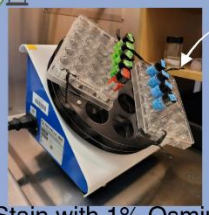

Stain with 1% Osmium and 1% K-ferrocyanide for 45 minutes on a rotary mixer.

39 

Wash quickly and then for 10 minutes in dH_2O on a rotary mixer, repeat 3-5 times.

40 1.25hrs 

Stain with 2% uranyl acetate for 1.25 hours on a rotary mixer.

41 20min x 4 

Dehydrate in graded ethanols: 50%, 75%, 85%, 95% rinsing once quickly and then for 20 minutes each on a rotary mixer. Do 2 quick final rinses with 100% ethanol.

Day 7 - Continued

42 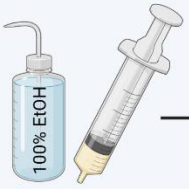

Treat each vial with 1:1 100%EtOH and Spurr resin. Leave rotating overnight.

Day 8

43 
Change vials to pure resin in the morning. Repeat after >4hrs and leave rotating overnight.

Day 9

44 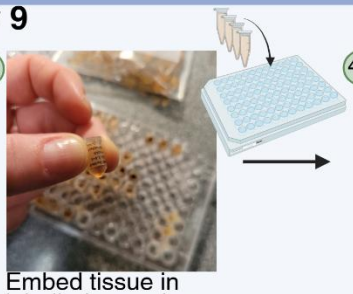
Embed tissue in labelled capsules filled with resin.

45 
Polymerize in oven at >60°C overnight.

Day 10

46 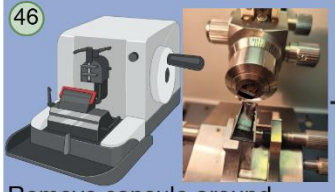
Remove capsule around solidified resin block. Cut sections on the ultramicrotome, first with a glass knife (LM) and then with a diamond knife at 50-70nm (EM; silver/gold visible).

47 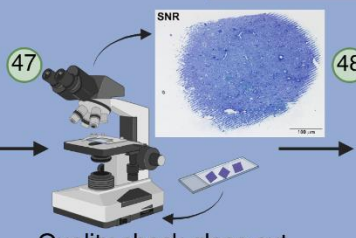

Quality check glass cut sections.Collect tissue on a glass slide, stain with toluidine blue and visualize under a light microscope.

48 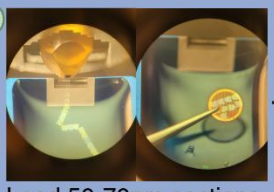
Load 50-70nm sections onto copper grids.

49 
Visualize with the transmission electron microscope.